PAUL SCHERRER INSTITUT

PSI

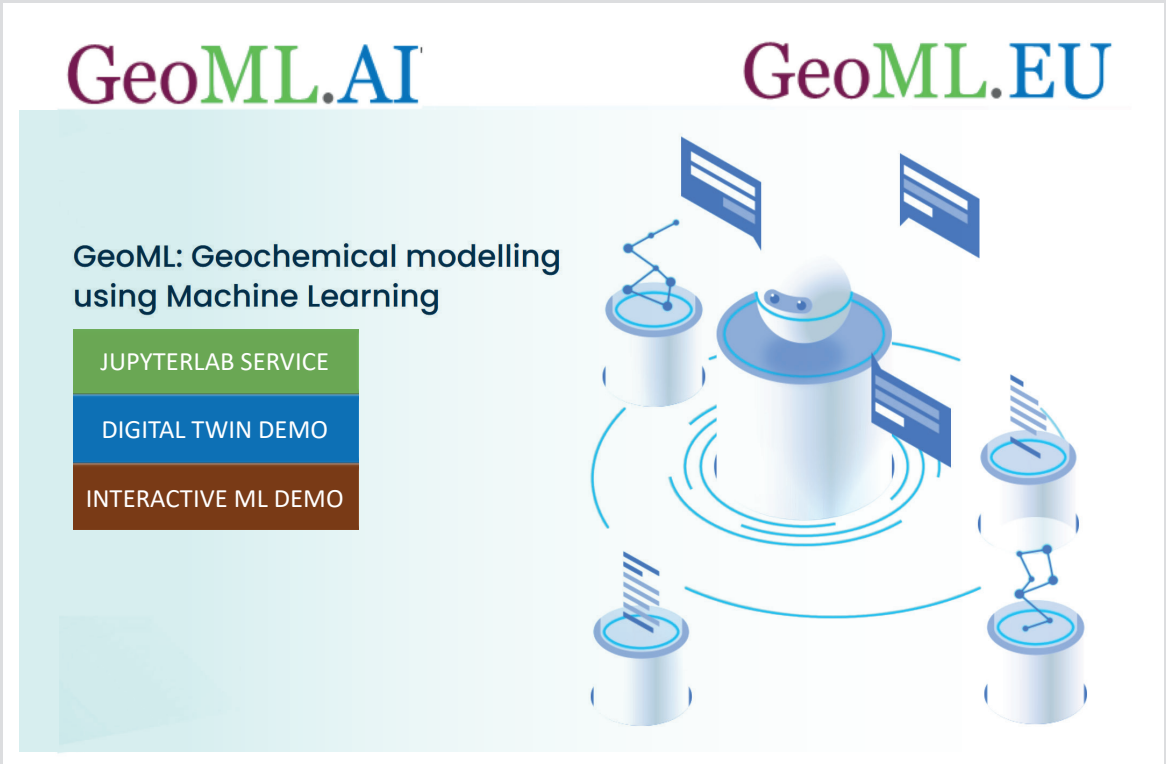

Progress Report 2021

Laboratory for Waste Management :: Nuclear Energy and Safety Department

Cover
Collaborative web platform for process simulations in repository systems: Machine Learning (ML) is a frontier development in data driven scientific approach. In geochemical modelling, ML is applied for accelerating reactive transport simulations using fast and accurate surrogate models replacing direct reactive transport solvers (see Chapter 2).

PAUL SCHERRER INSTITUT

PSI

Progress Report 2021

Laboratory for Waste Management
Nuclear Energy and Safety Department

See also our web-page
http://www.psi.ch/les/

Preface

The mission of the Laboratory for Waste Management (LES) is to carry out a comprehensive research and development (R&D) programme in support of Swiss radioactive waste disposal options. In particular, the aim is to be one of the world-leading laboratories in the fields of geochemistry of disposal systems and transport mechanisms of radionuclides, including geochemical retardation and immobilisation.

The laboratory serves an important national role by supporting the Swiss Federal Government and Nagra in their tasks to safely dispose of radioactive wastes from medical, industrial and research applications as well as from nuclear power plants. The research activities cover fundamental aspects of repository geochemistry, chemistry and physics of radionuclides at geological interfaces, radionuclide transport and retardation in geological and technical barriers. The work performed is a balanced combination of experimental activities conducted in dedicated laboratories for handling radioactive isotopes, field experiments and computer simulations. The work is directed towards repository implementation and the results are used by Nagra in their comprehensive performance assessments studies. The finalisation of the site selection process and the implementation of a repository in the next decades will require strong expertise in model-based assessments of the repository *in situ* conditions for specific repository designs. The long-term strategy of LES is thus to develop experimental and modelling expertise necessary for fully coupled description of relevant processes in a repository in order to assist safety driven implementation of disposal options in Switzerland.

Together with two other laboratories in the department of Nuclear Energy and Safety, LES maintains best practices and standards in the laboratory management and data processing according to the ISO9001:2015 certified Integrated Quality Management System. In 2021, LES has successfully passed the recertification audit conducted by the Swiss Safety Center (www.safetycenter.ch). The certification covers the research and scientific services for agencies in the area of nuclear waste disposal and environmental sciences.

The present report summarises the research activities and results achieved in 2021. It gives a detailed overview of research projects, personnel management, national and international collaborations, and individual contributions achieved by scientists in the four research groups at PSI and the Chair of Mineralogy at the University of Bern.

We gratefully acknowledge the support of our work by the PSI management, Nagra, and numerous research programmes within National and European Funding agencies (e.g. SNSF, Eurad).

Table of Contents

1 OVERVIEW

Churakov S.V.

1.1 Introduction

The overall progress made in the Laboratory for Waste Management (LES) from January 1st, 2021 to December 31th, 2021 is summarised in the first part of the report. The report is organised thematically according to the eight overarching research topics. These topics are multidisciplinary in nature and include contributions from different research groups at LES and the Mineralogy Group in the Institute of Geological Sciences at the University of Bern.

1.2 General

The site selection process for geological disposal of radioactive waste in Switzerland has entered its final stage. On November 22nd, 2018, the Swiss Federal Government has approved the further investigation of the "Jura Ost", "Nördlich Lägern" and "Zürich Nordost" areas for the final selection of a disposal site for a nuclear waste repository in Switzerland. All proposed siting regions are located in the Opalinus Clay formation. In 2019, Nagra has started a deep drilling campaign with the aim to characterise the local site-specific geological and hydrological conditions. First diffusion and sorption measurements on the samples extracted from the drill cores obtained at potential siting regions have started at LES in January 2020 and continued in 2021. The diffusion and sorption measurements on the drill cores and the interpretation of obtained data were the most prominent activities in 2021. Complete data sets for the Bülach, Trüllikon and Bözberg sites have become available by the end of 2021. These data provide a solid scientific basis for the performance assessment calculations and the decision making in the site selection process.

It is anticipated that the site intended for the General Licence Application (*Rahmenbewilligungsgesuch (ger.)*, RBG) will be announced in 2022. The development of the scientific basis and the documentation of the arguments to justify the site selection for the general licence application to be submitted in 2024 are the main driving forces in the current research phase. The corresponding documentation will have to be reviewed by the Swiss regulator (ENSI) and international experts up on submisson.

Following the period of very intensive site-specific explorations leading to the submission of the RBG, the implementation phase is expected to start soon after 2030 given that the approval of the proposed site is supported by the regulator and approved by the Parliament. During the implementation phase, the underground exploration studies will be continued to confirm the findings obtained during the site exploration campaign. Further, the implementation phase foresees the optimisation of the repository design and includes a detailed specification of the materials to be used for the repository implementation. In this context, LES' national role is to maintain know-how in the field of waste disposal geo-chemistry, and relevant aspects of material sciences. Accordingly, LES continues research on the main pillars of repository safety namely the mechanistic description of radionuclide interaction with repository barriers and of the processes in the repository near field. Present and future research activities focus on the behaviour of modern spent fuel under repository conditions, the chemical evolution of the repository near field, sorption competition phenomena, the behaviour of redox-sensitive radionuclides, the role of mineral surface-induced redox reactions, and the transfer of sorption models and data from dispersed to compacted systems. In preparation of the optimisation phase, LES puts strong emphasis on the further development of advanced capabilities for reactive transport simulations. These capabilities are particularly important for understanding the long-term evolution of *in situ* repository conditions and the interaction between repository barriers causing an alteration of their retention and transport properties. Such expertise is the essential basis for the optimisation of repository design.

Future research in nuclear waste disposal will strongly rely on the process-based multiscale modelling using high fidelity simulation platforms, coupling complex physical phenomena in repository systems. Particularly challenging in this context is the parameter transfer between models at different scales and efficient process coupling in complex realistic 3D models. LES is taking a leading role in the development of so-called data driven surrogate models based on modern algorithms developed in the field of artificial intelligence and machine learning. Particularly promising are the applications of Deep Neural Networks (DNN) and surrogate models for geochemical simulations in fully coupled THMC reactive transport codes. To foster international collaboration LES has launched a web based platform (https://www.geoml.ai) offering a python-based environment for the training of DNN for geochemical applications. These surrogate models are the basis for the development of digital twins for

coupled geochemical processes. Several demonstrations of such applications are provided at (https://www.geoml.eu).

In 2019, the Joint European Research Proposal COFUND-EJP NFRP-2018-6: *"European Joint Research Programme in the management and disposal of radioactive waste Eurad"* has been approved by the European Commission. This project is a joint venture of 52 mandated research agencies, waste management organisations and technical safety organisations focusing on the most urgent research issues of nuclear waste disposal in Europe. In the first phase of the project, LES joined six individual work packages (WPs):

FUTURE: Fundamental understanding of radionuclide retention (WP Lead and Task lead)

DONUT: Modelling of process couplings and numerical tools applied to performance assessment (Task co-Lead)

ACED: Assessment of chemical evolution of ILW and HLW disposal cells (Task Lead)

GAS: Mechanistic understanding of gas transport in clay materials (Contributor)

CORI: Cement organics radionuclide interactions (Contributor)

UMAN: Uncertainty management multi-actor network (Contributor)

In the beginning of 2020 a second call for the follow up projects within Eurad consortium has been launched, which lead to the formulation of additional work packages. Within this second wave call, LES participates to the extension of the UMAN project (Sub-Task Lead) and two new work packages:

MAGIC: Chemo-Mechanical AGIng of Cementitious materials (Task Lead)

MODATS: Monitoring equipment and data treatment for safe repository (Contributor)

Within the EURATOM NFRP-2019-2020-10 RIA call LES participates in the project *"Pre-disposal management of radioactive waste, PREDIS"*. This 4 years EU project was approved in spring 2020 and started in September 1st, 2020. The consortium includes 47 partners from 18 Member States. In this project, LES has a leading role in the development of a model based digital twin for the evolution of cementitious waste packages in extended intermediate storage scenarios.

The reactive transport codes developed at LES are versatile and applicable in broad cross-disciplinary applications. Complementary to geochemical applications, the codes are also used in collaborative research projects including thermohydraulic applications for nuclear reactors, desalination membranes, and pharmaceutical applications. Recently, an existing collaboration with GlaxoSmithKline Vaccines, Belgium (GSK), a science-led pharmaceutical company, focused on research, development and manufacturing of innovative pharmaceutical products, was extended. With support of Swissnuclear, further development of multiscale simulation codes for the modelling of boiling phenomena in nuclear reactors is ongoing.

Scientific exchange is an essential component of research and development programmes. Particularly important is the cross dissemination of knowledge in the adjacent areas. LES actively maintains collaborations with national and international research institutes in the field of waste management and environmental research. The main multi- and bi-lateral co-operations with external institutions and universities are summarised in Table 1.1.

Participation in international research projects and independent acquisition of project funding for PhD and postdoc projects is an essential driving force for developing state-of-the-art research capabilities, knowledge transfer and education of young generation scientists. Ongoing MSc/BSc/PhD projects and postdoc fellowships approved or started in 2021 are listed below along with ongoing ones.

A. Bucher (BSc student): *"Atomic scale structure of magnetite water interface"* (UniBe 2021-2022).

R. Haller (MSc student): *"Geochemical modelling of reactive transport processes with deep neural networks"* (UniBe 2019-2021).

N. Krattiger (BSc/MSc student): *"Comparative study of C-S-H and ASR-products in cement by GCMC modelling"* (UniBe 2019-2022).

D. Roos (MSc student): *"Structural changes and thermal stability of Pb^{2+} -modified zeolites"* (UniBe 2019/2021).

P. Chen (PhD student/UBern): *"Behaviour of Tc in illite in presence of Fe"*. Start date: November 2018 (Funding: Chinese Academy of Sciences).

P. Krejci (PhD student): *"Multispecies cation transport in compacted clays"*. Start date: December 2016 (Funding: Swiss National Science Foundation, SNSF).

P. Luraschi (PhD student): *"Evolution of transport properties, mineralogy and porosity of cement-clay interfaces"*. Start date: April 2017 (Funding: Nagra, PSI).

M. Mahrous (PhD student): *"Resolving dissolution-precipitation processes in porous media: Pore-scale Lattice Boltzmann modelling combined with synchrotron-based X-ray characterisation"*. Start date: March 2018 (Funding: SNSF).

J. Owusu (PhD student): *"Pore-scale simulations of gas molecules in saturated and partially saturated clays"*. Start date: November 2019 (Funding: HORIZON 2020, Eurad).

H. Peng (PhD student): *"In situ Chemical Tomography and Modelling of Reactive Transport Processes in Porous Media".* Start date: November 2021 (Funding: PSI-Cross).

Y. Qian (PhD student): *"Adsorption of redox sensitive radionuclides on Fe-bearing clay minerals"*. Start date: November 2019 (Funding: HORIZON 2020, Eurad).

R. Schliemann (PhD student): *"Dissolution, growth and ion uptake at phyllosilicate surfaces: Coupling atomistic interactions at the mineral water interface with Kinetic Monte Carlo model"*. Start date: July 2016 (Funding: SNSF).

V. Stotskyi (PhD student): *"Molecular scale understanding of competitive cation adsorption on swelling clay minerals"*. Start date: May 2021 (Funding: SNSF).

M. Wolffers (PhD student/UBern): *"Genesis and characterisation of fly ash in Swiss waste incineration plants".* Start date: March 2019 (Funding: Industry).

Dr. Y. Chen (postdoc): *"Diffusive transport of gaseous species at saturated and partially saturated conditions"*. Start date: September 2019 (Funding: EU Horizon 2020 Marie Skłodowska-Curie grant, PSI-FELLOW-II-3i).

Dr. P. Cruz Hernandez (postdoc): *"Sorption mechanisms of Zn and U on Opalinus Clay"*. Start date: August 2019 (EU Horizon 2020 Marie Skłodowska-Curie grant, PSI-FELLOW-II-3i).

Dr. F. Di Lorenzo (postdoc): *"Molecular scale understanding of competitive cation adsorption on swelling clay minerals"*. Start date: June 2021 (Funding: SNSF).

Dr. T. L. Guillemot (postdoc): *"Development of C-14 AMS based analytical methods for the identification and quantification of dissolved and volatile organic compounds".* Start date: January 2019 (Funding Nagra).

Dr. F. Marafatto (postdoc): *"Cryo-microspectroscopy at the microXAS beamline for the investigation of redox- and radiation-sensitive samples"*. Start date: June 2017 (Funding: PSI, EAWAG).

Dr. A. Mokos (postdoc): *"Boiling crisis in nuclear reactor"*. Start date: March 2021 (Funding: Swissnuclear).

Dr. A. Rajyaguru (postdoc): *"In situ Chemical Tomography and Modelling of Reactive Transport Processes in Porous Media".* Start date: August 2021 (Funding: PSI-Cross).

Tab. 1.1: National and international co-operations.

Co-operations
National Nagra* (Major financial contribution, various technical working groups) Swissnuclear* (Reactor safety, material aging)
Multinational NEA Thermodynamic Database Project EURATOM HORIZON2020 (Eurad) EURATOM HORIZON2020 (PREDIS) EURATOM HORIZON2020 (DISCO) Mont Terri Projects* (diffusion retardation, clay-cement interaction)
Universities University of Bern*, Switzerland (mineralogy, petrography, water chemistry, C-14 AMS) EPFL, Switzerland (cement systems) Université de Bourgogne, Dijon, France (molecular modelling) ETH*, Zurich, Switzerland (GEMS) Hiroshima University, Japan (clay-cement interaction) University of Luxembourg* (porous media) Sino-French Institute of Nuclear Engineering and Technology, Sun Yatsen University (diffusion)
Research Centres CEA*, France (chemistry of near and far field) Eawag, Switzerland (Gas MS analytics) EMPA*, Switzerland (cement) IRE, HZDR*, Germany (XAS, TRLFS, atomistic modelling, reactive transport) INE, KIT*, Germany (near and far field; TRLFS) FZJ, Germany (sorption/diffusion of Ra, reactive transport, thermodynamics of solid solutions) SCK/CEN, Belgium (clay and cement systems) UFZ*, Germany (reactive transport, clay systems)
Industrial Partners GlaxoSmithKline* NanoCem Congineer

**formal co-operation agreements*

Two PhD students have defended their PhD thesis in 2021:

L. Hax Damiani (PhD student): *"A novel reactive transport framework for fluid-rock interaction analysis: Computational approach, applications and benchmarks"*. PhD Defence October 22nd, 2021, University of Bern, (Funding: EU).

A. Glauser (PhD student/UBern): *"Development of quality of bottom ash from municipal solid waste incineration in Switzerland"*. PhD Defence March 30th, 2021, University of Bern (Funding: Various Industrial Partners).

LES has an aging research team. The personnel planning and knowledge transfer is one of the main concerns of the LES management. A broad consensus has been established that experimental research expertise at LES has to cover the main pillars of repository safety such as diffusion, sorption and the reactive transport phenomena. To keep the long-term leadership of LES in experimental studies of reactive transport phenomena a tenure track position was announced in December 2020. After careful evaluation of highly qualified applications, the position was offered to Dr. B. Ma, who has broad knowledge of transport processes in cement and clays systems.

The organisational chart of LES comprises four research groups located at PSI (Fig. 1.1). A fifth research group is located at the Institute of Geological Sciences (IfG) at the University of Bern. The mineralogy group at IfG is complementing the expertise in the field of mineral dissolution kinetics, structural studies of high porous materials and X-ray diffraction-based structure refinement and the geochemistry of conventional waste disposal. In particular, the mineralogy group hosts the Competence Centre for Secondary Raw Materials conducting applied research in the field of environmental geochemistry and secondary raw materials.

The LES annual report 2021 is organised in seven thematic research projects addressing specific aspects of repository geochemistry and radionuclide transport:

Chapter 2: Geochemical evolution of repository systems

Chapter 3: Development of mechanistic sorption models and experimental validation

Chapter 4: Radionuclides transport and retention in compacted systems at full and partial saturation

Chapter 5: Radioactive waste characterisation

Chapter 6: Thermodynamic models and databases

Chapter 7: Fundamental aspects of mineral reactivity and structural transformations

Chapter 8: Geochemical Aspects of waste materials and their disposal

The following section provides an overview of activities related to the Sectoral Plan for Deep Geological Disposal, repository near and far field, reactivity of barrier systems and code benchmarking.

1.3 Sectoral plan for deep geological disposal

The potential radiological impact of a repository is one of the main safety relevant criteria employed in the site selection process. Sorption and diffusion data are the basis for dosis calculations. The sorption databases for *in situ* repository conditions are derived using a thermodynamic approach. A new major update of LES thermodynamic database was released in 2020 in an electronic form. It is available in the GEMS geochemical solver together with detailed documentation of recommended thermodynamics parameters. Maintenance of the database is an ongoing process. In 2021, new data for radium halogens and sulphate were revised and included in the database (see section 6.2).

Calcium silicate hydrates (C-S-H) are the most important phases in cementitious systems responsible for chemical stability of cement, its mechanical strength and, in case of repository system, the retention of radionuclides. A highly versatile and accurate model CASH+ has been developed and maintained at LES since several years. The CASH+ model is formulated based on a sublattice solid solution model allowing an incremental extension of the chemical complexity keeping the core data unchanged. In 2021, the model has been extended to describe uptake of alkali metals (Li, Na, K, Rb, Cs) and alkaline earth metals (Mg, Sr, Ba, Ra). For this aim, thermodynamic properties of the corresponding endmembers were fitted to available experimental data or, when not available, estimated theoretically (see section 6.3).

1.4 Repository near field

1.4.1 Repository chemistry

Dissolution of spent fuel and vitrified nuclear waste defines the radionuclides release after breaching of the disposal casks containing high-level radioactive waste. Because of its high importance, this source term has been intensively studied for decades. In the framework of the Horizon 2020 EU project DisCo (Modern spent fuel Dissolution and chemistry in failed Container conditions) LES is developing thermodynamic models of UO_2 fuels under in-pile conditions and consider various scenarios of SF dissolution. To this aim, thermodynamic equilibrium calculations were carried out to model chemical conditions after canister breaching and intrusion of pore water from the

surrounding bentonite buffer material, based on the disposal concept currently foreseen in Switzerland. Two types of models were applied: (i) A batch equilibration model in which progressively increasing amounts of the materials involved (UO_2 spent fuel, Zircaloy, steel canister and other structural materials) react with intruded bentonite pore water filling the open spaces in the canister and (ii) A reactive transport model simulating thermodynamic equilibrium during counter-diffusion of solutes from saturated bentonite on one side and oxidatively corroding SF on the opposite side. The simulations show that redox kinetics and H_2 chemical reactivity under faithful repository conditions (realistic temperature, radiation field, clay compaction) has a profound effect on the water chemistry inside a breached steel canister in contact with UO_2. It could be further suggested that experimental studies aiming at better constraining the conditions of H_2 and S(VI) reduction are necessary (see section 5.3).

The composition and characteristics of pore waters in equilibrium with compacted bentonite (the backfilling material of the repository tunnels) is the basis for determining solubility limits and sorption coefficients of dose-relevant nuclides. The corresponding pore water model should be consistent with the sorption models used for the radionuclide retention, the thermodynamic data and activity models for reactive transport simulations. Accordingly, a unified pore water modelling approach has been developed and tested based on chemical analyses of Opalinus Clay aqueous extracts obtained during Nagra's borehole campaign for SGT-3 (see section 2.2.2).

The anoxic corrosion of activated steel in the near field of a L/ILW repository leads to the release of ^{14}C-containing low molecular weight (LMW) carbon compounds. The high mobility of ^{14}C-carrying gaseous and dissolved compounds is caused by weak interaction with mineral surfaces in the far field. Knowledge of the chemical nature of the carbon compounds acting as ^{14}C carriers to the liquid and gas phases enables a more detailed assessment of their retention in the near field of the L/ILW and SF/HLW repositories. To support future safety assessment, a laboratory-scale corrosion experiment with irradiated stainless steel was set up to identify and quantify the ^{14}C-containing carbon compounds released under anoxic and strongly alkaline conditions that simulate long-term conditions in a cement-based repository for L/ILW. The project was started in 2012 with the acquisition of the necessary analytical instruments. In further phases, a compound-specific radiocarbon analysis based on ^{14}C quantification by accelerator mass spectrometry as well as the experimental set-up were developed. Finally, the corrosion experiment was started in 2016 and has been sampled regularly since then. The experimental phase of the project was completed at the end of 2021. The technical report summarising the experimental results and the summary of data interpretation are in preparation. An extension of the project with further samplings from the reactor containing the irradiated steel samples is currently planned (see section 5.2).

1.4.2 Clay systems

In the frame of the Swiss Sectoral Plan for Deep Geological Repositories (SGT), LES is carrying out sorption experiments involving different radionuclides i.e. Cs^{I}, Ni^{II}, Eu^{III}, Th^{IV} and U^{VI} on samples from three potential siting regions. The aim is to compare the adsorption properties of the different argillaceous rocks and to test the robustness of the "bottom-up approach". For the safety analysis applied in the general licence application a simplified component additive approach, the so-called "bottom-up approach" is applied to calculate site-specific sorption databases (SDBs). In this approach, solid-liquid distribution ratios (R_d values) are calculated directly, including aqueous speciation, solubility and concentration-dependent adsorption of the radionuclides for site-specific argillaceous rock/porewater systems by using element specific adsorption models for illite developed at LES during the last 20 years. Sorption experiments in a synthetic pore water (SPW) were carried out on seven different samples from the Bülach-1 borehole in the siting region of Nördlich Lägern. In view of the uncertainties related to the complexity of the natural rocks and the sorption model, the blind predictions were in very good agreement with the measurements of Cs adsorption on different sedimentary rocks (see section 3.2).

Sorption models contain a number of variables with different uncertainties. All these uncertainties contribute to the performance of the model in a complex way. In order to quantify the integral effect of the relevant model variables (e.g. stability of surface species, site capacity, stability of hydrolysis species, clay content, etc.) on the calculated distribution coefficients, a new tool, the UpSaGems (Uncertainty propagation and Sensitivity analysis for Gems) has been developed to perform uncertainty propagation and global sensitivity analysis of thermodynamic models. The uncertainty propagation allows to quantify the effect of the errors in the input parameter on the total uncertainties of the model output, for instance, in form of statistical confidence intervals. The global sensitivity analysis quantifies the relative importance of different input parameters and their interactions onto variations of the model output (see section 3.4).

Several studies on radionuclide retention and transport in clays and argillaceous materials are performed in framework of the Eurad project FUTURE. Ba and Ra uptake on 2:1 clay minerals is investigated in collaboration between Forschungszentrum Jülich (FZJ) and PSI-LES. The available results indicate that the uptake of Ra on montmorillonite is governed by well-known adsorption mechanisms, i.e. cation exchange and surface complexation, and can be quantified by well established adsorption models (see section 3.3). Coupled adsorption and electron transfer interface reactions governing the retention of redox-sensitive Se and Tc on clay minerals in presence of Fe^{2+}/Fe^{3+} are investigated in a joint project between PSI and BRGM. The project focuses on the interface redox reactions between radionuclides Se/Tc and structural Fe in the clay matrix. The aim of the project is to quantify and characterise the coupled sorption and reduction mechanism (i.e. electron transfer, reactivity of Fe^{2+}, $Fe^{2+}/Fe^{/3+}$ ratio, and its crystallographic location) of these redox sensitive radionuclides by iron bearing clay minerals (see section 3.7). The sorption and diffusion of Co^{2+}, Mn^{2+}, Eu^{3+} tracers in compacted illites was measured by in-diffusion experiments at varying concentrations of background electrolytes represented by the alkaline earth and transition element series (Ca^{2+}, Mn^{2+}) under different pH and ionic strength. The ions in background electrolytes are expected to compete for the sorption sites with the tracer elements. The results of these experiments were in good agreement with the predictions of the 2-site protolysis non-electrostatic surface complexation and electrical double layer (2SPNE-SC/EDL) diffusion and sorption model. The competing cations not only exhibit an effect on the sorption behaviour (depending on the type of sites and competing cation involved), but also influence diffusivities of the studied tracers. These observations are interpreted as a competitive effect in the diffuse layer governing the concentrations of mobile cationic surface species (see section 4.1- 4.3).

To access role of Fe^{2+}, aqueous and adsorbed, on the diffusive behaviour of ^{99}Tc in compacted illite, the sorption of Fe(II) on illite has been studied as a function of pH and concentration. Fe^{2+} is assumed to play a key role in the retention of ^{99}Tc in clay rocks by acting as a reducing agent that reduces Tc^{7+} towards lower oxidation states, most probably to Tc^{4+}. The sorption of Fe^{2+} on illite was similar to its sorption behaviour on montmorillonite and modelled using 2 SPNE SC/CE surface complexation model (see section 4.7).

The success of the sorption model and “bottom-up approach” applied for sorption studies in poly-mineral rocks depends on the mechanistic understanding of the sorption mechanisms. Particularly, promising are the combination of wet chemical studies and spectroscopic investigations. Further refinement of the model using such a combined approach was applied for Zn uptake by Illite du Puy, Opalinus Clay and Boda Claystone (see section 3.5). New structural data were obtained to improve the description of Pb uptake in illite (see section 3.6). The molecular mechanism of sorption competition between divalent and tri-valent cation on 2:1 swelling clay is investigated by combination of various spectroscopic techniques and atomistic simulations in framework of an SNF project (see section 3.8).

Significant quantities of gas are expected to emerge in a repository, either resulting from corrosion of metallic materials or due to degradation of organic waste compounds. The gas should be able to migrate through the multi-barrier system to prevent potential pressure build up, which can lead to the loss of barrier integrity otherwise. One of the most important parameters controlling the gas dissipation in a disposal system of engineered barriers is the diffusive mobility of gaseous species in host rocks. Diffusion of gas in partially saturated bentonite was studied in the framework of a Marie Skłodowska-Curie COFUND postdoc project. To this end, a new gas-tight equipment (GD-MS) was designed and developed to keep the clay sample at a well-defined saturation degree during a through-diffusion experiment with He (see section 4.5). Complementary to experimental studies theoretical atomistic simulations are applied to investigate the transport mechanism of dissolved gases in interlayers of swelling clays within the EURAD project GAS (see section 4.6).

1.4.3 Cement systems

The Horizon 2020 EU project PREDIS (“The pre-disposal management of radioactive waste”) aims to develop new methods, processes and technologies for the management of radioactive waste during interim storage. LES is contributing to the development of digital twins of cemented waste packages by experimental investigations of old waste packages and model development. The work carried out during the first year mainly consisted of the development of a concept for a digital twin of cemented waste packages during predisposal period. The digital twin of cemented waste packages is envisaged as a user-friendly and accessible tool designed to predict and evaluate different scenarios of waste package evolution during interim storage using specific input information, such as the dimensions, the initial composition of the waste package and the storage conditions. The numerical models for waste package evolution are computationally time-consuming. The computational efficiency of the tools is improved using most advanced machine learning algorithms and surrogate models

based on deep neural networks. These models are trained based on large amounts of chemical, physical and mechanical data for the evolution of waste packages based on full scale process simulators. To validate these numerical models, simulations results will be compared with experimental data obtained by characterisation of old cemented waste packages stored for many years in an interim storage facility under known conditions (see section 5.5).

In the framework of the Eurad project CORI ("Cement-Organics-Radionuclides-Inter-actions") LES is investigating the extent of the abiotic degradation of cellulose and isosaccharinic acid (ISA) under the anaerobic, alkaline conditions relevant to a cement-based L/ILW repository. This project aims at investigating whether abiotic degradation occurs at elevated partial pressure of H_2 and in the presence of iron as a possible catalyst under alkaline conditions. Cellulose degradation and α-ISA stability is being investigated in artificial cement pore water (ACW) with pH 13.3 in the presence of portlandite and metallic Fe powder at a temperature of 90°C to accelerate potential degradation reactions. The presence of metallic Fe gives rise to increased H_2 partial pressures caused by progressive corrosion, which creates reducing conditions (see section 5.4).

1.4.4 Interface processes

The evolution of the cement-clay interface is of relevance for the long-term safety assessment of the underground radioactive waste repositories because it modifies the mobility of ions and molecules across the interface compared to unreacted materials. Mineral reaction and porosity evolution at cement-clay interfaces is investigated in the laboratory through diffusion experiments. Chemical interaction between these materials results in dissolution-precipitation reactions of minerals that lead to the changes in porosity and pore space connectivity at the interface. Through-diffusion experiments have shown significant reduction of the diffusivity at the interface after 2 years of interaction time. The changes are explained by precipitation of C-S-H phases at the clay compartment of the interface (see section 2.2.1).

Alkali-silica reaction (ASR) is one of the most important concrete durability issues worldwide. The sorption properties of ASR products are barely known experimentally. A comparative study of the sorption properties of ASR products and C-S-H was conducted using reactive Grand Canonical Monte Carlo simulations. It could be shown that due to the differences in the surface site density of the ASR products and C-S-H, Ca ions are strongly partitioned to C-S-H, whereas K has a higher affinity for ASR products. Current studies are continued with the aim to investigate the chemical conditions for attractive and repulsive interactions between the C-S-H and ASR particles. These inter-particle interactions are expected to be the key factors controlling the swelling of ASR products (see section 7.4).

Thick-wall steel casks are used to store radioactive waste in deep geological repositories and to prevent the release of radionuclides into the environment. Steel corrodes slowly under repository conditions forming mixed iron oxides, mainly magnetite (Fe_3O_4). The radionuclides, especially redox sensitive ones, are expected to interact strongly with the corrosion products and either form surface complexes or become incorporated into the crystal structures of the iron oxides. The surface properties of magnetite and potential for incorporation of Pu and Tc are investigated by quantum mechanical calculations and XAS spectroscopy. The first necessary preparatory step for the theoretical modelling of radionuclide uptake on the magnetite surface is the validation of methodology based on available structural and electronic properties of bulk magnetite (see section 7.3).

1.5 Model development, code benchmarking, advanced analytical tools, thermodynamic databases

Reactive transport simulations are the main tool applied for the long-term performance assessment of the repository *in situ* conditions and geochemical evolution of repository near field. Coupled THMC simulations of large spatial domains performed for a long time scale are particularly challenging due to high computational resources and costs. For complex geochemical systems the performance of coupled THMC-codes is often limited by the geochemical solvers which can account for up to 90 % of the simulation time. The second challenge is related to the coupling of models at different scale and the corresponding parameter transfer.

Several projects are focused on reactive transport simulations of crystallisation processes at pore scale using most advanced modelling algorithms. In the framework of the PSI-funded CROSS project *"In situ 4D micro X-ray chemical imaging and a digital twin of miniaturized counter-diffusion experiments: co-precipitation of metals with carbonates in porous media"* numerical models are developed for real time simulations of nucleation and growth of carbonate mineral crystals in presence of traces of secondary elements (e.g. Ni, Zn, Pb). These models are essential for the process understanding and are used to assist in steering the experimental conditions for automated observation of crystallisation process (see section 2.3.1). Computer Vision is applied for automated crystal detection in microfluidic reactive transport

experiments (see section 2.3.3). In collaboration with the Institute of Energy and Climate Research (IEK-6), Forschungszentrum Jülich, Germany, counter-diffusion microfluidic experiments are used to investigate co-precipitation of (Ba,Sr) sulphate solid solutions in transport and kinetic controlled regimes. The interpretation of the experimental data and the process mechanism is conducted based on a pore scale LB code coupled to classical nucleation theory (see section 2.3.4).

Within Eurad-DONUT project a benchmark is designed to test a variety of ML techniques relevant to geochemical and reactive transport simulations in the framework of radioactive waste disposal, aiming at identifying benefits and limitations of ML (see section 2.3.1).

A web service for cement hydration modelling CemGEMS (https://cemgems.app) has been launched online in 2020. CemGEMS is a no-code web application for cement chemists, students and researchers, aimed to facilitate thermodynamic modelling of cement hydration processes, visualization and tabulation of results. In the back-end, the web app runs the conventional GEMS3K code. Recently, the web app was extended to account for heat effects of cement hydration in isothermal and adiabatic conditions (see section 2.4).

The models and codes developed at LES are highly versatile and find further applications in different adjacent areas. Pore Scale Lattice Boltzmann simulations are used in computational fluid dynamics applications to simulate the boiling phenomena in nuclear reactors (see section 2.5.1), multiphase fluid flow in desalination membranes (see section 2.5.2) and pharmaceutical applications (see section 2.5.4).

1.6 Environmental impact of conventional waste disposal, secondary raw material recycling and fundamental aspects of mineral reactivity

PSI/LES and the Institute for Geological Science at the University of Bern (UBERN/IfG) have a long standing collaboration in the field of environmental mineralogy and applied geochemical engineering. The research of the Mineralogy Group at the University of Bern covers fundamental and applied aspects of mineral dissolution and precipitation, chemical factors of crystal structure stability and temperature driven phase transitions in minerals. The dedicated laboratories operated by the mineralogy group are equipped with powder and single crystal diffractometers for structural studies of minerals, and with an atomic force microscope for *in situ* characterisation of mineral surfaces. The experimental studies are widely supported by modelling activities.

The Competence Centre for Secondary Raw Materials (CCSRM, Project Leader Dr. U. Eggenberger) is embedded in the Mineralogy group and conducts applied research in the field of environmental geochemistry and secondary raw materials. The core competences of the CCSRM cover the topics of circular economy and disposal quality of conventional non-radioactive waste materials. Geochemical aspects and challenges related to the *in situ* conditions in conventional and radioactive waste disposal rely on common scientific backgrounds and modelling tools. Shared expert knowledge provides the fruitful basis for collaboration and mutual synergies between LES/PSI and CCSRM/UBERN. Recently, CCSRM has established a collaboration project with the Wyss Academy for Nature (www.wyssacademy.unibe.ch) on the topic of circular economy.

Approximately six million tons of solid municipal waste are incinerated annually in Switzerland. Nearly half of the incinerated residuals is disposed of in landfill sites. These residuals are composed of boiler- and electrostatic precipitator ashes and show significant concentrations of heavy metals (e.g. Zn, Cu, Cd, Pb, Sb). From the year 2026 onwards, heavy metal recovery has to be conducted before landfill disposal. Acid leaching represents the state-of-the-art method for heavy metal recovery prior to deposition. However, it has not yet been legally determined, whether the obligation for treatment also applies to the boiler ash. The available data to boiler ashes are very limited, thus their metal recovery potential has not yet been explored. Using a broad combination of methods (XRF, XRD, SEM), the ashes from six Swiss waste incineration plants were characterised with respect to the chemical and mineralogical composition of major- and minor phases. Key parameters to estimate the recovery potential are the contents of recoverable heavy metals and the extractability of the ashes. The obtained results provide important insights into the formation of the different ash fractions and their geochemical characteristics (see section 8.2).

Cement manufacturers are looking for new raw materials for clinker production. Conventionally used raw materials such as limestone is becoming less attractive due to the high CO_2 emissions arising from calcination reactions and land use conflicts often related to open-pit mines. Currently used supplementary cementitious materials such as coal fly ash were previously thought to be environmentally friendly alternatives, but they are expected to become unavailable in Europe since their production is, again, often related to high-carbon-emission. Bottom ashes from fluidised bed boilers are especially attractive to the cement industry. Potential for the use of bottom ashes from fluidised bed boilers has been investigated

in laboratory as a preparatory step for industrial scale applications (see section 8.3).

Swiss waste disposal ordinance defines an aftercare period of 50 years for the monitoring of the landfill sites. The time horizon of landfill aftercare reflects only a small part of its life cycle and is not based on scientific studies. Therefore, reliable predictions for future behaviour of Type D landfills are challenging. To close the knowledge gap, the dynamics of pollutants leaching from landfills is investigated in detail based on laboratory and field investigations (see section 8.4).

Heavy-metal-exchanged zeolites are attractive materials that find applications in several research fields, from environmental remediation to catalysis. Pb-exchanged zeolites have received special attention because of their importance in environmental related problems (i.e. removal of Pb from wastewater and food) and their use in industrial processes. The crystal structure of a natural zeolite, stellerite, fully exchanged with Pb, was investigated by Single Crystal X-ray Diffraction, Molecular Dynamics simulations and X-ray Absorption Spectroscopy to determine eventual structural changes induced by the lead uptake and determine the lead speciation (see section 7.3).

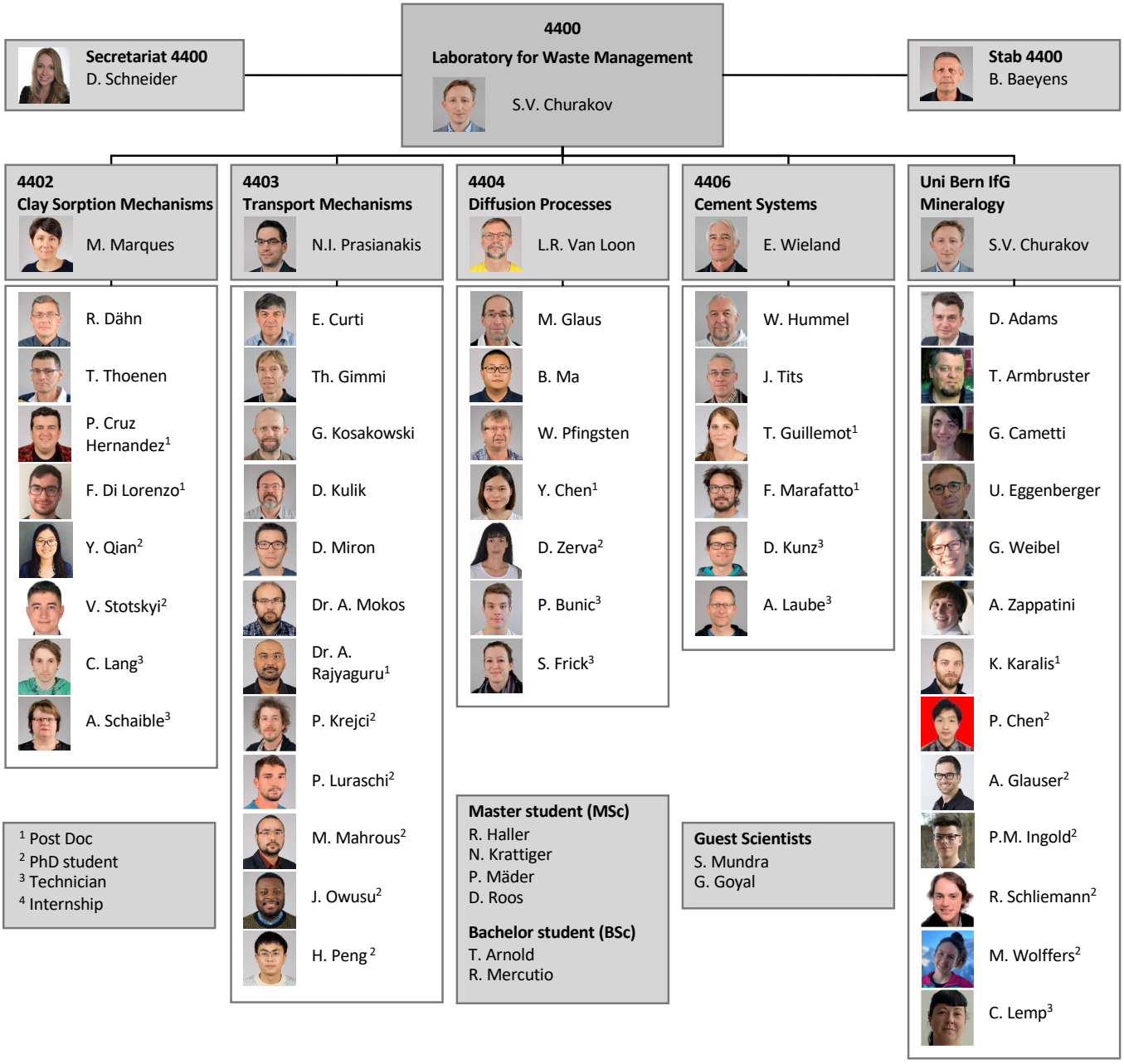

Fig. 1.1: Organisational chart of LES.

2 GEOCHEMICAL EVOLUTION OF REPOSITORY SYSTEMS

Prasianakis N.I., Churakov S.V., Curti E., Gimmi T., Pfingsten W., Kulik D.A., Miron G.D., Mokos A., Rajyaguru A. (postdoc), Damiani L.H. (PhD student), Luraschi P.(PhD student), Mahrous M. (PhD student), Peng H. (PhD student), Haller R. (MSc student), G. Goyal (internship)

2.1 Introduction

This project aims at developing cross scale THMC-numerical models and simulation tools for describing the long-term evolution of the multi-barrier repository system and geotechnical engineering. This expertise is essential for the safety assessment and cross comparison of various repository designs as a part of the site selection process in the Sectoral Plan for Deep Geological Disposal (SGT) Stage 3, and the following general license application. Geotechnical engineering is a steadily growing research field aiming at optimization of the subsurface reservoirs properties, for geothermal energy production and for resource exploration.

The project is focusing on three main topics: 1) Experimental characterisation and numerical modelling of the evolution of the technical barriers and their respective interfaces e.g. cement evolution and cement-clay interaction; 2) Fundamental understanding of reactive transport mechanisms including sorption through multiscale modelling and upscaling techniques; 3) The benchmarking and application of state-of-the-art coupled codes as well as the development and coupling of thermodynamic modelling and database tools. Overarching thematic contributions and modelling support is provided in the area of contaminants retention and transport in host rock, heterogeneities, uncertainties and diffusion in disperse and compacted systems.

In the area of repository design and the temporal evolution of the repository *in situ* conditions, the study of the evolution of cement-clay interfaces, has been finalized. Within the Nagra supported PhD project: "*Evolution of transport properties, mineralogy, and porosity of cement-clay interfaces*" (P. Luraschi), the interaction between various cement types and Opalinus Clay (OPA) was investigated using several analytical methods. Diffusion coefficients through the interfaces have been measured in the lab.

Within the SNSF PhD project "*Resolving dissolution-precipitation processes in porous media: Pore-scale Lattice Boltzmann modelling combined with synchrotron based X-Ray characterisation*" (M. Mahrous), and the EU project Eurad WP4-DONUT funding from the European Union's Horizon 2020 research and innovation programme under grant agreement no. 847593, the pore-level reactive transport modelling capabilities have been enhanced using machine learning techniques and more specific artificial neural networks (ANN). Chemical calculations were accelerated by four orders of magnitude by replacing the native geochemical solver with an ANN based surrogate model without loss in accuracy. The efficiency and accuracy were demonstrated after implementing the ANN technique in the digital twin of a microfluidic lab-on-a-chip experiment conducted at FZ-Jülich. The overall calculations were significantly accelerated and the oscillatory zoning mechanism has been investigated.

GEM Software (GEMS, lead scientist D.A. Kulik) development has been continued, and a transformation towards web-based microservices has been advanced. To cover the needs of a dedicated tool, easy to learn and to use for students or non-chemists working on cements, and with little to no maintenance efforts, the CemGEMS (https://cemgems.app) web application was developed within a project funded by NANOCEM. CemGEMS web application can potentially model cement leaching, degradation and salt attacks, it can be used with benefits in (radioactive) waste management studies in addition to applications in cement research and industrial engineering.

CROSS project *"In situ 4D micro X-ray chemical imaging and a digital twin of miniaturized counter-diffusion experiments: co-precipitation of metals with carbonates in porous media"* has been initiated in 2021 (PI: N.I. Prasianakis, A. Rajyaguru, experimental techniques and MSc H. Peng, PhD candidate on numerical modelling). The overarching research goal of the project is elucidate the role of trace metals (Ni, Zn, Pb) in polymorph selection and growth kinetics of calcium carbonate in porous media (silica gel, mineral powders). Machine learning is a core technology for enabling the development of the digital twin technology for the crystallisation experiments.

GeoML: Computer vision for classification of geological core samples has been investigated within the Internship of Ms. G. Goyal.

Several projects on multiscale multiphysics computational fluid dynamics are currently on-going, based on the advanced modelling capabilities that exist at LES. In the realms of a collaborative project with the Laboratory for scientific computing and modelling at PSI (LSM-PSI) and under the umbrella of Swissnuclear funding agency through the project "*Numerical prediction of boiling crisis considering surface characteristics*" (A. Mokos), the fundamental understanding of boiling processes from atomistic to reactor scale is pursued. Also, an industrial research project with the pharmaceutical company "*GlaxoSmithKline*" has been continued in 2021.

2.2 *In situ* conditions in repository near field

2.2.1 Interactions at cement-clay interfaces

The experimental cell developed in previous projects was used to investigate the interaction between various combinations of cement and clay types, by means of through-diffusion experiments and X-ray and neutron measurements (Luraschi et al., in prep.). The studied materials comprise a hardened, high porosity Ordinary Portland Cement (OPC) paste, ESDRED mortar (ESD, drilled out from samples from the CI experiment at the Mont Terri rock laboratory far from any material interface), Opalinus Clay (OPA, also from a drill core from the CI experiment at Mont Terri) and bentonite. The samples were connected to a reservoir filled with the corresponding pore waters on each side, and diffusion experiments with HTO as tracer were performed. After the experiments, the samples were characterised by SEM/EDS, X-ray tomography, and thermogravimetry (TGA). Fig. 2.1 presents the results of the diffusion experiments. For all samples, a clear decrease of the effective diffusion coefficient (D_e) during the reaction time of ~25 months was observed. In general, samples with bentonite as clay component display a higher reactivity (faster/stronger decrease of the diffusion coefficient) than those with Opalinus Clay. For bentonite-OPC samples, D_e, HTO decreased by ~58% in two years with respect to the initial unaltered sample (Fig. 2.1a), while for OPA-OPC samples, D_e, HTO decreased only by ~41% with respect to the initial calculated value in the same time. Similarly, for bentonite-ESD samples, a decrease by ~56% was observed after two years, while for ESD-OPA samples, D_e, HTO decreased by only ~36% during this time.

The results for the bentonite-OPC samples are very similar to previously obtained results for montmorillonite-OPC samples, as expected. The ESDRED cement mortar has a lower porosity and therefore a lower diffusion coefficient compared to the OPC. Therefore, the initial D_e, HTO of unaltered samples is lower for ESDRED-clay samples compared to OPC-clay samples. The slightly lower reactivity of ESDRED compared to OPC is probably related to the lower initial pH of this material compared to OPC, but it may also be related to its lower diffusion coefficient, leading to slower mass transfer across the interface.

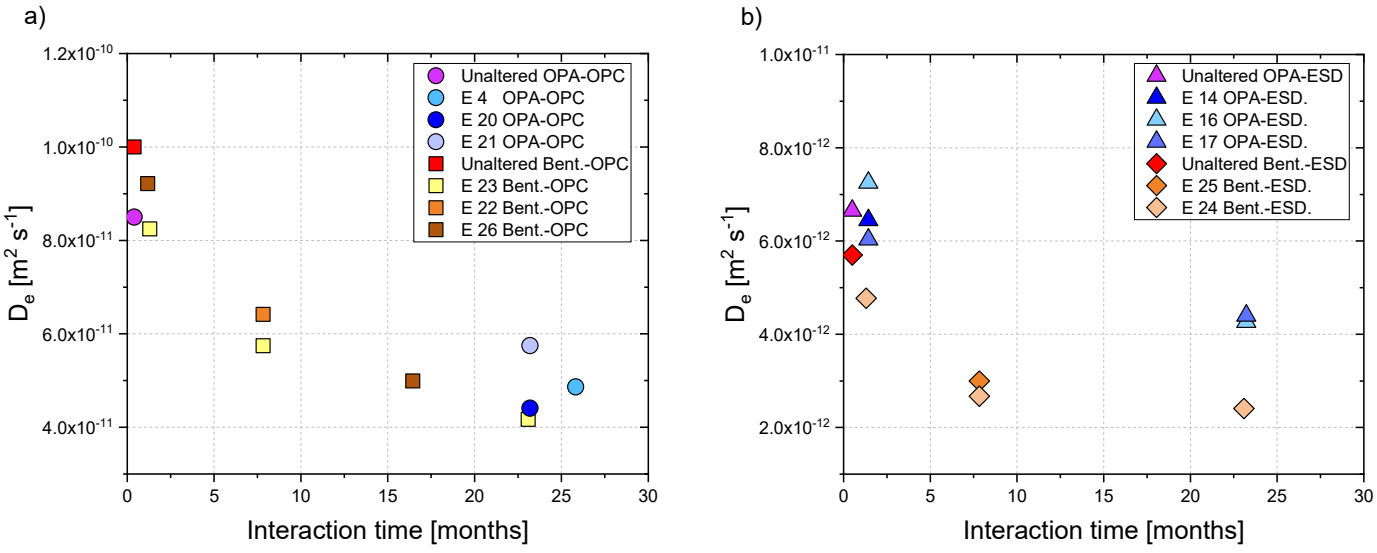

Fig. 2.1: Evolution of the effective diffusion coefficient D_e of HTO for (a) OPC paste in contact with bentonite or OPA; and (b) ESDRED mortar from a Mont Terri experiment in contact with bentonite or OPA, for various samples. Purple and red symbols represent calculated values for completely unreacted interfaces. For these calculations, the following values where considered: OPA De, HTO = 5 × 10^{-11} (Bossart et al. 2017), bentonite De, HTO = 6.1 × 10^{-11} (Na-montm. value after Luraschi et al. 2020), OPC paste D_e, HTO = 2.8 × 10^{-10} (Tits et al. 2003), ESDRED D_e, HTO = ~3.6 × 10^{-12} (estimated from data of a diffusion experiment).

2.2.2 Modelling of Bentonite Pore Water (BPW) compositions for safety assessment

On behalf of Nagra, LES is committed to provide basic data for the safety assessment of the Sectoral Plan for Deep Geological Repositories (Stage 3). The definition of composition and characteristics of pore waters in equilibrium with compacted bentonite (the backfilling material of the repository tunnels) is a key dataset to be supplied, as it is the basis to determine solubility limits and sorption coefficients of dose-relevant nuclides.

A model was developed and tested (Curti 2021), based on the long-standing 2SPNE SC/CE sorption model (Bradbury & Baeyens 1997) recently implemented in GEM-Selektor (Kulik et al. 2018). The model includes cation exchange equilibria with montmorillonite and surface protonation/deprotonation on three distinct sites, as well as dissolution/precipitation reactions with minor reactive solids detected in MX-80 bentonite samples. Redox conditions are controlled by iron minerals.

The operational components of the BPW model are shown in the flow diagram of Fig. 2.2. The starting point are chemical analyses of Opalinus Clay aqueous extracts obtained during Nagra's borehole campaign for SGT-3, supplied by Bern university's rock-water interaction group. After small adjustments and application of different aqueous activity models, eight slightly different Opalinus Clay water (OPAw) compositions, saturated with celestine, gypsum and calcite were obtained, all at equilibrium with the same CO_2 partial pressure. The tested activity models were Truesdell-Jones (TD), five variants of Debye-Hückel (DH-), Davies and the Specific Ion interaction Theory (SIT). The OPAw obtained from the SIT activity model was preferred and selected for the further development of the BPW model. The calculations assume specific initial Solid/Water (S/W) ratio and anion porosity (ε_{an}) reflecting the degree of bentonite compaction and ionic strength of the pore water, respectively. In addition, equilibrium with a pre-defined *in situ* pCO_2 is assumed. Finally, experimental information on the initial state of the bentonite is considered (populations of exchangeable cations, speciation of surface hydroxyl groups and inventories of minor minerals). The result is an equilibrium system consisting of bentonite pore water (BPW), a final exchanged ion population, a distribution of protonated and deprotonated surface sites and an assemblage of minor solids at equilibrium.

Test calculations based on provisional pore water data from the Bülach borehole were carried out for three representative degrees of bentonite compaction (1300, 1450 and 1600 kg m^{-3}), leading to anion porosities between 11% and 24%. Thermodynamic equilibria

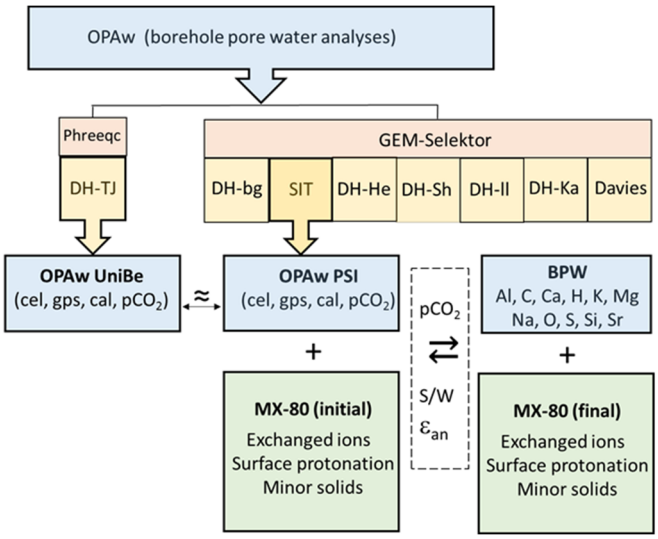

Fig. 2.2: Flow chart for development of Bentonite Pore Water model.

were calculated for water volumes corresponding to the maximum anion porosity at each degree of compaction, i.e. including the volume assigned to the diffuse double layer (DDL). This choice was made because the 2SPNE SC/CE sorption model is non-electrostatic and thus does not specify the DDL explicitly. Fig. 2.3 shows the calculated volumetric partitioning of solids, interlayer, and free water (anion porosity + DDL) for a dry bulk density of 1450 kg m^{-3}. The results of the corresponding calculation are shown in Table 2.1.

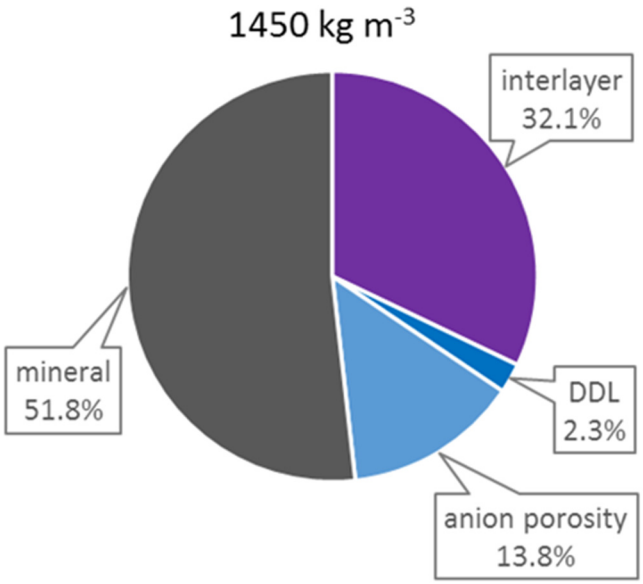

Fig. 2.3: Volumetric distribution of water and solids in compacted bentonite at 1450 kg m^{-3} dry bulk density.

Tab. 2.1: Results of BPW calculations for 1450 kg m^{-3} dry bulk density and a fixed pCO_2 of $10^{-2.83}$ bar.

	Initial state (ACW3a / MX-80)	Final state (BPW / MX-80)	Difference (Final – Initial)
T [°C]	25	25	0
p(tot) [bar]	1	1	0
log (pCO_2 [bar])	*-2.83*	-2.83	0
pH	7.28	7.41	0.13
Eh [V]	-0.204	-0.180	0.024
IS [mol/kgw]	0.510	0.586	0.076
MX-80 bentonite	*(mol)*	*(mol)*	
BaZ_2	5.00E-04	1.41E-07	-5.00E-04
CaZ_2	3.30E-02	3.42E-02	1.20E-03
KZ	1.30E-02	1.29E-02	-6.08E-05
MgZ_2	2.00E-02	1.99E-02	-1.05E-04
NaZ	6.68E-01	6.70E-01	2.33E-03
SrZ_2	2.00E-03	3.06E-04	-1.69E-03
Z^-(tot)	7.92E-01	7.92E-01	0
$=S^sOH_2^+$	2.10E-07	1.40E-06	1.19E-06
$=S^sOH$	6.50E-04	1.13E-03	4.83E-04
$=S^sO^-$	8.50E-04	3.66E-04	-4.84E-04
$=S^{w1}OH_2^+$	4.20E-06	2.79E-05	2.37E-05
$=S^{w1}OH$	1.30E-02	2.27E-02	9.66E-03
$=S^{w1}O^-$	1.70E-02	7.32E-03	-9.68E-03
$=S^{w2}OH_2^+$	9.40E-05	1.14E-03	1.04E-03
$=S^{w2}OH$	3.00E-02	2.92E-02	-7.69E-04
$=S^{w2}O^-$	3.00E-04	2.37E-05	-2.76E-04
=SOH(tot)	4.38E-02	5.54E-02	1.15E-02
Aqueous solution	(molality)	(molality)	
Al	---	1.67E-08	1.57E-08
Ba	---	1.47E-07	1.46E-07
C (inorganic)	8.42E-04	1.10E-03	2.62E-04
Ca	3.95E-02	2.77E-02	-1.18E-02
Cl	4.06E-01	4.04E-01	-1.34E-03
Fe	1.12E-12	1.25E-05	1.25E-05
K	1.93E-03	2.46E-03	5.35E-04
Mg	1.78E-02	1.87E-02	8.72E-04
Na*	5.04E-01	4.83E-01	-2.12E-01
S	2.84E-02	5.79E-02	2.96E-02
Si	---	1.78E-04	1.78E-04
Sr	3.13E-04	2.41E-04	-7.16E-05
Net charge (eq)	1.81E-02	6.53E-03	-1.15E-02
Gas	*(mol)*	*(mol)*	
CO_2	0.00E+00	7.24E-02	7.24E-02
CH_4	0.00E+00	8.77E-14	8.77E-14
H_2	0.00E+00	9.60E-08	9.60E-08
N_2	0.00E+00	4.85E+01	4.85E+01
O_2	0.00E+00	0.00E+00	0.00E+00
H_2S	0.00E+00	3.39E-09	3.39E-09
Solids	*Initial (mol)*	*Equilibrium (mol)*	
Baryte	1.00E-12	5.00E-04	5.00E-04
Calcite	3.00E-01	3.14E-01	1.36E-02
Pyrite	5.00E-01	5.04E-01	3.91E-03
Celestine	1.00E-12	1.70E-03	1.70E-03
Kaolinite	3.90E-02	3.90E-02	-1.00E-09
Gypsum	2.35E-02	1.01E-02	-1.34E-02
Siderite	8.60E-02	0.00E+00	-8.60E-02
Magnetite	4.30E-01	4.57E-01	2.74E-02
Quartz	1.66E+00	1.66E+00	-2.03E-05

*Na concentration includes Na^+ initially adsorbed on the (negatively charged) clay surface.

2.3 Fundamental understanding of reactive transport and sorption mechanisms

2.3.1 Digital Twin of counter diffusion experiments

The CROSS project *"In situ 4D micro X-ray chemical imaging and a digital twin of miniaturized counter-diffusion experiments: co-precipitation of metals with carbonates in porous media"* has been initiated in 2021 (PI: N.I. Prasianakis, Dr. A. Rajyaguru, experimental techniques, and MSc H. Peng, PhD candidate on numerical modelling). The overarching research goal of the project is elucidate the role of trace metals concentrations (Ni, Zn, Pb), radionuclides and other toxic contaminants, in the polymorph selection and growth kinetics of calcium carbonate porous media (silica gel, mineral powders). In the next step, the planned experiments and modelling will shed the light on the effect of precipitation processes on the transport properties of the porous medium itself. LES will develop a digital twin of the transport and crystallisation phenomena based on the pore-scale coupling chemical-physical processes (diffusion, precipitation, pore space evolution), aiming at reproducing the microscopic phenomena observed in the experiments. Machine-learning algorithms for the on-line classification of crystal morphologies (trained on the initial experimental results) will play a central role in supporting the rapid assessment of experimental observations. Neural networks will be used to accelerate the computationally expensive numerical solvers required to model the experiments. The project will provide a new cross-disciplinary methodology paradigm for investigating and understanding reactive transport phenomena at an unprecedented level of details, specifically the effects of kinetically-driven crystallization processes. In Figure 2.4 a schematic of the process of applying deep reinforcement learning to the classification of reaction products is shown. It is expected that this methodology will be applicable to many disciplines, including energy and environmental research, degradation of construction materials, and biomedical research (e.g. bone tissue).

2.3.2 Model developments in Eurad WP-DONUT: GeoML Benchmark

Thanks to the recent progress of technology, the fields of artificial intelligence (AI) and machine learning methods (ML) are growing at a very fast pace. The Eurad (European Joint Programme on Radioactive Waste Management) community has recently started using ML for a) accelerating numerical simulations, b) improving the efficiency of multiscale and multiphysics couplings, c) uncertainty quantification and sensitivity analysis. A number of case studies indicate that overall acceleration of geochemical and reactive transport calculations, between one to four orders of magnitude (Laloy et al. 2019, Prasianakis et al. 2020). The observed speed up depends on the chemical system, simulation code, application and problem formulation. Within Eurad-DONUT (Development and Improvement Of Numerical methods and Tools for modelling coupled processes) a benchmark is currently designed to test a variety of ML techniques relevant to geochemical and reactive transport simulations in the framework of radioactive waste disposal, aiming at providing basic guidelines about the benefits and limitations of using ML techniques (Lead: N.I. Prasianakis). More specifically, the benchmark aims at providing a point of reference

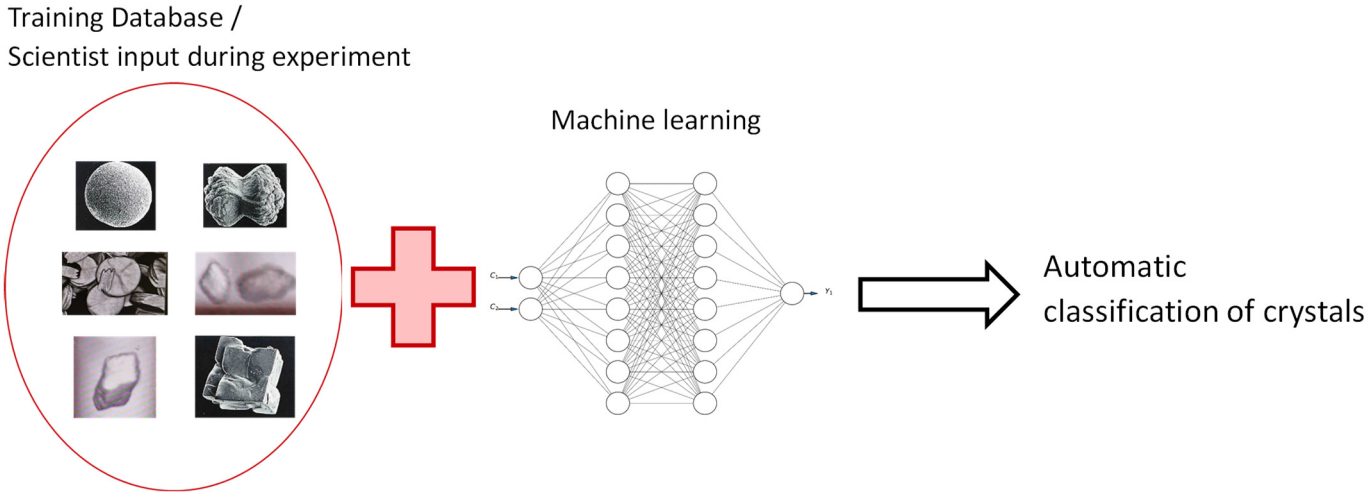

Fig. 2.4: Machine learning algorithms are trained on the available multi-dimensional data of the characterisation techniques. This provide real-time input to the experimentalist and to the digital twin of the experiment. Ultimately, it will be possible to predict crystal shapes and kinetic rates based on the local thermodynamic conditions.

for testing codes and models and for addressing the challenges relevant to:

(i) producing high quality training datasets, which will be usable by all available ML techniques,

(ii) using deep learning neural network, polynomial chaos expansion and Gaussian processes to learn from the generated data,

(iii) testing the accuracy of predictions for geochemical calculations, reactive transport simulations, and uncertainty analysis.

Joint efforts of BRGM, ISTO (CNRS/INSU-BRGM), SCK-CEN, NRG, ENRESA (UDC), UFZ, and PSI resulted in the definition of computational benchmarks relevant for the nuclear waste management. Three major geochemical solvers PHREEQC, ORCHESTRA and GEMS, are applied to model the chemical systems of interest.

2.3.3 Computer Vision and Machine learning from experimental observations

Within the Internship project of Ms. G. Goyal, computer vision techniques and machine learning have been used to analyse experimental observations and datasets. In a first step, crystal detection and determination of the region of interest has been successfully programmed and applied on the video feed of microfluidic crystallization experiments. In a second on-going step, material characterisation is enabled by combining computer vision and mineralogical information.

2.3.4 A Bridging Experimental-Modelling Approach Towards Mechanistic Understanding of Minerals Co-precipitation

Minerals co-precipitation is one of the main mechanisms of demobilizing safety relevant radionuclides in nuclear waste repositories. However, understanding mineral co-precipitation phenomena in porous media is challenging due to the complexity of the processes involved, which incorporate nucleation, crystallization, solute species transport, homogeneous and heterogeneous chemical reactions. Often the equilibrium thermodynamic approach to describe minerals co-precipitation fails to quantify the solid solution composition in a time-evolving system, especially if it is reaction limited. Inclusion of reaction kinetics is needed to obtain a better understanding of the solid solution formation and the evolution of its composition with time. This is a difficult task, as it requires dedicated experiments, advanced characterisation tools, and state-of-the-art modelling.

In 2021, the members of the transport mechanisms group (LES) in collaboration with the Institute of Energy and Climate Research (IEK-6), Forschungszentrum Jülich, Germany addressed this topic using a combined experimental-theoretical-modelling approach. The experiments are a set of

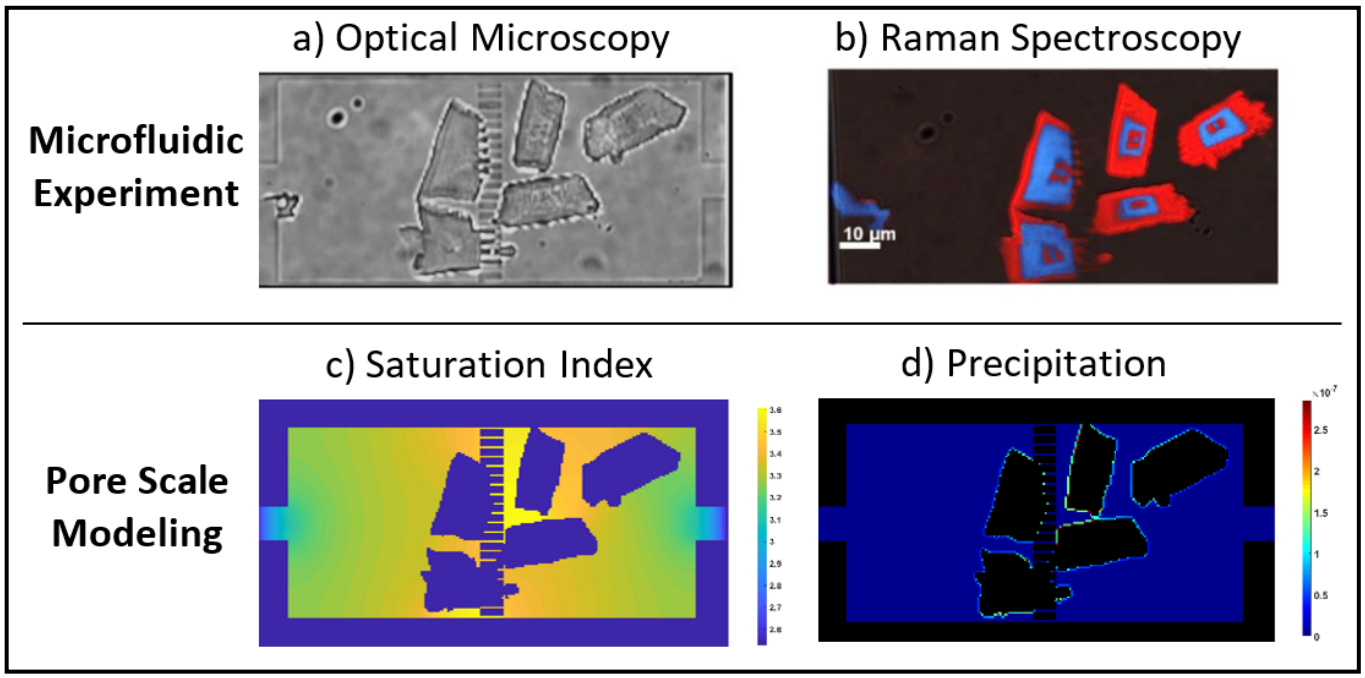

Fig. 2.5: Scheme of the experimental-modelling approach: (a) microfluidic chamber after 360 minutes using optical microscopy. (b) color coded composition of the precipitated $Ba_xSr_{1-x}SO_4$ solid solution using in-operando Raman spectroscopy (red and blue regions indicate high Sr and Ba mole fractions, respectively). (c) saturation index calculation for $(Ba_{0.5}Sr_{0.5})SO_4$ solid solution using pore scale modelling. (d) the precipitated $(Ba_{0.5}Sr_{0.5})SO_4$ represented as percentage of the pixel volume, computed from the pore scale simulations (Poonoosamy et. al. 2021).

counter-diffusion experiments in a microfluidic chamber, in which barium and strontium ions co-precipitate from a supersaturated sulphate-rich solution to form concentric layers of Sr and Ba enriched $Ba_xSr_{1-x}SO_4$ solid solution via oscillatory zoning. During the experiment, the formed solid solution was monitored using optical microscopy and its composition identified using Raman spectroscopy. The experiments were then modelled numerically to give further insights into the system spatiotemporal evolution.

The modelling was done on macroscopic as well as on a pore scale level using a passive scalar approach. Solute species transport was modelled via the Lattice Boltzmann Method (LBM). The transport step was coupled to chemical reactions using a Sequential Non-Iterative Approach (SNIA). Aqueous homogeneous reactions were assumed to be at instantaneous equilibrium using full speciation calculations, while heterogeneous precipitation reactions were kinetically constrained. Nucleation is accounted for using the Classical Nucleation Theory (CNT), while crystal growth is modelled using a discrete composition approach. The applied experimental-modelling methodology is capable of describing, as a function of time and location at high spatial resolution (micrometer scale), a number of observables, including the spatial distributions of each aqueous species, saturation indices, solid solution compositions, the nucleation induction times, showing the interplay between transport and reaction kinetics. Results were presented in the 7th International Workshop on Crystallization in Porous Media (CRYSPOM VII) (M. Mahrous), and published in (Poonoosamy et. al. 2021). The applied experimental-modelling will bring us one step closer towards a better mechanistic understanding of minerals co-precipitation and its role in the deep geological nuclear waste repositories.

2.4 Thermodynamic modelling of cement hydration: NANOCEM CemGEMS project

CemGEMS (https://cemgems.app) is a no-code web application for cement chemists, students and researchers, aimed at facilitating the thermodynamic modelling of cement hydration processes, visualization and tabulation of results. In the back-end, the web app runs the GEMS3K code (Kulik et al. 2013, Wagner et al. 2012) with a pre-configured chemical system file using the Cemdata18 (Lothenbach et al. 2019, https://www.empa.ch/cemdata) and the PSI/Nagra GEMS chemical thermodynamic databases.
CemGEMS has been developed for the Nanocem consortium (https://nanocem.org) since summer 2018 at LES (Kulik et al., 2021) and Congineer GmbH in collaboration with Empa, EPFL, HTC and other organizations. The web-application was launched online in 2020 (see LES progress report 2020). The present section contains a progress update for one year since then, in a partial fulfillment of the goals of Nanocem P06 Internal Project for extension of CemGEMS web application.

The commonly used modified Parrot and Killoh (mP&K) model (Lothenbach et al. 2008), also implemented in CemGEMS, describes the general progress of the clinker reaction after one day and longer

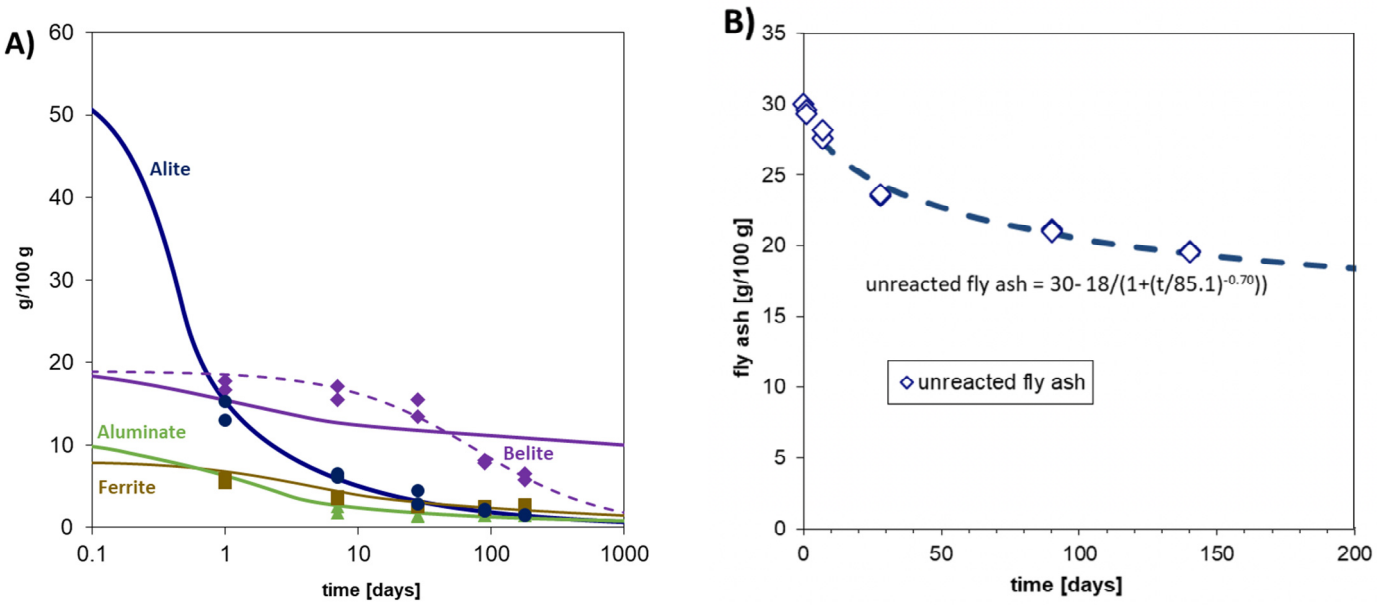

Fig. 2.6: (A) measured (symbols) and modelled (mP&K model: solid lines; 4PL fit: dashed line) clinker reaction in Portland cement as a function of time. (B) measured (symbols) and modelled (curve) fly ash reaction in a blend containing Portland cement, fly ash and limestone using the 4PL fit (from Kulik et al. 2021, Fig. 4).

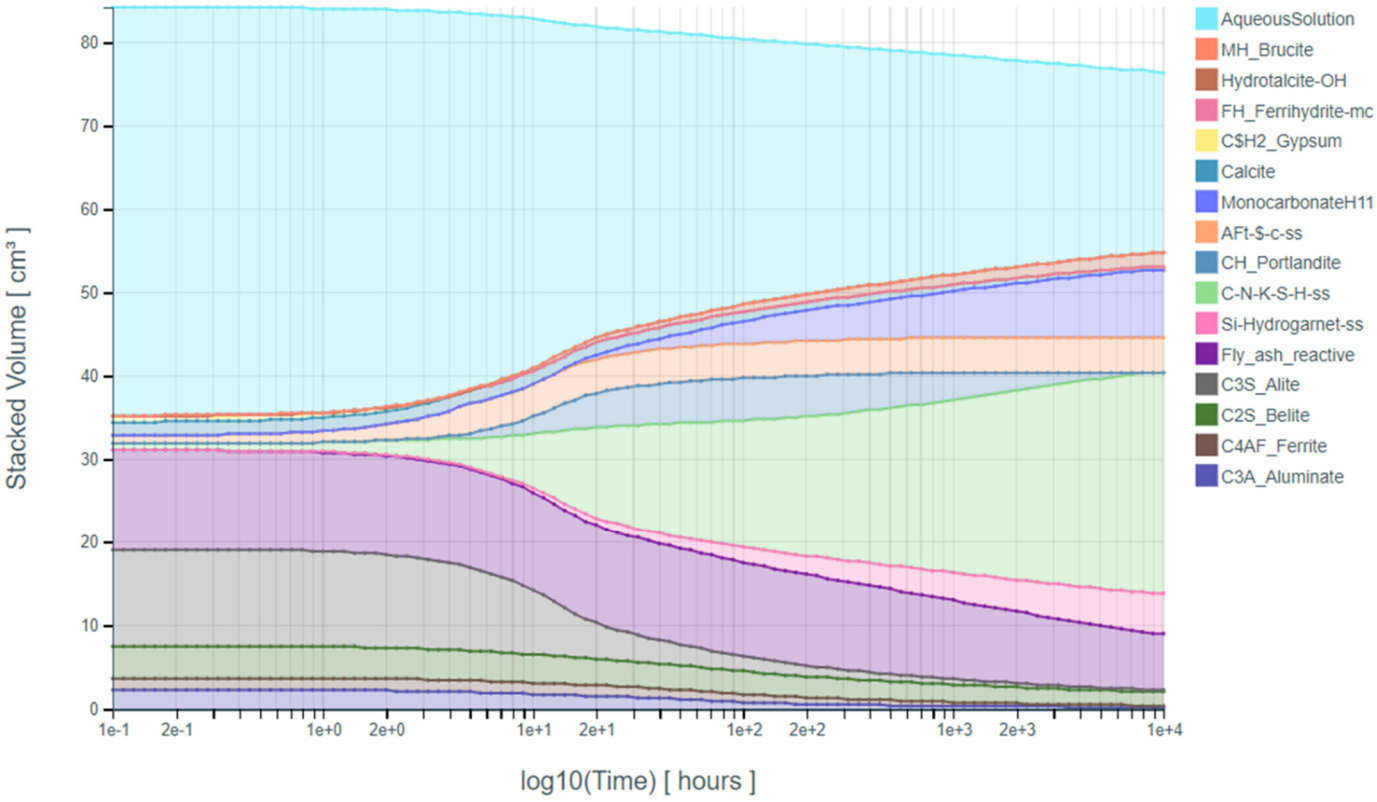

Fig. 2.7: Thermodynamic modelling of phase volumes in cm³ per 100 g of anhydrous binder as a function of time, for fly-ash blended cement composition, mP&K and 4PL parameters from (De Weerdt et al. 2011) (see Fig. 1) at water/binder ratio of 0.5 and temperature of 20°C. To obtain such diagram in CemGEMS, create a new recipe of "CEM-II-BV" cement type and "min" data type, then create a new process of "Hydration-MPK" process type with "Time-log" lead, and simulate the process. From (Kulik et al. 2021, see Fig. 6).

in Portland cements (PCs) relatively well (Figure 2.6A). However, this model does not capture very early hydration reactions during the first hours, or the reaction of supplementary cementitious materials (SCM) such as coal fly ash. In such cases, other models directly fitted against the time-resolved QXRD data should be used instead or along with the mP&K model. The so-called 4PL or 5PL logistic fits, often used for this purpose, were implemented in CemGEMS.

The empirical non-linear regression equation known as the four-parameter logistic (4PL) fit is a special case of the more general five-parameter logistic (5PL) equation (Gottschalk & Dunn 2005) when $g = 1$:

$$rx = d + \frac{(a-d)}{\left(1+\left(t/c\right)^{b}\right)^{g}} \quad (1)$$

where *rx* is the reaction extent in percent, *t* is the hydration time in days, *a* is the asymptote minimum *rx* value (usually 0), *d* is the asymptote maximum *rx* value (<=100%), *b* is the maximum steepness ($b > 0$ for reaction extent, $b < 0$ for the fraction of unreacted solid), *c* is the (time) position of the inflection point, and *g* is the asymmetry (1 by default). This simple logistic fit describes well the hydration of calcium sulfoaluminate cements, of SCMs (see Figure 2.6B for the case of fly ash), and also of clinker phases (exemplified in Figure 2.6A for belite).

Although the mP&K model can be used as such to predict Portland cement hydration (with some minor parameter refitting), 4PL or 5PL fit parameters always need first to be adjusted against the measured reaction data (e.g. by QXRD). More about the CemGEMS functionality regarding mP&K and 5PL models can be found in (Kulik et al. 2021); both the mP&K and the 5PL fits for different clinker constituents and SCMs can be used simultaneously, as in a run on Fig. 2.7, based on kinetics shown in Fig. 2.6.

Estimation of heat effects of cement hydration has been implemented in CemGEMS in a simplified form for *(i)* isothermal and *(a)* adiabatic edge cases. This was possible because the GEMS thermodynamic database provides the data on the standard enthalpy H^{o}_{T} and heat capacity Cp^{o}_{T} for all substances. *(i)* The heat generated at each step *s* of a hydration process at isothermal

conditions can be calculated from the masses and specific (per unit mass) enthalpies H^o_T; *(a)* The adiabatic temperature change (i.e. at no heat exchange with the environment) can be estimated from masses, the heat generated at step s, and the specific heat capacities Cp^o_T of all involved substances (equilibrated or residual).

Isothermal case: The heat generation rate $rQ(t)$ at T = const at step s is found after computing (by GEMS) the total enthalpy H_{eq} and the total heat capacity Cp_{eq} of the equilibrated part, and calculating the respective totals for the residual part H_{re} and Cp_{re}. The total for the whole recipe: $H_{s,T} = H_{eq,s} + H_{re,s}$

The isothermal heat effect at step s: $cQ_{s,T} = H_{s,T} - H_{(s-1),T}$. The isothermal *heat rate* at time t and time step length Δt: $rQ_{t,T} = \left(H_{(t+\Delta t),T} - H_{t,T}\right)/\Delta t$.

The accumulated heat production uQ_s until step s at constant T equals to $uQ_s = uQ_{s-1} + cQ_s$ or from time $t_0 = 0$ to time (step) t: $uQ_t = \sum_{t_0}^{t} rQ_t \Delta t$. Here, a stepwise partial dissolution of clinker minerals and SCMs constituents, and an instant formation of equilibrium hydrates are assumed.

Adiabatic case: The temperature change at step cT_s is approximated from the heat effect $cQ_{s,T}$:

$cT_s = \frac{cQ_{(s-1),T}}{cCp_{(s-1),T}}/\alpha_{s-1}$ where $\alpha_{s-1} = 1 + (aT_{s-1} - T_0)/\kappa$; $aT_{s-1} = aT_{s-2} + cT_{s-1}$; and $\kappa = 7.7$ is an empirical calibration constant. The temperature change rate at time t (step s) is then $rT_t = cT_s/\Delta t$.

The total temperature rise aT_s until step s and from start temperature T_0: $aT_s = aT_{s-1} + cT_s$ $(T_{s=1} = T_0)$

or from time $t_0 = 0$ to time (step) t: $aT_t = rT_t + aT_{t-\Delta t}$. Note that in the process, $dU \approx dH$; $dH = mCpdT$, where U is internal energy, H is enthalpy, Cp is heat capacity, m is mass of the system, and T is in Kelvin. Hence, upon the discretization, $T_{t+\Delta t}$ can be found from $mCp_t(T_{t+\Delta t} - T_t) = \Delta H_t = H_{t+\Delta t} - H_t$.

Fig. 2.8 left, shows both rate curves calculated in CemGEMS for Portland cement hydration process, and Fig. 2.8 right, shows both accumulated effect curves.

At present (January 2022), CemGEMS has > 350 registered users. The last release of online community variant https://cemgems.app is v.0.6.1 beta (19.02.2021), so far 100% uptime. The 1st hands-on training on zoom (>50 participants) took place on 19.02.2021 (as zoom videoconference), recorded and put on a YouTube channel "CemGEMS" created 23.02.2021. On-going work includes: improvements and preparation of the next release v.0.7; research and modification of GEMSW code to run in webassembly on the browser client (delayed due to issues with the Cheerp compiler used for xGEMS, GEMS3K and GEMSW compilation into WebAssembly). Changes in the front-end to use p2p communication instead of sending the user data to/from the back-end server database, pending until WebAssembly GEMSW is running along with the launch of CemGEMS v.1.0 and the user data-secure enterprise counterpart https://cemgems.com.

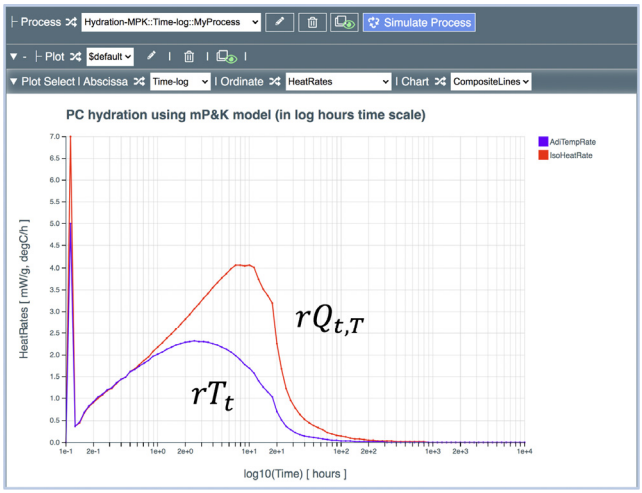

Fig. 2.8: Edge-case heat effects of the ordinary Portland cement hydration process simulated using the mP&K model, estimated and plotted in CemGEMS web app: (left) – rates of isothermal heat generation $rQ_{t,T}$ (mW/g) and of adiabatic temperature change rT_t (K/hour); (right) – total accumulated heat at isothermal conditions uQ_t and adiabatic temperature rise aT_t (in ^{o}C).

2.5 Multiscale Multiphysics computational fluid dynamics

2.5.1 Numerical prediction of boiling crisis considering surface characteristics

In collaboration with the Laboratory for Scientific Computing and Modelling at PSI (LSM-PSI) and under the umbrella of the project *"Numerical prediction of boiling crisis considering surface characteristics"* under the Swissnuclear funding agency an understanding of boiling processes on the surface of fuel rods within nuclear reactors from atomistic to reactor scale is pursued. The LES laboratory (A. Mokos, N.I. Prasianakis) focus on the mesoscopic scale aiming to provide parameter inputs to the macroscopic boiling code PSI-Boil, developed at LSM-PSI. To achieve this target, a LB algorithm was developed at LES, based on Yantra (Lead: Dr. R. Patel) to simulate boiling on rough surfaces where the density ratio between the two phases is ~20, as dictated by the conditions within the pressurized water reactor. The code has been applied in multiple test cases related to bubble generation and flow near a rough surface as shown in Figure 2.9. Additionally, computer-generated porous media have been algorithmically created to simulate the rough 3D micro-surface on a fuel rod.

2.5.2 Membrane Distillation: Multiphase flow within membranes

Under a collaborative project (A. Mokos) with the University of Luxembourg (T. Jager and Prof. S. Leyer), the in-house LB code was used to simulate multiphase flow within membranes used for distillation. The membrane material used here is Polytetrafluoroethylene (PTFE) with a pore diameter of about 200nm. In particular, the Shan and Chen multi-phase model is used to simulate multi-phase flow at pore level (Jäger et al. 2021). Fig. 10 shows the results for the membrane geometry (simulation of 0.6 billion voxels) and a subdomain; the field is initialized with a random density and is allowed to evolve, generating separate vapour and water phases until it reaches an equilibrium state. A new Python code was developed in order to allow visualization of the larger geometry.

2.5.3 Smoothed particle Hydrodynamics: Membrane Distillation: water sheet falling under gravity

In collaboration with Electricité de France (EDF), Laboratoire d'Hydraulique Saint-Venant (LHSV) at Ecole Nationale des Ponts et Chaussées and the company Nextflow Software, the simulation of a waterfall was finalized (Mokos et al. *in press*). In particular, this work uses the Smoothed Particle Hydrodynamics (SPH) meshless numerical method in order to investigate the behavior of a water sheet falling under gravity by reproducing the experimental results of a laboratory chute of 9.5m height (Bercovitz et al. 2016). This flow occurs typically over dam ogee-type spillways. The focus is on the trajectory and velocity of the water sheet as well as on the pressure upon impact on a plate. The SPH simulations using an adaptive particle refinement technique show good agreement with the experimental pressure results for all comparisons, while using air friction allows correct modelling of the falling velocity distribution as shown in Figure 2.11.

2.5.4 Research projects with GlaxoSmithKline Vaccines

In 2021, two industrial project with the pharmaceutical company GlaxoSmithKline Vaccines, Belgium (GSK) have been initiated (PI: N.I. Prasianakis). GSK is a science-led global healthcare company focused in the research, development and manufacturing of

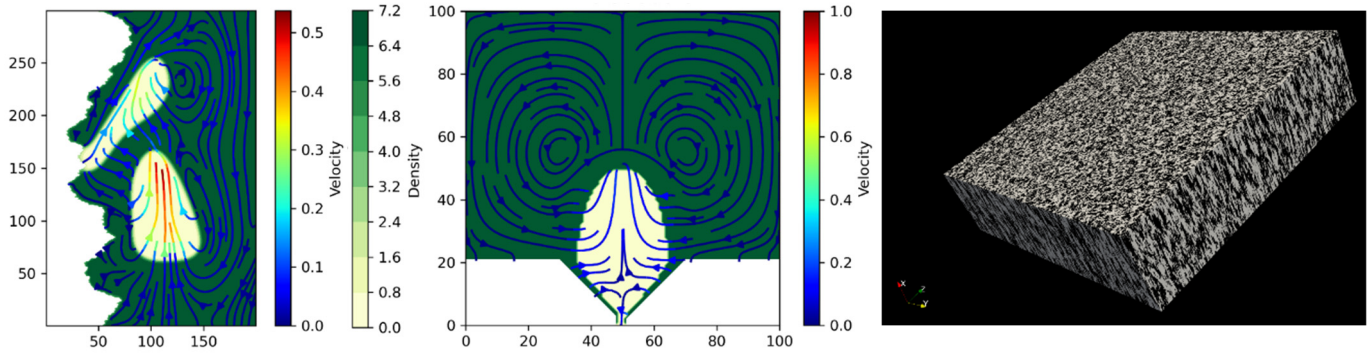

Fig. 2.9: (left) LB simulation of multiple bubbles interacting with a rough surface of ZrO_2 with a hydrophobic contact angle; (middle) LB simulation of bubble generation in an idealized surface in the presence of dent. (Yantra code); (right) a computer generated porous medium, discretized with 750×750×200 grid points with high porosity spatial correlation in the x-direction (for use with the in-house multiphase LB code).

innovative pharmaceutical medicines, vaccines and consumer healthcare products. Advancements in specific areas within the aforementioned domains can be based on advanced theoretical and numerical modelling. For this project, the state-of-the-art multiscale models and methods developed at LES are fully utilized.

2.6 Next generation of computational tools: online platforms and services GeoML.AI and GeoML.EU

The GeoMLplatform (.ai and .eu domains) has emerged due to the need to intensify and explore in a collaborative manner the impact of key enabling technologies: machine learning (ML) and artificial intelligence (AI), on multiscale multiphysics geochemical and material modelling. Moreover, it is an effort to make machine learning technologies more easily accessible to scientists-experimentalists and students without explicit computer science background. For that reason, a new online educational and dissemination platform GeoML with advanced functionality, user and demonstrator spaces has been deployed by the members of the transport mechanisms group in collaboration with Congineer GmbH (https://congineer.com) (PI: N.I. Prasianakis). The platform is available via https://geoml.ai/ and https://geoml.eu/ links with .ai being of general purpose, and .eu reserved for the European Union project-based collaborations (Fig. 2.11).

For collaboration projects and joint developments (within and outside LES), a fully functional JupyterLab server loaded with all necessary machine learning, reactive transport and geochemical modelling packages has been set up. Results can be presented in form of Jupyter notebooks or lab books, Python codes, data files, as well as publicly available interactive demonstrators and digital tools. Key advantage of GeoML is that the user can login and work via web browser from any device, without the need for special computer hardware or for the installation of multiple software packages, which sometimes are even incompatible or unavailable for specific operating systems.

Fig. 2.11: https://geoml.ai/ An online educational and dissemination platform with advanced functionality, user and demonstrator spaces.

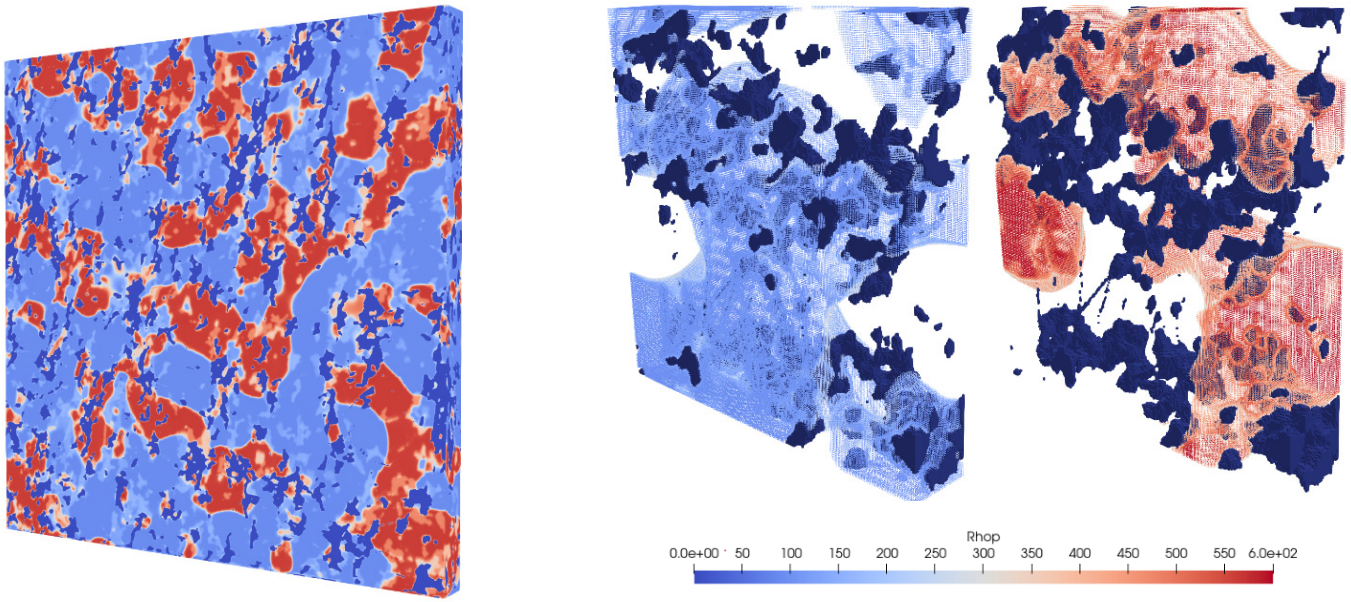

Fig. 2.10: (left) a slice (10%) of the membrane domain for the 0.6B voxel simulation showing the LB density of simulation. Higher density signifies higher water concentration. The membrane is shown in dark blue. (right) simulation of a subdomain (7M voxels) showing the areas dominated by liquid and gas.

First two interactive demonstrators are already online: a) Waste Package Digital Twin (G.D. Miron, D.A. Kulik, J. Tits) on https://geoml.eu; b) Neural Network accelerated reactive transport (L.H. Damiani, R. Haller, S.V. Churakov, N.I. Prasianakis) on https://geoml.ai.

2.6.1 GeoML.EU: Waste Package Digital Twin tool

In the context of the ongoing EURAD PREDIS project, the aim is to build a proof-of-concept Digital Twin that can be used in waste predisposal applications. The digital twin is developed as a friendly and accessible tool for assessing / predicting different waste package evolution scenarios. In its final form, the user will be able to run different geochemical and chemo-mechanical models for given waste package properties (input) to retrieve parameters (output) relevant for waste package integrity evolution as a function of time (Fig. 2.12). This allows to produce datasets of waste package evolution scenarios that combined with experimental observations, can be used to train fast surrogate multiphysics models. This will allow to efficiently test different compositions for potential problems of existing and future waste packages, and to perform uncertainty propagation, sensitivity analysis and waste package multi-objective optimization.

A demo prototype of the Digital Twin is operational on the GeoML platform (https://digitaltwin.geoml.eu/) (Fig. 2.13). As a running example, the user can select to run the "Cement Hydration" geochemical process and test the volume evolution of a waste package cement recipe during hydration (Fig. 2.14 top).

A second example is running a 2D cement carbonation scenario (Fig. 2.14 bottom) and assessing the evolution as a function of time of a waste package integrity parameter (function of pH). The digital twin allows to combine different independent or coupled processes into one digital toolkit. The results of one process can be used as input for another, and all output results can finally be used to train surrogate models.

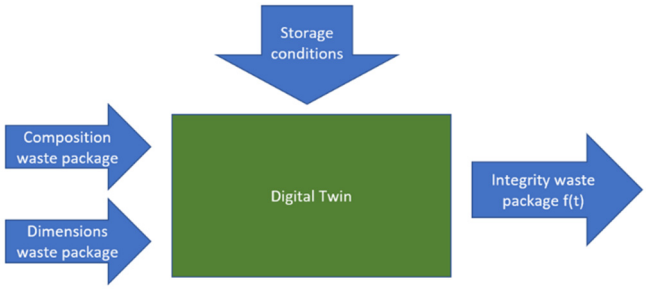

Fig. 2.12: EURAD PREDIS proof-of-concept Digital Twin that can be used in waste predisposal applications.

2.6.2 GeoML.AI: Machine Learning accelerated reactive transport

Reactive transport simulations play a key role in process understanding and modelling of the geochemical evolution of waste repositories. These simulations combine diffusive / advective mass transport, solute transport, and homogeneous and heterogeneous chemical reactions calculations. The main computational cost is in the computation of aquatic chemical equilibria (Geochemical Speciation

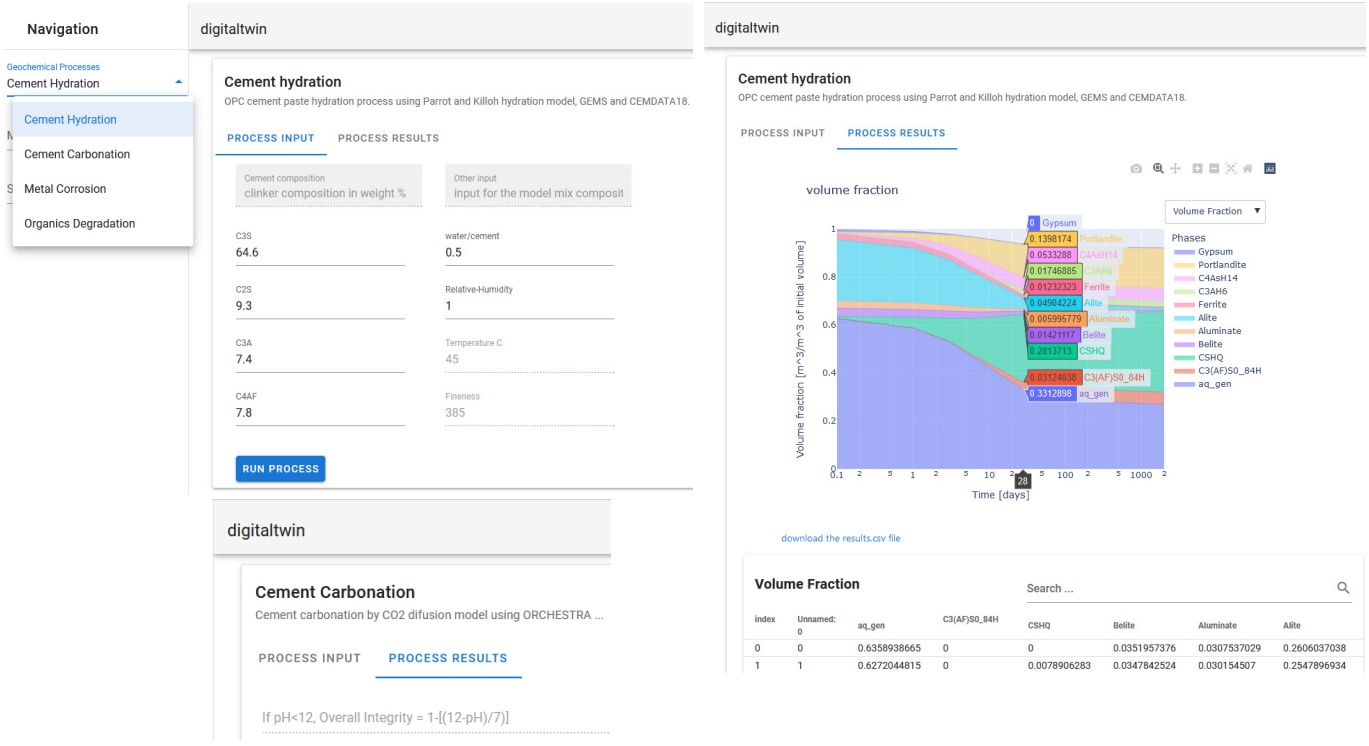

Fig. 2.13: A demo prototype of the Digital Twin is running on the GeoML platform (https://digitaltwin.geoml.eu/).

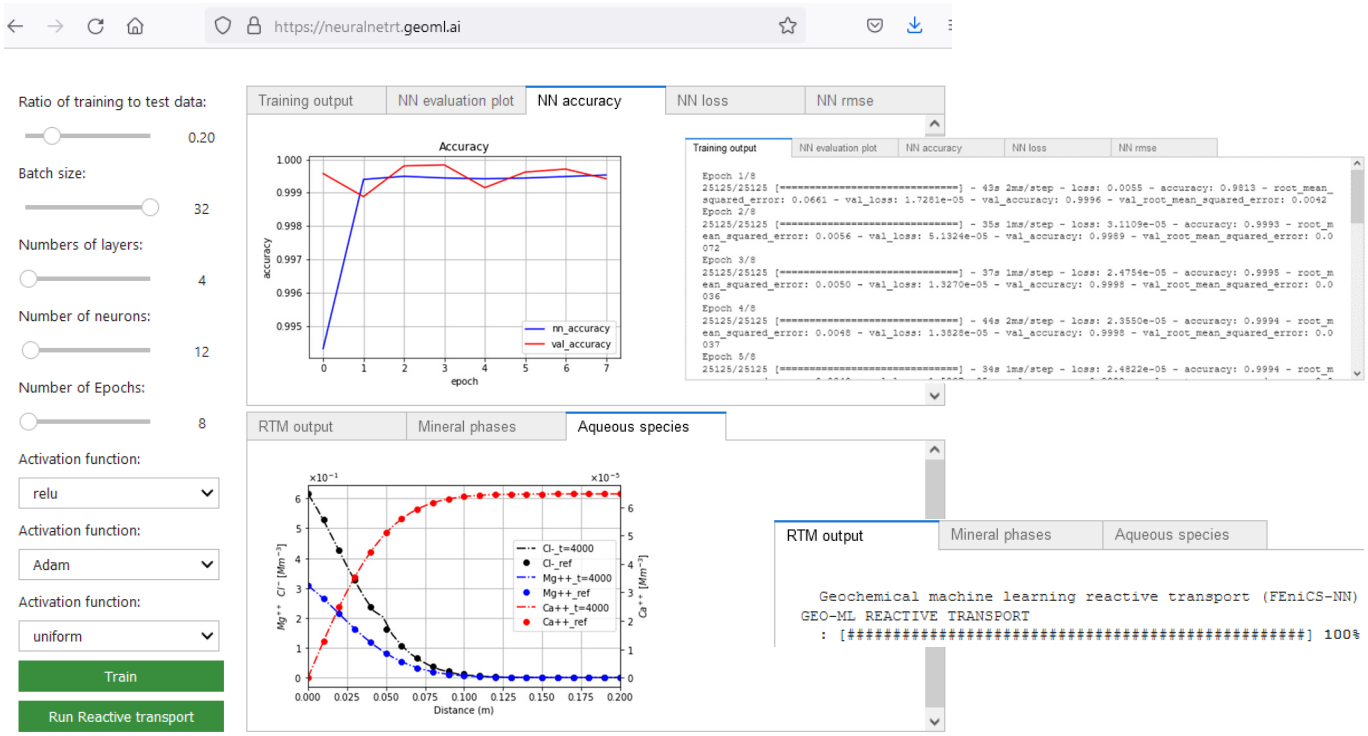

Fig. 2.14: A demo prototype of the neural network accelerated reactive transport calculation which is running on the GeoML platform (https://neuralnetrt.geoml.ai/).

Calculations), which consumes 70%-99% of the total simulation time. Hence, a direct coupling of a transport solver with any external geochemical solver would significantly reduce the speed of reactive mass transport calculations. However, surrogate models based on artificial neural networks have a potential to speed up the geochemical speciation calculations by several orders of magnitude (as demonstrated by several authors), bringing the geochemical calculation cost at a level comparable to that of the mass transport simulation. Combining machine learning techniques with reactive transport simulations will therefore eventually lead to more accurate and reliable field-scale simulations within reasonable computational times. A chain of numerical tools has been built, starting from producing the training dataset using the geochemical solvers, continuing with the training and testing of neural networks, and running the reactive transport simulation alternatively with the fully coupled geochemical solver or with the trained neural network. The whole process is now fully automated, allowing for exploring and testing different neural network architectures and chemical systems.

A demonstrator which allows the user to interactively parameterize the training process and the neural network architecture, as well as to compare the efficiency of the machine learning instance with the fully coupled simulator, is accessible via the link: https://neuralnetrt.geoml.ai/. In Fig. 2.14, such an example is presented, relevant to the calcite-dolomite chemical system. The user may select the neural network architecture e.g. number of hidden layers, number of neurons per layer, may control the activation function and the machine learning algorithm before starting the training. After the training is finished, all relevant metrics of accuracy of the network are plotted (Fig. 2.14 top). The user can then run the full reactive transport problem and obtain several plots that compare the fully coupled and the neural network accelerated solution.

2.7 References

Bercovitz Y., Lebert F., Jodeau M., Buvat C., Violeau D., Pelaprat L., Hajczak A. (2016)
LS-PIV procedure applied to a plunging water jet issuing from an overflow nappe. In Proceedings of the 4th IAHR Europe Congress.

Bossart P., Bernier F., Birkholter J., Bruggeman C., Connoly P., Devonck S., Fukaya M., Herfort M., Jensen M., Matray J., Mayor J., Möri A., Oyama T., Schuster K., Shigeta S., Vietor T., Wieczorek K. (2017)
Mont Terri rock laboratory, 20 years of research: introduction, site characteristics and overview of experiments. Swiss J. Geosci. 110, 1-20.

Bradbury M.H. & Baeyens B. (1997)
A mechanistic description of Ni and Zn sorption on Na-montmorillonite. 2. Modelling. J. Contam. Hydrol. 27, 223-248.

Bradbury M.H., Berner U., Curti E., Hummel W., Kosakowski G., Thoenen T. (2014)
The Long Term Geochemical Evolution of the Nearfield of the HLW Repository. Nagra Technical Report 12-01, chapter 9.

Curti E. (2021)
Bentonite Pore Waters (BPW) for the Sectoral Plan, phase SGT-3: model development and testing. Internal Technical Report TM-44-21-02. Paul Scherrer Institut, Villigen, Switzerland.

De Weerdt K., Ben Haha M., Le Saout G., Kjellsen K.O., Justnes H., Lothenbach B. (2011)
Hydration mechanisms of ternary Portland cements containing limestone powder and fly ash. Cement and Concrete Research 41, 279-291.

Gottschalk P.G. & Dunn J.R. (2005)
The five-parameter logistic: A characterization and comparison with the four-parameter logistic. Analytical Biochemistry 343, 54-65.

Hummel W. & Curti E. (2020)
The PSI Chemical Thermodynamic Database 2020: Data Selection for Phosphorous and Application to HLW near-field pore water modelling. Technical Note TM 44-20-06, Paul Scherrer Institut.

Jaeger T., Mokos A., Prasianakis N.I., Leyer S. (2021)
Pore-level Multiphase Simulations of Realistic Distillation Membranes for Water Desalination. 16th conference on Sustainable development of Energy, Water and Environment Systems (SDEWES 2021), 10–15 October 2021, Dubrovnik, Croatia

Kulik D.A., Marques Fernandes M., Baeyens B. (2018)
The 2SPNE SC/CE sorption model in GEM-Selektor v.3.4 code packagec (ClaySor): Implementation, tests, and user guide. Work Report NAB 18-27, Nagra, Wettingen, Switzerland.

Kulik D.A., Wagner T., Dmytrieva S.V., Kosakowski G., Hingerl F.F., Chudnenko K.V., Berner U.R. (2013)
GEM-Selektor geochemical modeling package: revised algorithm and GEMS3K numerical kernel for coupled simulation codes. Computers and Geosciences, 17, 1-24.

Kulik D.A., Winnefeld F., Kulik A., Miron G.D., Lothenbach B. (2021)
CemGEMS – an easy-to-use web application for thermodynamic modeling of cementitious materials. RILEM Technical Letters, 6, 36-52.

Lothenbach B., Kulik D.A., Matschei T., Balonis M., Baquerizo L., Dilnesa B., Miron G.D., Myers R.J. (2019)
Cemdata 18: A chemical thermodynamic database for hydrated Portland cements and alkali-activated materials. Cement and Concrete Research 115, 472-506.

Lothenbach B., Le Saout G., Gallucci E., Scrivener K. (2008)
Influence of limestone on the hydration of Portland cements. Cement and Concrete Research 38, 848-860.

Luraschi P., Gimmi T., Van Loon L.R., Churakov S.V., Shafizadeh A. (2020)
Evolution of HTO and $^{36}Cl^-$ diffusion through a reacting cement-clay interface (OPC paste-Na montmorillonite) over a time of six years. Applied Geochemistry 119 (2020) 104581.

Mokos A. et al. (2021)
SPH Modelling of the Water Nappe Gravity Fall over a Dam. Journal of Hydraulic Research, 2021. Accepted, in press.

Tits J., Jakob A., Wieland E., Spieler P. (2003)
Diffusion of tritiated water and 22Nafl through nondegraded hardened cement pastes. J. Contam. Hydrol. 61, 45–62.

Wagner T., Kulik D.A., Hingerl F.F., Dmytrieva S.V. (2012)
GEM-Selektor geochemical modelling package: TSolMod Library and data interface for multicomponent phase models. Canadian Mineralogist 50, 1173-1195.

3 DEVELOPMENT OF MECHANISTIC SORPTION MODELS AND EXPERIMENTAL VALIDATION

Marques Fernandes M., Baeyens B., Dähn R., Miron G.D., Kulik D.A., Churakov S.V., Schaible A., Lang C., Di Lorenzo F. (postdoc), Cruz P. (postdoc), Qian Y. (PhD student), Stotskyi V. (PhD student)

3.1 Introduction

In the framework of the deep drilling programme carried out by Nagra, the sorption of Cs^{I}, Ni^{II}, Eu^{III}, Th^{IV} and U^{VI} are being measured on drilling core samples from three different siting regions. The "bottom-up approach" (Ref) was tested on sorption isotherms obtained for Cs^{I} on seven samples with different mineralogies from the Bülach-1 borehole.

The activities in the EU project Eurad FUTURE have continued this year. In collaboration with the Forschungszentrum Jülich (FZJ), the study on the adsorption behaviour of ^{226}Ra and Ba on montmorillonite was completed and the results were published in 2021 in Applied Geochemistry (Klinkenberg et al. 2021). In the subtask "*Redox reactivity of radionuclides on mineral surfaces*", a PhD student has performed different types of sorption experiments studying the uptake of Tc^{VII} and Se^{IV} on clay minerals with different Fe^{II}/Fe^{III} ratios. First extended X-ray absorption fine structure (EXAFS) spectroscopic measurements were performed to unravel the Tc/Se surface speciation as a function of different geochemical parameters (e.g. clay reduction degree, metal loadings and pH).

UpSaGems (Uncertainty propagation and Sensitivity analysis for Gems), which is a new tool (currently under development) for performing error propagation and sensitivity analysis in GEMS, was used to quantify the impact of uncertainties of the Ni surface species stability and aqueous speciation on calculated adsorption isotherms.

Over the past years, the "bottom-up approach" was applied on many different sedimentary rocks. Published isotherms obtained on Opalinus Clay, Boom Clay/Oxford Clay/Marl and Boda Claystone (Baeyens et al. 2014, Bradbury & Baeyens 2000, Bradbury & Baeyens 2011, Marques Fernandes et al. 2015) as well as unpublished in-house data were re-modelled with a state-of-the-art sorption database for illite (Bradbury & Baeyens 2017) and compiled in a Nagra Technical report (NTB-19-04). The sorption studies (wet chemical and spectroscopy) of Zn on illite and argillaceous rocks were published in 2021 in Geochimica et Cosmochimica Acta.

In a previous study, the adsorption of Pb^{II} onto illite and montmorillonite was investigated in terms of batch experiments and the uptake was subsequently modelled using a thermodynamic adsorption model. In the continuity of this study, the retention of Pb on illite was further investigated by EXFAS to elucidate its structural environment over a larger range of Pb^{II} concentrations and to verify the adsorption model developed for illite (Marques Fernandes & Baeyens 2019).

The SNSF-funded PhD and postdoc project entitled "*Molecular scale understanding of competitive cation adsorption on swelling clay minerals*" (SNF Nr. 200021-129947) started in spring this year. The PhD project focusses on Density Functional Theory (DFT) analysis and first calculations have been started. Within the Post-doc project, pure saponite clay minerals doped with Ni^{II} and Lu^{III} were synthesized. Preliminary Ni adsorption experiments on synthetic saponite were performed and EXAFS spectra were recorded of Lu/Ni doped saponites as well as of Ni/Lu aqueous complexes. The EXAFS spectra, will later be used to benchmark the DFT calculations.

3.2 Cs sorption on samples from the Bülach-1 borehole: measurements and application of the Generalized Cs Model (GCM)

In the frame of the Swiss Sectoral Plan for Deep Geological Repositories (SGT), LES is carrying out sorption experiments involving different radionuclides i.e. Cs^{I}, Ni^{II}, Eu^{III}, Th^{IV} and U^{VI} on samples from the three siting regions. The aim is to compare the adsorption properties of the different argillaceous rocks and to test the robustness of the "bottom-up approach" (Bradbury & Baeyens 2011, Marques Fernandes et al. 2015). For the safety analysis for the general licence application, we intent to apply a simplified component additive approach, the so-called "bottom-up approach" to calculate site-specific sorption databases (SDBs). In this approach, solid-liquid distribution ratios (R_d values) are calculated directly, including aqueous speciation, solubility and concentration-dependent adsorption of the radionuclides for site-specific argillaceous rock/porewater systems by using element specific adsorption models developed for illite within LES during the past 20 years (Bradbury & Baeyens 2000, 2009a, b, 2017). In view of the upcoming safety assessment, the validation of the "bottom-up approach" is of key importance to justify its applicability.

Sorption experiments in a synthetic pore water (SPW) were carried out on seven different samples from the Bülach-1 borehole. The different samples were taken at different depth, covering (-845m to -1017m) in the siting region of Nördlich Lägern. The rock samples were crushed inside a glove box at a particle size ≤ 1 mm and conditioned with the SPW. The pore water composition and rock mineralogy of the different samples are given in Tables 3.1 and 3.2. The total clay content of the investigated samples varies from 1% up to 69 wt.%.

Sorption isotherms for the nuclides Cs^{I}, Ni^{II}, Eu^{III}, Th^{IV} and U^{VI} were measured at element concentrations ranging from trace up to concentrations where the element concentrations are still below the calculated solubility limit. In the present report, only the Cs^{I} isotherms are shown. The entire experimental data and blind predictive modelling will be compiled in a Nagra Technical report in 2022.

The blind prediction of the Cs adsorption isotherms measured on Bülach samples in their corresponding porewaters was performed with the generalised caesium sorption (GCS) model (Bradbury & Baeyens 2000). According to this model the uptake of Cs in argillaceous rocks is assumed to be controlled predominantly by illite (Bradbury & Baeyens 2000). To model the adsorption of Cs^{I} on the rock samples the capacity of the different Cs specific cation exchange sites (i.e. frayed edge sites (FES), type 2 sites (T2S) and planar sites (PS)) were scaled only to the illite end-member content in the natural rocks (see Table 3.2). Since FES and T2S are not present in smectites nor in kaolinite, the retention of Cs at trace and medium concentration is expected to be solely governed by adsorption on illite. The sorption behaviour of Cs is essentially influenced by the clay content and the competitive Cs exchange with Na, K, Mg and Ca on the PS, and Na and K on FES and T2S. Selectivity coefficients K_c for the cation exchange equilibria on the three site types are given in (Marques Fernandes & Baeyens 2021).

The Cs isotherms measured on the different Bülach samples are shown in Fig. 3.1. All isotherms exhibit the typical non–linear uptake indicative for adsorption on different site types and in agreement with adsorption of Cs on illite. The measured R_d values reflect well the different illite contents of the samples (see Table 3.1). Blind predictions using the GCS model predict very well the Cs adsorption behaviour along the depth profile, with an illite variation of 0.7 wt.% to 37 wt.% (solid black lines in Fig. 3.1). A slight over estimation of sorption on the T2S at Cs_{eql} concentration between ~ 10^{-5} M to 10^{-3} M is observed for all samples.

In view of the uncertainties related to the complexity of the natural rocks and to the sorption model, it can be concluded that the simplified "bottom-up approach" provides a quite good blind prediction tool for the adsorption of Cs on different sedimentary rocks.

Tab. 3.1: Composition of the synthetic pore water for the Bülach-1 drill cores (Mäder, pers. comm.).

pH	7.6
I.S. (M)	0.4
pCO_2 (bar)	$10^{-3.4}$
	Concentration (M)
Na	0.325
K	0.0019
Mg	0.0176
Ca	0.0383
Sr	0.0003
Cl	0.402
SO_4	0.0275
TIC	0.00041

Tab. 3.2: Mineralogical composition of the Bülach-1 rock samples (Mazurek, pers. comm.).

[wt.%]	**-845.05 m**	**-861.00 m**	**-921.43 m**	**-955.62 m**	**-995.09 m**	**-1002.19 m**	**-1017.33 m**
C(org)	0.10	0.56	0.85	1.01	0.98	4.03	0.67
Quartz	1	27	28	15	16	9	37
K-feldspar	-	6	5	4	5	3	5
Plagioclase	-	3	3	3	3	2	4
Calcite	98	14	10	4	9	47	7
Dolomite / Ankerite	-	-	-	-	-	-	2
Siderite	-	-	3	3	2	-	2
Pyrite	-	1.1	1.2	0.5	1.1	2.0	0.3
Illite end-member	0.7	37	23	33	29	21	21
Smectite end-member	0.2	7	2.6	3.9	3.4	3.1	2.2
Kaolinite end-member	0.0	2.7	18	25	23	6	12.5
Chlorite end-member	0.1	2.1	5	7	7	3.1	6.1

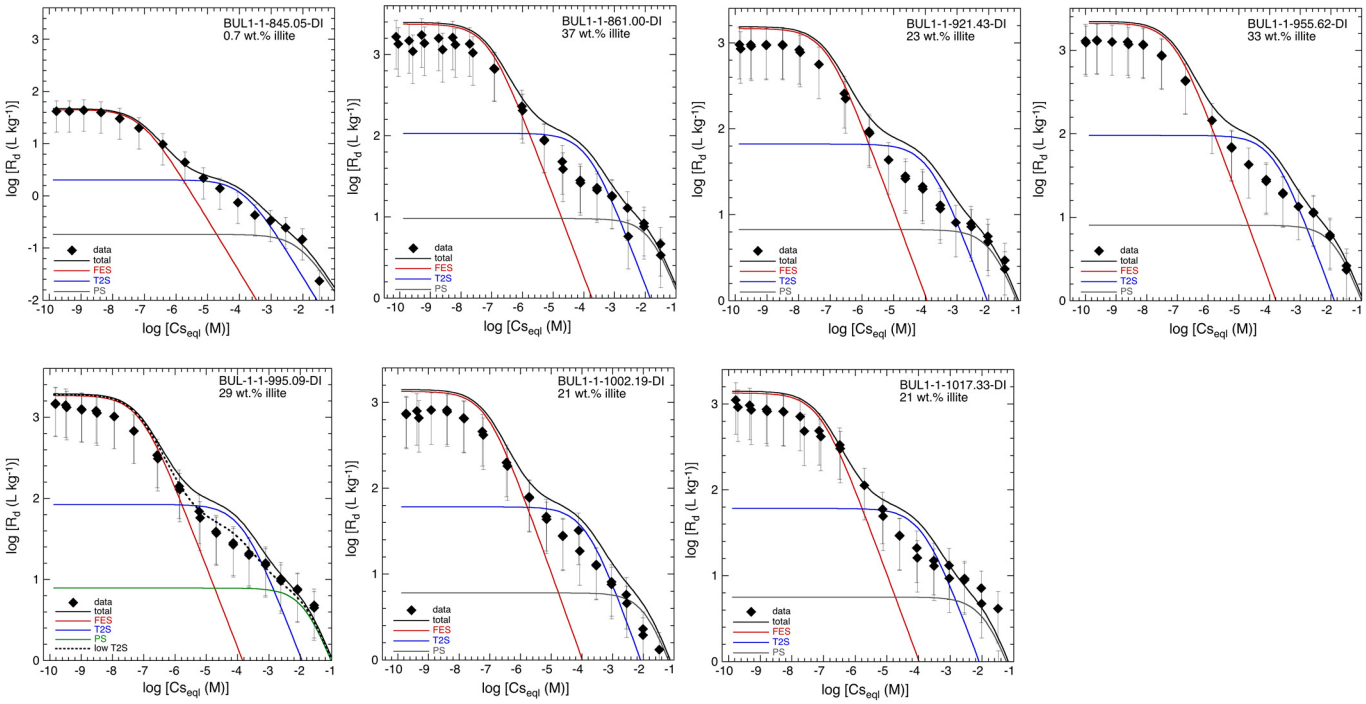

Fig. 3.1: Sorption isotherms of Cs^I on drill core samples from the Bülach-1 borehole. Experimental and blind predictions.

3.3 Ba and Ra adsorption on montmorillonite

In the framework of an international cooperation with Forschungszentrum Jülich (FZJ) and PSI-LES, embedded in the EU programme FUTURE (Eurad project FUTURE), adsorption studies of Ba and Ra on 2:1 clay minerals are under investigation. The adsorption studies on montmorillonite (SWy) are completed and recently published in Applied Geochemistry (Klinkenberg et al. 2021), whereas the studies on illite are on-going.

Adsorption edges of Ba and ^{226}Ra at trace concentrations as a function of pH at fixed ionic strength and an adsorption isotherm with Ba in an equilibrium range varying from 10^{-9} to 10^{-2} M at fixed pH and ionic strength were carried out on homo-ionic Na-SWy-2 in NaCl background electrolyte. The adsorption of trace Ra was also investigated in the presence of increasing stable Ba concentrations. This experiment can be regarded as a competitive adsorption experiment between stable Ba and ^{226}Ra.

Fig. 3.2 shows the log R_d values (symbols) of two Ba adsorption edges on Na-SWy in 0.03 M and 0.3 M NaCl in the pH range 5 to 9.5. The experimental data show that the adsorption of Ba is dependent on ionic strength (up to pH ~ 8) which is indicative for cation exchange. At ionic strength of 0.3 M and pH > 8 the sorption of Ba increases at increasing pH which is indicative for surface complexation.

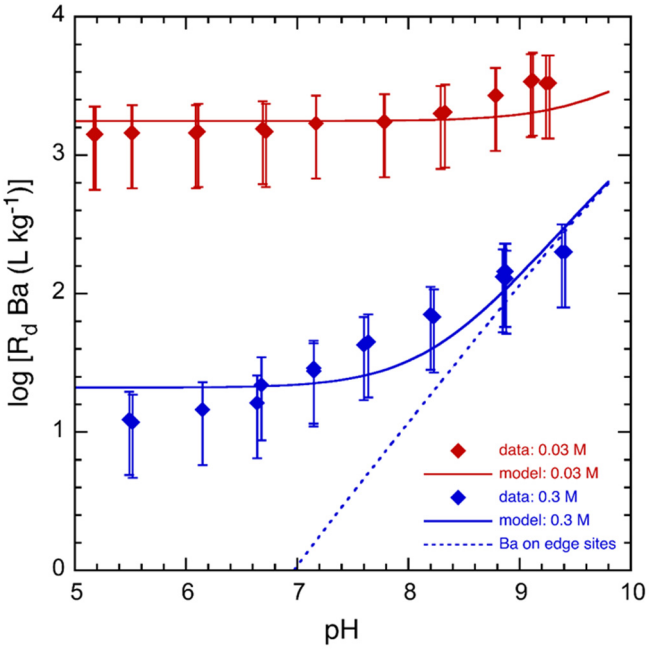

Fig. 3.2: Experimental and modelling results for adsorption edges of Ba in 0.03 M and 0.003 M NaCl.

Fig. 3.3 shows the log R_d values (symbols) of three Ra adsorption edges on Na-SWy in 0.02 M, 0.14 M and 0.3 M NaCl in the pH range 5 to 10. The experimental data are very reminiscent to the Ba results and show that the adsorption of Ra is dependent on ionic strength and becomes pH dependent at higher pH and ionic strength.

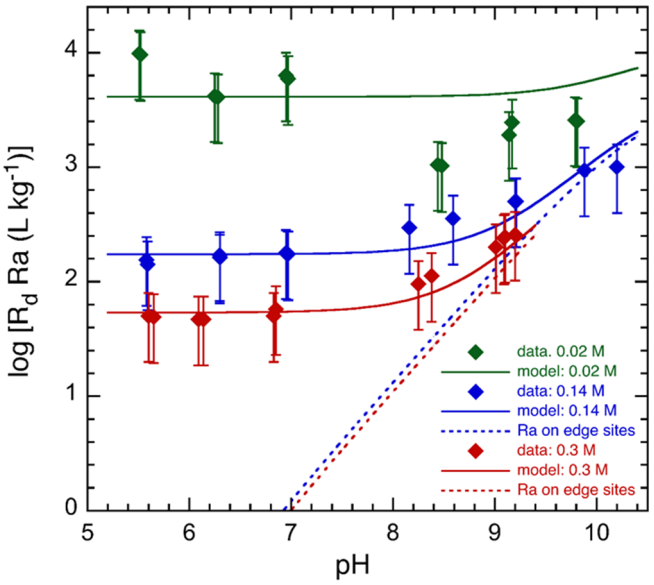

Fig. 3.3: Experimental and modelling results for adsorption edges of Ra in 0.02 M, 0.14 M and 0.3 M NaCl.

Fig. 3.4 shows an adsorption isotherm of Ba in the presence of trace ^{226}Ra at pH 7 in 0.02 M NaCl on SWy as log R_d Ba as function of Ba equilibrium (Ba_{eql}) concentration. The ^{226}Ra R_d values follow exactly the measured Ba R_d values along the isotherm indicating that for these experimental conditions Ba and Ra are behaving as chemical analogues.

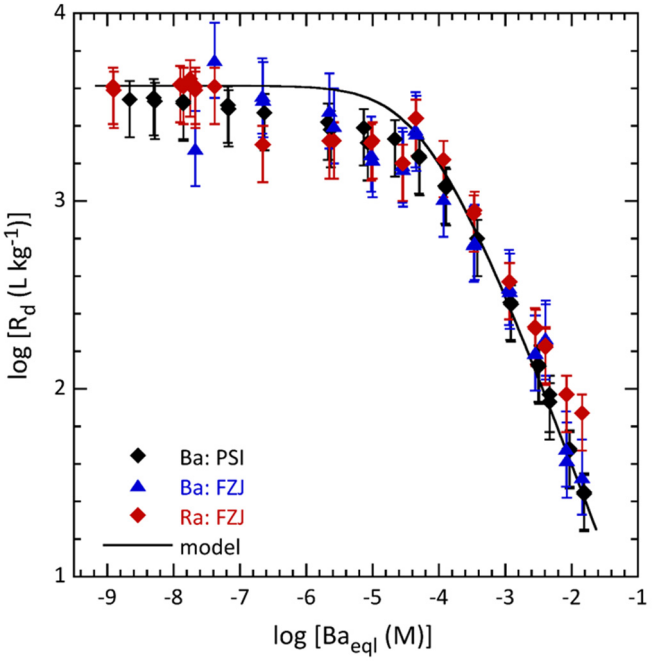

Fig. 3.4: Adsorption isotherm of ^{137}Ba/^{133}Ba and ^{137}Ba/^{226}Ra on Na-SWy at pH 7 in 0.02 M NaCl.

The experimental data presented in Fig. 3.2 to 3.4 could be modelled by considering Ra^{2+}-Na^+ and Ba^{2+}-Na^+ cation exchange equilibria on the planar sites of montmorillonite. The cation exchange reaction can be written by

$$2\text{Na-SWy} + X^{2+} \Leftrightarrow \text{X-SWy} + 2\ Na^+$$

with X^{2+} being Ra^{2+} or Ba^{2+}. The selectivity coefficient (K_c) convention from Gaines & Thomas (1953) was used and is defined by

$$ {}^{X}_{Na}K_c = \frac{N_X}{N_{Na}^2}\frac{[Na]^2}{[X]}\frac{(\gamma_{Na})^2}{(\gamma_X)} $$

where N_X and N_{Na} are the equivalent fractional occupancies, defined as the equivalent of Na or X (Ra or Ba) adsorbed per kg of clay mineral divided by the cation exchange capacity (CEC) [eq·kg^{-1}], [Na] and [X] are the aqueous molar concentrations and γ_{Na} and γ_X are aqueous phase activity coefficients.

The selectivity coefficients for Ba^{2+}-Na^+ and Ra^{2+}-Na^+ exchange summarised in Table 3.3 could quantitatively describe the linear parts of the adsorption edges (Fig. 3.2 and 3.3) and the isotherm (Fig. 3.4).

As already mentioned before, the pH dependent adsorption at pH > 8 could only be quantified by considering a surface complexation reaction at the edge sites of montmorillonite. The 2 site protolysis non-electrostatic surface complexation and cation exchange model (2SPNE SC/CE) for montmorillonite (Bradbury & Baeyens 1997) was used to model the adsorption edges up to pH 10. The dotted lines in Fig. 3.2 and 3.3 illustrate the contribution to Ba and Ra uptake at high ionic strength and high pH. The contribution of surface complexation is negligible at low ionic strength because cation exchange is the dominant uptake process. The results of the cation exchange and surface complexation reactions together with the corresponding fitted parameters are summarised in Table 3.3.

The K_c values in Table 3.3 indicate a trend in the values. The K_c values increase at increasing ionic strength and at the highest ionic strength (0.3 M NaCl) the K_c values for Ra are higher compared to Ba. Based on the higher ionic radius of Ra compared to Ba a selectivity behaviour which is more pronounced in higher ionic strength media could be postulated.

An important outcome from this study is that the uptake of Ra on montmorillonite is governed by well-known adsorption mechanisms, i.e. cation exchange and surface complexation, and can be quantified by well established adsorption models.

Tab. 3.3: Summary of selectivity coefficients for Ba/Ra-Na exchange and surface complexation constants for Ba/Ra surface complexation on montmorillonite.

Cation exchange reaction	**log K_c**
$2Na\text{-}SWy + Ba^{2+} \Leftrightarrow Ba\text{-}SWy + 2Na^{+}$	0.70 – 0.90
$2Na\text{-}SWy + Ra^{2+} \Leftrightarrow Ra\text{-}SWy + 2Na^{+}$	0.70 – 1.34
Surface complexation reaction	**log K**
$\equiv S^{W2}OH + Ba^{2+} \Leftrightarrow \equiv S^{W2}OBa^{+} + H^{+}$	-5.0
$\equiv S^{W2}OH + Ra^{2+} \Leftrightarrow \equiv S^{W2}ORa^{+} + H^{+}$	-5.0

3.4 UpSaGEMS: Uncertainty propagation and sensitivity analysis for sorption calculations

In order to quantify how the errors in different input parameters (e.g. stability of surface species, site capacity, stability of hydrolysis species, clay content, etc.) affect the calculated distribution coefficients (log R_d), an uncertainty propagation and global sensitivity analysis can be used. The uncertainty propagation allows to quantify the effect of the input parameter errors onto the total uncertainties of the model output, for instance, in form of statistical confidence intervals. The global sensitivity analysis quantifies the relative importance of different input parameters and their interactions onto variations of the model output (Saltelli 2002, Zhou et al. 2008). Input parameters are varied simultaneously to account for their interactions in complex nonlinear models. Uncertainty propagation is a straightforward task for simple mathematical models with analytical explicit formulations of parameters dependencies. Uncertainty propagation in geochemical simulations is a challenging task due to the large number of parameters, non-linearity and stiffness of governing thermodynamic equations as well as buffering effects in chemical systems. In such cases, numerical methods like Monte Carlo sampling and polynomial chaos expansion can be used. The Monte Carlo method uses random sampling of the input parameter distribution to generate many model outputs that are then used for calculating statistics. The same method is also used for calculating fitted parameter uncertainties in the GEMSFITS code (Miron et al. 2015), where hundreds of parameter fitting tasks are generated by varying the input experimental data within their uncertainties, then solving these tasks, and collecting statistics on the values of fitted parameters. The polynomial chaos expansion is a method that replaces the model with a polynomial surrogate model, which is then used for the statistical analysis.

The UpSaGems (Uncertainty propagation and Sensitivity analysis for Gems) is a new tool (currently under development) for performing error propagation and sensitivity analysis in GEMS (Kulik et al. 2013) calculations. It is implemented in Python on the LES JupyterLab service (https://thermohub.net) in JupyterLab (https://jupyter.org) environment and can be used directly from the web browser. UpSaGems uses the Uncertainpy python library (Tennøe et al. 2018) for conducting the statistical analysis. The library supports the estimations of the error propagation and sensitivity analysis on already existing models using the Monte Carlo or the polynomial chaos expansion methods. The setup in UpSaGems is based on the more efficient polynomial chaos expansion method, which has been tested to produce the same results as the Monte Carlo sampling method.

In the present example, UpSaGems is used to quantify the impact of uncertainties of the Ni sorption species stability and aqueous speciation on the calculated sorption isotherm. The confidence intervals of the standard Gibbs energy of formation (G°_{298}) for the surface species, representing 95% confidence intervals (2σ), were separately retrieved during the GEMSFITS parameter optimization procedure using the Monte Carlo method. To run the statistical analysis for a sorption isotherm, the user provides the values of the model parameters and their uncertainties (2σ). The results of the analysis are the calculated model mean (best fit model value), standard deviation, the 95% confidence interval, and the first order indices (S_i) and total Sobol (S_T) indices. The first order Sobol indices quantify how much do the input parameters contribute to the overall variability of the model. The total Sobol indices additionally include the effect on the sensitivity due to the interaction of a given parameter with all the other parameters.

For the Ni sorption example, an isotherm at 0.1 M ionic strength for pH 7 to 7.24 was evaluated for four parameters (G°_{298}) with their respective errors: ClayNi@ -28186 ± 483, =iSsONi+ -287151 ± 256, iSvONi+ 272284 ± 735 J/mol sorption species and Ni(OH)2@ -411519 ± 10900 aqueous species. The results of the statistical analysis are shown in Fig. 3.5. The 95% confidence interval band (Fig. 3.5a) does not cover most of the experimental data points. This is due to the additional experimental data that was used for the parameter error estimation such as pH edge data and isotherm data at different pH and ionic strengths, which are not shown. In addition, with the increasing number of measurements used in the model fit, the standard deviation of the mean model value (Fig. 3.5b) becomes smaller and the model becomes increasingly more precise. The first order Sobol indices (Fig. 3.5) that

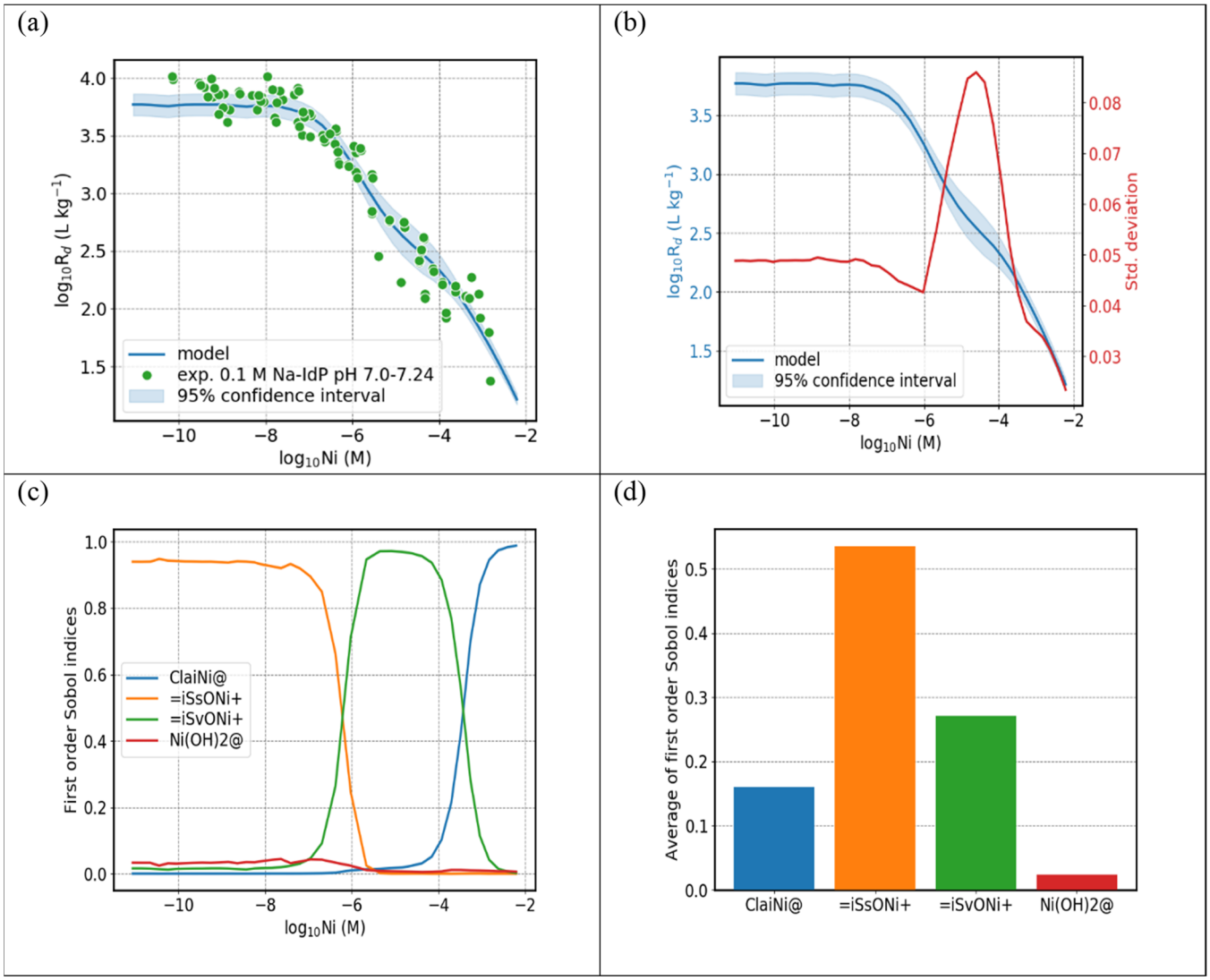

Fig. 3.5: Results of the propagation and sensitivity analysis of ClayNi@, =iSsONi+, =iSvONi+ sorption species and Ni(OH)2@ aqueous species onto the calculated Ni sorption isotherm.

are directly related to the contribution of surface species to R_d and average values (Fig. 3.5d) show that the stability of =iSsONi+ species has the largest effect on the model variability in the investigated Ni concentration interval with S_i = 0.54, which signifies that roughly half of the variability in the model is due to this parameter. The Ni(OH)2@ neutral aqueous species has a small contribution to the overall variability of the model with S_i = 0.024, even though it has a large uncertainty of its G°_{298} value.

The UpSaGems tool is under development and will further be extended with the possibility of adding different types of input parameters to the statistical analysis, such as the input composition for assessing the site capacity and the clay content effects. Additionally, other models and GEMS processes can be implemented, and the statistic effects of their input parameter variations can then be analysed.

3.5 Zn uptake by illite and argillaceous rocks

The uptake of Zn by illite (Illite du Puy,IdP) and two argillaceous rocks, Opalinus Clay (OPA) and Boda Claystone (BODA) was investigated by EXAFS and the results were recently published in Geochimica et Cosmochimica Acta (Dähn et al. 2021). The uptake of Zn by illite was studied in 0.1 M NaCl at near-neutral pH and a Zn loading of 2.1 mmol/kg. The Zn uptake by the two argillaceous rock systems was carried out in 0.1 M NaCl at pH 7.2 and in their respective porewaters at pH 8.0 to evaluate the influence of porewater composition. The Zn loadings were 1.8 mmol/kg and 1.7 mmol/kg on OPA and BODA, respectively. Elemental analysis of illite and both argillaceous rocks indicates an intrinsic Zn content of 2.9 mmol/kg in illite, 4.1 mmol/kg in OPA and 2.2 mmol/kg in BODA.

The $k^3\chi(k)$ EXAFS spectra of intrinsic Zn (Zn_{incor}) in IdP, OPA and BODA samples are very similar (Fig. 3.6a). The split in the oscillation at 3.8 $Å^{-1}$ is slightly

stronger in the BODA sample compared to IdP and OPA. Since this split is absent in the FT^{-1} spectra of the IdP, OPA and BODA samples it indicates that this spectral feature is caused by the presence of higher atomic shells > 4.0 Å. The spectra indicate that the Zn intrinsically present in the samples is located in the octahedral sheets of the clay platelets (Dähn et al. 2011). The spectra of the Zn loaded OPA and BODA samples show remarkable similarities, indicating that in the three uptake systems the formation of similar inner-sphere complexes prevail (Fig. 3.6b), and that the local structural environment is alike of the intrinsically present Zn.

Data analysis for the IdP, OPA and BODA samples with only intrinsic Zn indicate that ~3 Zn-Al backscattering pairs are present. This indicates that Zn is located in the octahedral sheets of the dioctahedral clays and is not filling empty octahedral position (in this case 6 would be expected). The observed $CN_{Zn\text{-}Si}$(OPA) = 2.5(9) and $CN_{Zn\text{-}Si}$(BODA) = 1.9(9) are smaller compared to the value obtained for IdP (4.4(9)), and are also smaller than the theoretical expected 4 indicating a higher disorder compared to the IdP system. The $CN_{Zn\text{-}Al}$ and $CN_{Zn\text{-}Si}$ and the Zn-Al and Zn-Si bond distances agree well, within the uncertainties, with the values obtained for the pure systems. The obtained structural data indicate that in all three investigated systems Zn at low metals loadings formed inner sphere surface complexes at clay edge sites. Thus, IdP and both argillaceous rocks show the same uptake behaviour, indicating that the clay minerals are predominantly responsible for the uptake of Zn.

3.6 Pb^{II} adsorption on illite

The adsorption behaviour of Pb^{II} on illite under different experimental conditions (pH, ionic strength and Pb concentrations) was quantified and a sorption model developed (Marques Fernandes & Baeyens 2019). Up to now, however, structural information on the adsorption mechanisms of Pb on clay mineral surfaces are very sparse (Gräfe et al. 2007, Strawn & Sparks 1999). In order to gain molecular level information on the uptake processes of Pb by illite, three Pb loaded Na-illite samples were prepared in 0.1 M NaCl at pH ~7.1 along the adsorption isotherm (Fig. 3.7). The Pb loadings were 2 mmol/kg (Pb-1), 14 mmol/kg (Pb-2) and 140 mmol/kg (Pb-3).

The EXAFS data were collected at the beamline 11-2 of the Stanford Synchrotron Radiation Lightsource (SSRL). The k^3-weighted Pb L_{III}-edge EXAFS spectra show a small decrease in amplitude with increasing loading (Fig. 3.7a). The variations observed in the $k^3\chi(k)$ spectra are causing a decrease of the first and second peak in the RSF (Fig. 3.8b).

The data could be fitted well with Pb-O1, Pb-O2, Pb-Al and Pb-Si backscattering pairs indicative of the formation of inner-sphere surface complexes. The formation of Pb precipitates can be excluded. With increasing Pb loading the $R_{Pb\text{-}O1}$ and $R_{Pb\text{-}O2}$ stayed within the experimental error unchanged at 2.37(1) and 2.63(1) Å, respectively. The $CN_{Pb\text{-}O1}$ decreased from 2.6(2) to 2.3(2) whereas the $CN_{Pb\text{-}O2}$ decreased from 1.6(2) to 1.4(2). The Pb-Al and Pb-Si distances stayed constant at 3.35(3) Å and 3.54(3) Å, respectively.

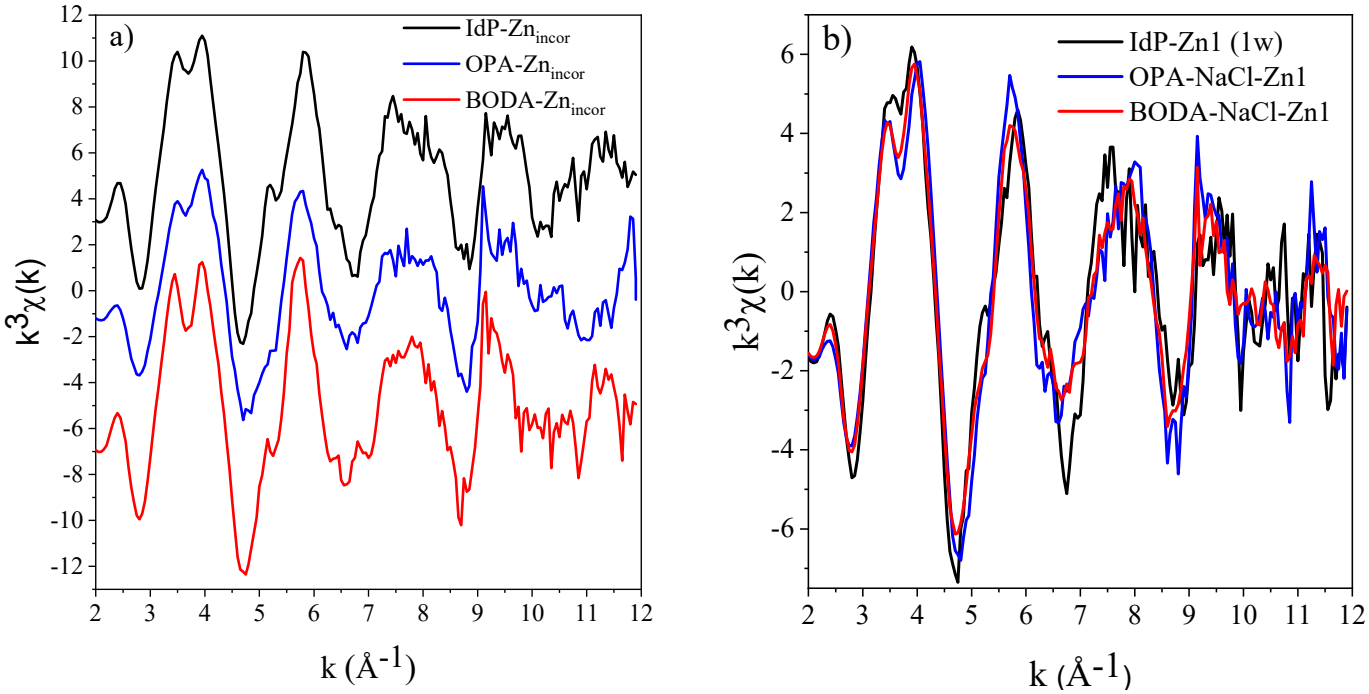

Fig. 3.6: (a) Comparison of k^3-weighted Zn K-edge EXAFS spectra of IdP, OPA and BODA with only incorporated Zn, (b) IdP loaded with 2.1 mm/kg (Idp-Zn1), OPA with 1.8 mmol/kg (OPA-NaCl-Zn1) and BODA with 1.7 mmol/kg (BODA-NaCl-Zn1).

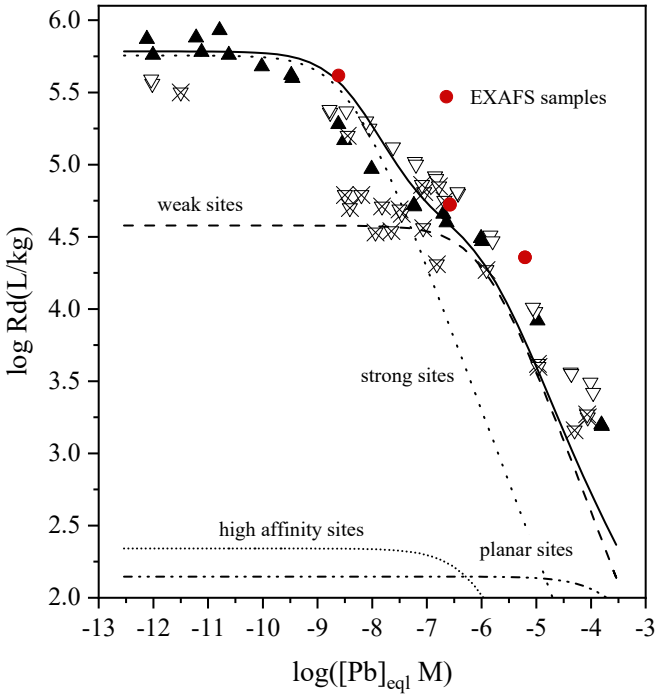

Fig. 3.7: Adsorption isotherm for Pb on Na-IdP at pH ~7 in 0.1 M NaCl. Red symbols: EXAFS samples. Continuous black line: modelled curve using the 2SPNE SC/CE model developed for Pb^{II} on Na-IdP. Dashed and dotted lines: contribution to the overall sorption of Pb on the different types of sites (experimental data and model parameters are taken from (Marques Fernandes & Baeyens 2019)).

The $CN_{Pb\text{-}AL}$ decreased from 1.8(3) to 1.3(3), and $CN_{Pb\text{-}Si}$ decreased from 1.9(3) to 1.3(3). The decrease of coordination numbers may indicate the transition of the Pb surface complexes from strong (Pb-1) to weak sites (Pb-2) and to planar sites (Pb-3) (Dähn et al. 2021).

3.7 Redox reactivity of TcVII and SeIV on mineral surfaces

The PhD project of Yanting Qian entitled "*Coupled adsorption and electron transfer interface reactions governing the retention of redox-sensitive Se and Tc on $Fe^{II/III}$ bearing clay minerals*" started in November 2019. The project focuses on interface redox reactions between radionuclides Se/Tc and Fe of the clay mineral. The aim of the project is to quantify and characterise the coupled sorption and reduction mechanism (i.e. electron transfer, reactivity of Fe^{II} & influence of amount Fe^{II}, $Fe^{II/III}$ ratio, and crystallographic location) of these redox sensitive radionuclides by iron bearing clay minerals.

First, clays with different Fe^{III} contents (Wyoming montmorillonite (SWy-2) and nontronite (Nau-2)) were reduced to different degrees (different Fe^{II}/Fe^{III} ratios) by a mixture of sodium Citrate, sodium Bicarbonate, and sodium Dithionite (CBD method) as proposed by Stucki (1984). The reduction degrees were controlled by either varying the dithionite amount and/or the contact time. In order to make sure that the reduction treatment did not alter the clay mineral, the availability of edge and interlayer sites of the reduced

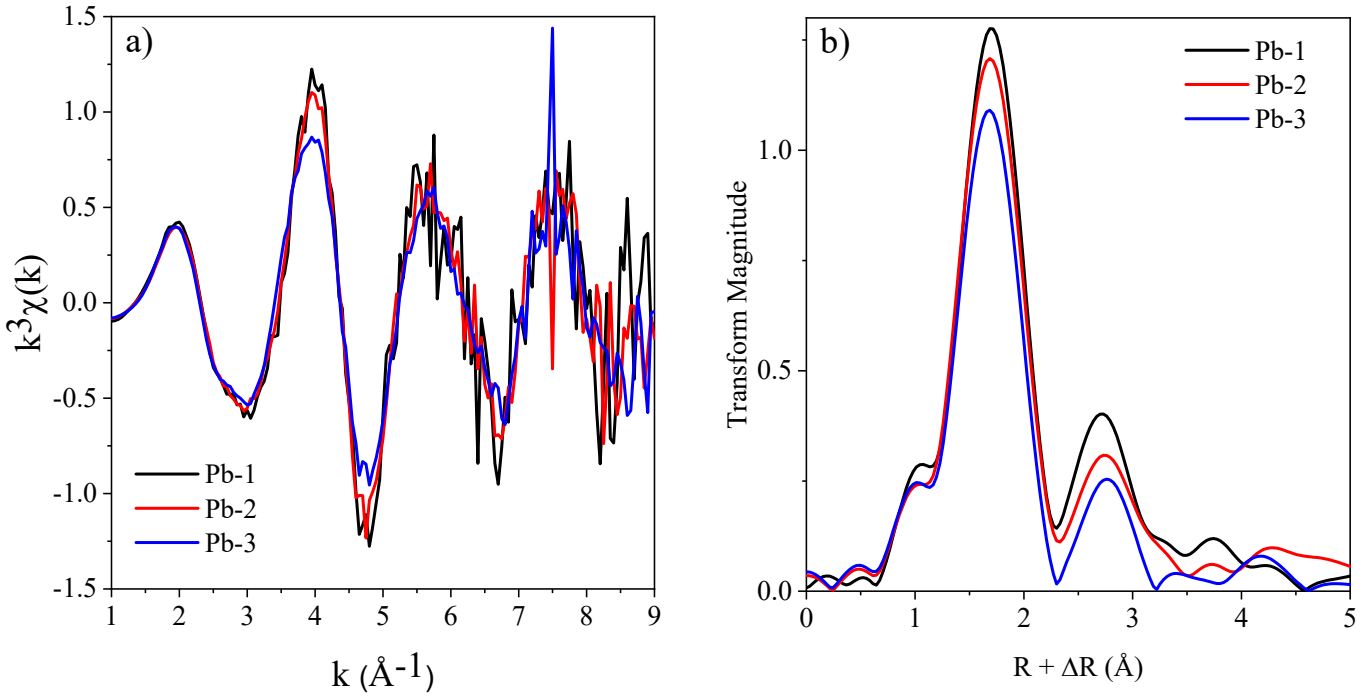

Fig. 3.8: (a) Comparison of k^3-weighted Pb L_{III}-edge EXAFS spectra of Pb treated illite samples and (b) the corresponding RSFs.

and non-reduced Fe-bearing clay minerals were verified by measuring the cation exchange capacity with Ni ethylenetridiamine and performing ^{152}Eu adsorption experiments respectively. Different Fe reduction degrees were observed on SWy and NAu samples by Moessbauer spectroscopy, which is consistent with the amount of the reducing agent added. These investigations are carried in a collaboration with the University of Le Mans. Other clay mineral characterisations, such as XRD and TEM, are also in the progress. These structural and morphological measurements are currently being carried out at BRGM, France.

The sorption of TcO_4^- was measured at pH 5 and 8 in 0.1 M NaCl on the different reduced and non-reduced SWy-2 and Nau-2 samples at S/L ratios ~2 g/L (Fig. 3.9a). For all reduced samples, an increased sorption is observed (up to log R_d of 3.5 L/kg) compared to the non-reduced samples where no sorption at all is observed (Fig. 3.9a). Only high-red Nau-2, which has the highest Fe content and is expected to have the highest reduction degree, shows higher sorption than the other reduced samples (up to 1.5 log units). The reduction products of first Tc loaded high-reduced Nau-2 samples were investigated at 15 K by EXAFS spectroscopy in fluorescence mode at the Rossendorf beamline ESRF in Grenoble. Preliminary data analysis of the EXAFS data suggests that essentially $TcO_2 \cdot nH_2O$ precipitates have formed on high-reduced Nau-2, even at low loadings of 60 ppm (Fig. 3.9b.) With respect to SeO_3^{2-}, pH dependent sorption experiments have been started and first EXAFS measurements were carried out. Data analysis is currently on-going.

3.8 Molecular scale understanding of competitive cation adsorption on swelling clay minerals

In spring 2021, the project entitled *"Molecular scale understanding of competitive cation adsorption on swelling clay minerals"* funded by the Swiss National Science Foundation has started (SNF Nr. 200021-129947). The overall aim of the two-part project is to improve the molecular scale understanding of the retention of common di- and trivalent metal ions onto clay minerals and to foster advanced atomistic simulation approaches as well as spectroscopic techniques for the quantitative description of processes at mineral/fluid interfaces. Part one, carried out by a postdoc, Dr. Fulvio Di Lorenzo, focuses on the synthesis and characterisation of the clay mineral saponite, sorption experiments, thermodynamic modelling and EXAFS spectroscopy. Part 2 of the project, deals with atomistic simulations of the clay systems set up in Part 1 and is carried out by a PhD student, Vasyl Stotskyi.

In Part 1 of the project, pure and Lu/Ni-doped saponites were hydrothermally synthesized following a well-established protocol (Michot & Villiéras 2002, Rinnert et al. 2005). Synthetic analogues of natural swelling clay minerals are very attractive because of their high purity and adjustable composition. Saponites can relatively easily be synthesized under laboratory conditions (Michot & Villiéras 2002, Robert et al. 1993) and allow producing well-defined systems. The starting material was characterised with different techniques such as X-ray diffraction (XRD), infrared (IR) spectroscopy and atomic force microscopy

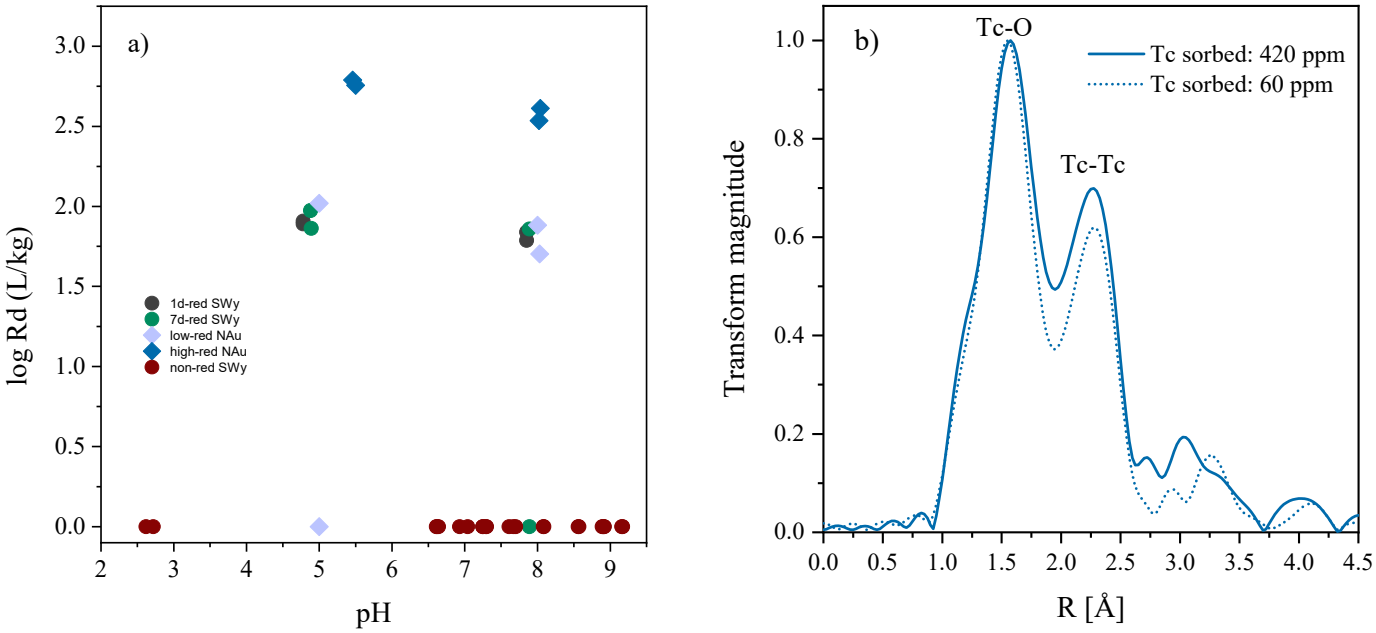

Fig. 3.9: (a) Tc sorption as a function pH on reduced and non-reduced clay minerals. (b) Tc K-edge EXAFS spectrum of Tc sorption on high reduced nontronite (Nau-2) obtained at pH ~7.

(AFM). AFM measurements allow to observe the morphology and therefore the aspect ratio between basal and lateral surface area of the clay mineral particles. For the synthesized pure saponite, this ratio corresponds to 35:65, as shown in Fig. 3.10a. As can be seen in the infrared spectra of the pure magnesian saponite and the Ni/Lu doped saponites (Fig. 3.10b), the increasing amounts of Lu and Ni induce a blue shift (i.e. an increase in the resonance energy of vibrations associated with the bending of Si-O-Si bonds (400-460 cm^{-1}) and the stretching of Si-O bonds 960-990 cm^{-1}, (Madejová et al. 2017). The blue shift is the result of a distortion of the Si-O bonds induced by the substitution of Mg^{2+} in the octahedral layer with Ni^{2+} and Lu^{3+}. First EXAFS measurements took place very recently at the Rossendorf beamline (ROBL) at the ESRF (Grenoble, France), and data analysis is ongoing. Spectra were recorded for aqueous Ni and Lu complexes and Ni doped saponites at 15K and at RT. The aim of these measurements is to compare the structural parameters derived by EXAFS with the structural parameters obtained by DFT in part two.

In part two of the project, a proposal has been successfully submitted to the Swiss National Supercomputing Centre (CSCS). For the coming year, 140'000 node hours have been granted for the project to perform the DFT calculations. To elaborate a robust and reliable atomistic understanding of the processes at the solid-water interface, it is judicious to

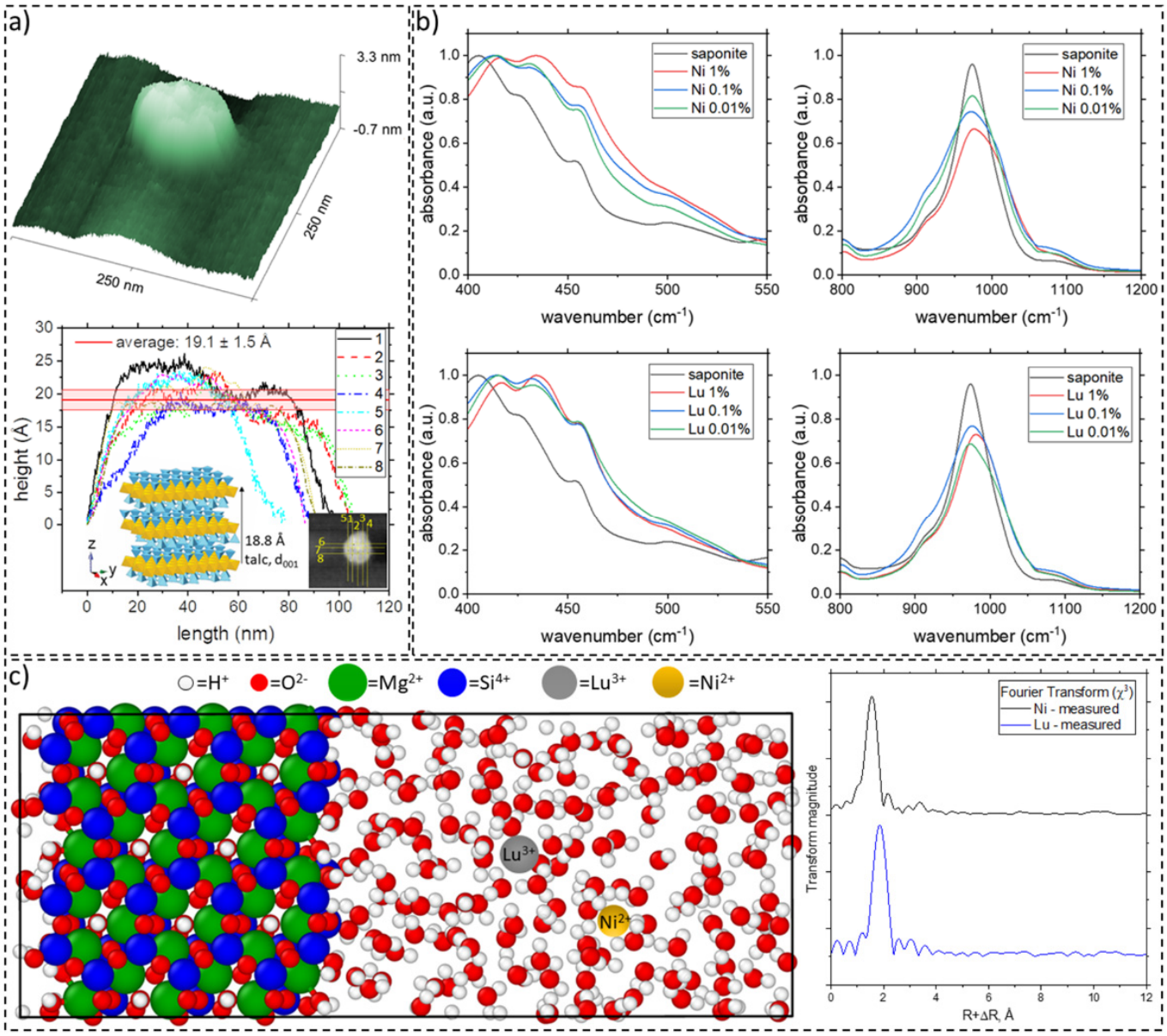

Fig. 3.10: (a) AFM image and geometrical parameters of saponite particles. (b) IR spectra of the pure as well Ni an Lu doped saponites. (c) The information about the coordination environment of the metals in water solution obtained by EXAFS is used to calibrate the Hubbard parameter in the DFT calculations to achieve a better description of the electronic state for transition metals.

verify/validate the consistency of the structural parameters derived from the atomistic calculations by the *in situ* spectroscopic technique EXAFS, which provides the similar structural information. In the first step, the structure of the aqueous Lu and Ni complexes as well as of the Ni/Lu doped saponites is calculated and directly compared to EXAFS data. As a next step towards the interface modelling, the surface energy of the edge saponite (talc) edges is estimated.

3.9 References

Baeyens B., Marques Fernandes M., Bradbury M.H. (2014)
Comparison of Sorption Measurements on Argillaceous Rocks and Bentonite with Predictions Using the SGT-E2 Approach to Derive Sorption Data Bases. Nagra technical report NTB 12-05, Nagra, Wettingen, Switzerland.

Bradbury M.H. & Baeyens B. (1997)
A mechanistic description of Ni and Zn sorption on Na-montmorillonite Part II: modelling. Journal of Contaminant Hydrology 27, 223-248.

Bradbury M.H. & Baeyens B. (2000)
A generalised sorption model for the concentration dependent uptake of caesium by argillaceous rocks. Journal of Contaminant Hydrology 42, 141-163.

Bradbury M.H. & Baeyens B. (2009a)
Sorption modelling on illite Part I: Titration measurements and the sorption of Ni, Co, Eu and Sn. Geochimica Et Cosmochimica Acta 73, 990-1003.

Bradbury M.H. & Baeyens B. (2009b)
Sorption modelling on illite. Part II: Actinide sorption and linear free energy relationships. Geochimica Et Cosmochimica Acta 73, 1004-1013.

Bradbury M.H. & Baeyens B. (2011)
Predictive sorption modelling of Ni(II), Co(II), Eu(IIII), Th(IV) and U(VI) on MX-80 bentonite and Opalinus Clay: A "bottom-up" approach. Applied Clay Science 52, 27-33.

Bradbury M.H. & Baeyens B. (2017)
The development of a thermodynamic sorption data base for illite and the application to argillaceous rocks. PSI Bericht Nr 17-06. Paul Scherrer Institut, Villigen PSI and NTB 17-14, Nagra, Wettingen, Switzerland.

Dähn R., Baeyens B., Bradbury M.H. (2011)
Investigation of the different binding edge sites for Zn on montmorillonite using P-EXAFS – the strong/weak site concept in the 2SPNE SC/CE sorption model. Geochimica et Cosmochimica Acta 75, 5154-5168.

Dähn R., Baeyens B., Marques Fernandes M. (2021)
Zn uptake by illite and argillaceous rocks. Geochimica et Cosmochimica Acta, 312, 180-193.

Gaines G.L.J. & Thomas H.C. (1953)
Adsorption studies on clay minerals. II. A formulation of the thermodynamics of exchange adsorption. Journal of Chemical Physics 21, 714.

Gräfe M., Singh B., Balasubramanian M. (2007)
Surface speciation of Cd(II) and Pb(II) on kaolinite by XAFS spectroscopy. Journal of Colloid and Interface Science 315, 21-32.

Klinkenberg M., Brandt F., Baeyens B., Bosbach D., Marques Fernandes M. (2021)
Adsorption of barium and radium on montmorillonite: A comparative experimental and modelling study. Applied Geochemistry, 135, 105117.

Kulik D.A., Wagner T., Dmytrieva S.V., Kosakowski G., Hingerl F.F., Chudnenko K.V., Berner U.R. (2013)
GEM-Selektor geochemical modeling package: revised algorithm and GEMS3K numerical kernel for coupled simulation codes. Computational Geosciences 17, 1-24.

Madejová J., Gates W.P., Petit S. (2017)
Chapter 5 - IR Spectra of Clay Minerals, in: Gates, W.P., Kloprogge, J.T., Madejová, J., Bergaya, F. (Eds.), Developments in Clay Science. Elsevier, pp. 107-149.

Marques Fernandes M. & Baeyens B. (2019)
Cation exchange and surface complexation of lead on montmorillonite and illite including competitive adsorption effects. Applied Geochemistry 100, 190-202.

Marques Fernandes M. & Baeyens B. (2021)
Application of the “bottom up” approach for the sorption of Cs(I), Co(II), Ni(II), Eu(III), Th(IV) and U(VI) onto sedimentary rocks. Nagra Technical Report NTB 19-04, Nagra, Wettingen, Switzerland.

Marques Fernandes M., Vér N., Baeyens B. (2015)
Predicting the uptake of Cs, Co, Ni, Eu, Th and U on argillaceous rocks using sorption models for illite. Applied Geochemistry 59, 189-199.

Michot L.J. & Villiéras F. (2002)
Assessment of surface energetic heterogeneity of synthetic Na-saponites. The role of layer charge, Clay Minerals, p. 39.

Miron G.D., Kulik D.A., Dmytrieva S.V., Wagner T. (2015)
GEMSFITS: Code package for optimization of geochemical model parameters and inverse modeling. Applied Geochemistry 55, 28-45.

Rinnert E., Carteret C., Humbert B., Fragneto Cusani G., Ramsay J.D.F., Delville A., Robert J.L., Bihannic I., Pelletier M., Michot L.J. (2005)
Hydration of a synthetic clay with tetrahedral charges: A multidisciplinary experimental and numerical study. The Journal of Physical Chemistry B 109, 23745-23759.

Robert J.-L., Beny J.-M., Della Ventura G., Hardy M. (1993)
Fluorine in micas : crystal-chemical control of the OH-F distribution between trioctahedral and dioctahedral sites. European Journal of Mineralogy 5, 7-18.

Saltelli A. (2002)
Sensitivity Analysis for Importance Assessment. Risk Analysis 22, 579-590.

Strawn D.G. & Sparks D.L. (1999)
The Use of XAFS to Distinguish between Inner- and Outer-Sphere Lead Adsorption Complexes on Montmorillonite. Journal of Colloid and Interface Science 216, 257-269.

Stucki J., Golden D., Roth C. (1984)
Preparation and Handling of Dithionite-Reduced Smectite Suspensions. Clays and Clay Minerals - CLAYS CLAY MINER 32, 191-197.

Tennøe S., Halnes G., Einevoll G.T. (2018)
Uncertainpy: A Python Toolbox for Uncertainty Quantification and Sensitivity Analysis in Computational Neuroscience. Frontiers in Neuroinformatics 12.

Zhou X., Lin H., Lin H. (2008)
Global Sensitivity Analysis, in: Shekhar, S., Xiong, H. (Eds.), Encyclopedia of GIS. Springer US, Boston, MA, pp. 408-409.

4 RADIONUCLIDES TRANSPORT AND RETENTION IN COMPACTED SYSTEMS AT FULL AND PARTIAL SATURATION

Van Loon L.R., Glaus M.A., Pfingsten W., Baeyens B., Marques Fernandes M., Frick S., Bunic P., Gimmi T., Churakov S.V., Chen Y. (postdoc), Krejci Ph. (PhD student), Chen P. (PhD student), Zerva D. (PhD student), Owusu J. (PhD student)

4.1 Introduction

The retention of radionuclides by clay minerals in engineered and geological barrier systems is a key process responsible for the radiological safety of a deep geological repository. Reliable sorption data (R_d values) and a mechanistic understanding of sorption and transport processes are thus mandatory for a proper evaluation of the barrier safety function. Sorption studies are mainly performed in batch systems using dispersed clays with a low solid to liquid ratio. In such an experimental setup the composition of the solution can be well controlled (e.g. pH, Eh, concentrations of anions and cations, organic and inorganic ligands) and/or varied in order to study their effect on the sorption. Undisturbed clay rocks, however, are very dense and are characterised by a high solid-to-liquid ratio. It is still an unanswered question whether the data and models derived from dilute dispersed systems can be transferred to the natural consolidated rocks and compacted clays. The aim of this project is to resolve conceptual difficulties in applying the existing sorption models to diffusion in compacted argillaceous rocks.

A second focus of the project deals with the question whether adsorbed ions should be treated as immobile or only partially immobile. These two conceptual model assumptions have fundamental implications for the transport behaviour of ions in compacted systems. In the case of full immobilisation, a pore diffusion model can describe transport whereas in the case of partial immobilisation surface diffusion models have to be applied.

Diffusion studies of gas molecules in fully and partially saturated compacted clay systems were performed in the framework of a Marie Skłodowska-Curie COFUND fellowship, partially financed by the EU. Diffusion parameters for the diffusion of helium (He) in partially saturated compacted bentonite at different degrees of saturation between 0.2 – 0.9 were obtained. In the framework of the Eurad-Gas Project, molecular dynamics simulations are used to investigate the mobility of small volatile inorganic molecules (H_2, Ar, CH_4, He) in compacted montmorillonite under fully and partially saturated conditions.

4.2 Sorption and diffusion in compacted illite

The sorption and diffusion of various radioactive tracers (Co^{2+}, Mn^{2+}, Eu^{3+}) was measured by in-diffusion experiments in compacted illite at varying concentrations of background electrolytes represented by the alkaline earth and transition element series (Ca^{2+}, Mn^{2+}) under different conditions of pH and ionic strength. The ions in background electrolytes are expected to compete for the sorption sites with the tracer elements. The results of these experiments were in good agreement with the predictions of the 2-site protolysis non-electrostatic surface complexation and electrical double layer (2SPNE-SC/EDL) diffusion and sorption model. The competing cations not only exhibit an effect on the sorption behaviour (depending on the type of sites and competing cation involved), but also influence diffusivities of the studied tracers. These observations are interpreted as a competitive effect in the diffuse layer governing the concentrations of mobile cationic surface species. It can be concluded from these experiments that the *in situ* concentrations of alkali earth metal cations in rock pore water have a significant effect on the diffusion of sorbing radiotracers, whereas those of competing representatives of transition metals (e.g. Fe(II)) do not. The situation regarding sorption is just the opposite. These findings are an important basis for a valuable extrapolation of the transport properties of a given radionuclide from model clay mineral systems to intact clay rocks. They shall be applied in the future compilations of diffusion data in data bases for the purpose of site comparison and the general license application of a final site for the geological disposal of radioactive waste. The results of the competition experiments between a $^{57}Co^{2+}$ tracer and Ca^{2+} was recently published (Glaus et al. 2021). Currently, similar diffusion measurements are conducted using small samples of Opalinus Clay in order to better corroborate the transferability of diffusion properties from the illite system to clay rocks. The abrasive peeling method (Van Loon & Mueller 2014) is used to investigate the tracer profiles in these experiments.

4.3 Eurad project FUTURE: Subtask mobility

The activities regarding the evaluation of the new in-/out-diffusion method with membrane-confined diffusion cells made from poly-etherether-ketone (PEEK) were abandoned. The reason is that unexpected tracer amounts (tritiated water) accumulated either in dead volumes in the diffusion cells or in the PEEK

material itself. Even with intensified efforts to avoid the first source of bias, it could not be avoided that larger amounts of tracer were recovered in the out-diffusion phase than can be expected from the capacity provided by the clay porosity. It is therefore concluded that the PEEK material itself is not appropriate for such experiments. Similar experiments with diffusion cells made from stainless steel were successful. Ongoing tests with cylindrical PEEK bodies will show whether a certain uptake of water and tritiated water can be demonstrated also for geometrically simple PEEK shapes.

A series of in-diffusion experiments with $^{57}Co^{2+}$ tracer were initiated using compacted homoionic forms of Na^+-, Li^+- and Cs^+-illite. The results of these experiments (not yet available) shall demonstrate the role of the index cation on the distribution of mobile and immobile surface tracer species near the basal surfaces of the illite and thus to provide more insight in the validity of the 2SPNE-SC/EDL diffusion and sorption model. They will be complemented by measurements of geometrical factors, anion accessibility and cation exchange properties in these clays.

Substantial contributions were made to the state-of-the-art report of the 'mobility' subtask in the Eurad project FUTURE (Maes et al. 2021).

4.4 Diffusion modelling of cations, anions and neutral tracers through Opalinus Clay and bentonite

The comparably large diffusion coefficients of sorbing cations in clays can partly be explained by electrical double layer (EDL) or Donnan models (Glaus et al. 2021). However, clays or clay rocks often exhibit different sorption sites for cations, and it seems that the mobility of cations on these different sites varies (Krejci et al. 2021). A model was thus proposed for multicomponent cation and anion diffusion in clays that combines diffusion of solutes in bulk pore water, in the diffuse layer as well as in the Stern layer. The model was applied simultaneously to diffusion data for various cations and for Cl in bentonite, or in Opalinus Clay. Parameters were chosen based on mineralogy and other independent data as far as possible, but cation mobilities in the Stern layer had to be estimated from the diffusion data. The model was successfully applied to describe simultaneously the diffusive tracer fluxes of HTO, several cations and Cl. The relevance of the contributions of different compartments to the diffusive flux was evaluated for differently sorbing cations under varying geochemical conditions.

4.5 Gas diffusion in partially saturated clay systems

Large amounts of gas will be produced in a repository due to corrosion of steel and degradation of organic waste forms (Diomidis et al. 2016). These gases should be able to migrate through the multi-barrier system to prevent potential pressure build up, which can lead to the loss of barrier integrity. One of the most important parameters controlling the gas dissipation in disposal system of engineered barriers is the diffusive mobility of gaseous species in host rocks. The diffusion mobility of gases in compacted clays and argillaceous rocks at saturated and partially saturated condition is being subject of intensive studies in field and laboratory scale diffusion experiments. These studies provide accurate measurements of macroscopic gas mobility at the sample scale. In the framework of a Marie Skłodowska-Curie COFUND postdoc project the diffusion of gas in partially saturated bentonite was studied. To this end, a new gas-tight equipment (GD-MS) was designed and developed to keep the clay sample at a well-defined saturation degree during a through-diffusion experiment. A detailed description of the equipment is given in Chen et al. (2021a). The diffusion of helium and argon in partially saturated bentonite started in late 2020. All diffusion measurements were carried out on compacted bentonite at a dry-bulk density of 1655 kg m^{-3}. The bentonite sample (diameter 25.6 mm, thickness 9.7 mm) was sandwiched between two stainless steel filters (diameter 25.5 mm, porosity 0.19), and porous endplates were mounted. Each test run consists of two steps: clay saturation and gas diffusion. A corresponding salt solution was placed in both reservoirs to maintain the desired clay S_w (degree of saturation, -). After ventilating the set-up with argon for 10 mins, both reservoirs were filled with argon to an absolute pressure, P_{abs}, of 1.1 bar, and the clay was equilibrated over six weeks. The argon in the high-concentration reservoir was replaced with Varigon® He 50 after saturation, and gas diffusion started at the following initial conditions: low-concentration boundary with argon at P_{abs} of 1.1 bar and the high-concentration reservoir with Varigon® He 50 at the same pressure. Helium and argon partial pressures were measured automatically with the inline mass spectrometry (MS) MiniRUEDI (Brennwald et al. 2016). The same procedure was followed for each saturation condition from 0.19 to 0.98. All diffusion experiments were performed in duplicate. The He concentrations in the high and low reservoirs for the test at a water saturation degree of 0.6 (saturated KCl solution) are shown in Figure 4.1. The experimental method enables a sensitive and accurate measurement of effective diffusion coefficients at varying saturation degrees (S_w = 0.2 – 0.98).

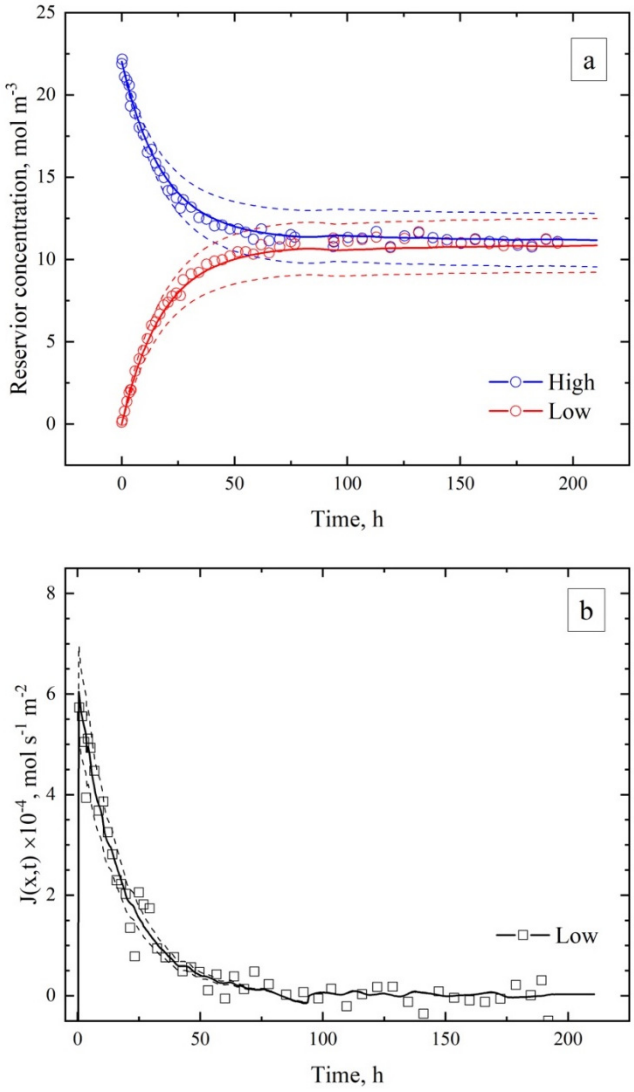

Fig. 4.1: The He concentrations in the high and low reservoirs (a) and the diffusive fluxes (b) in the low-concentration boundary for the test at a water saturation degree of 0.6 (saturated KCl solution). The solid lines represent best-fit D_e values, and the dash lines are the scenarios for applying the lower (-15%) and upper thresholds (+15%) of D_e.

4.6 Self-diffusion of gas molecules in montmorillonite at fully and partially saturated conditions

The molecular mechanism of the gas transport in clay rocks and compacted clay minerals remains unresolved in the macroscopic experiments. Therefore, complementary molecular simulations are conducted to investigate the role of confinement and the pore connectivity in gas transport by combination of the large scale molecular dynamics (MD) simulations and pore scale LB modelling. The initial part of the project has been dedicated to setting up clay mineral systems and parametrizations for classical MD simulation. In particular, the system size dependence and the performance of the different force fields was investigated.

Diffusion coefficient values obtained by MD simulations are influenced by the periodic boundary conditions of the simulation cell, Eq. 4.1 (Holmboe and Bourg (2013) Yeh and Hummer (2004)). The correction term is obtained in bulk simulations, where D_{PBC} is the diffusion coefficient predicted using periodic boundary conditions, D is the diffusion coefficient in the limit $L \rightarrow \infty$, k_B is Boltzmann's constant, ξ is the so-called self-term for a cubic lattice at the room temperature, and η is the viscosity of the medium.

$$D = D_{PBC} + \frac{k_B T \xi}{6\pi\eta L} \qquad \text{Eq. 4.1}$$

Predicted diffusion coefficients of water at different temperatures are shown in Fig. 4.2. In the next step the performance of different force field for gaseous molecules was benchmarked against literature data (Fig. 4.3). The verified potential parameters, and the correction coefficient for periodic boundary conditions, herewith are used to investigate diffusion of gases in saturated and partially saturated clay systems.

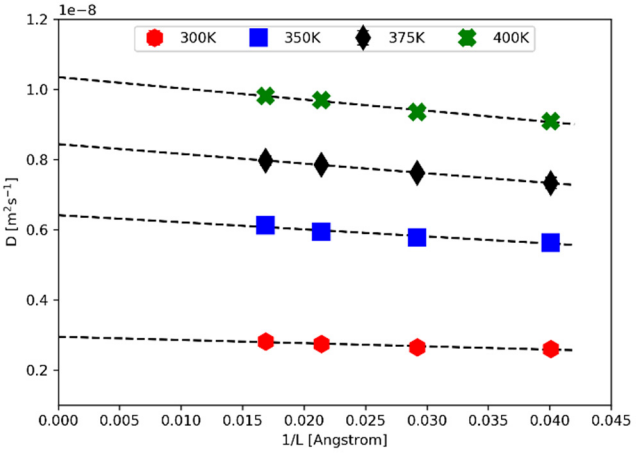

Fig. 4.2: Calculated diffusion coefficient of water D_{PBC} as function of inverse simulation cell size (for simulations with 512, 1331, 3375, and 6859 water molecules) at different temperatures. The size-corrected diffusion coefficient D is determined by linear regression (black line) to 1/L = 0.

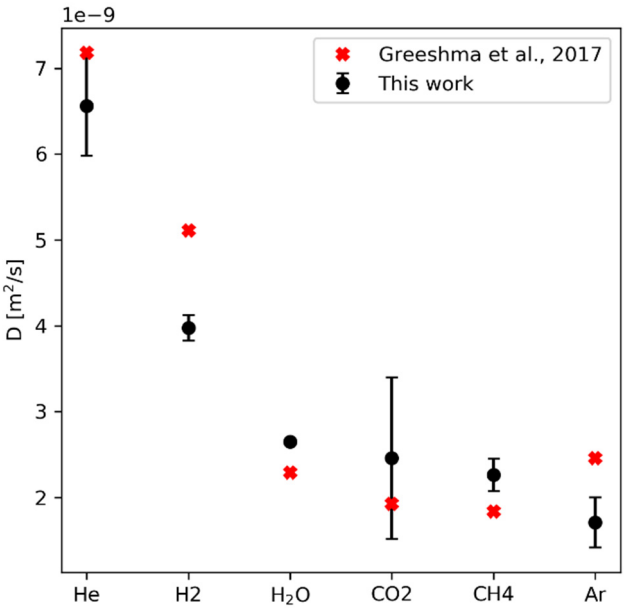

Fig. 4.3: Self-diffusion coefficients of gas molecules dissolved in bulk water. Black points are the D values obtained in this work at T=300K, and red symbols are the data from Greeshma et al. (2017), at T=298K.

4.7 Sorption of Fe(II) on illite

In the framework of a study on the diffusive behaviour of ^{99}Tc in compacted illite, the sorption of Fe(II) on illite has been studied as a function of pH and concentration. Fe(II) is assumed to play a key role in the retention of ^{99}Tc in clay rocks by acting as a reducing agent that reduces Tc(VII) towards lower oxidation states, most probably to Tc(IV). The sorption of Fe(II) on illite was similar to its sorption behaviour on montmorillonite (Soltermann et al. 2014). It could also be observed that Fe(II) on the surface oxidizes to Fe(III). Therefore the 2 sites protolysis non-electrostatic surface complexation/cation exchange model (2 SPNE SC/CE) was extended to account for surface oxidation of Fe(II). The results showed that most of the sorbed Fe(II) was oxidized at pH below 6.5. At pH above 6.5, the oxidation of surface complexes are more possibly, without unambiguously excluding the possibility of precipitation of Fe(III) species. The oxidized surface complexes further react with water forming surface iron hydroxides. Precipitation is possible formed at pH above 6.5 according to the modelling results of the sorption edge (Chen et al. 2021b).

4.8 References

Brennwald M.S., Schmidt M., Oser J., Kipfer R. (2016)
A portable and autonomous mass spectrometric system for on-site environmental gas analysis. Environmental Science and Technology 50, 13455-13463.

Chen Y., Brennwald M.S., Theile J.M., Prasianakis N.I., Mantzaras J., Van Loon L.R. (2021a)
A new experimental set-up for measuring gas diffusivity in compacted bentonite at various water saturation degrees. Submitted for publication in Applied Geochemistry.

Chen P., Van Loon L.R., Marques Fernandes M., Churakov S.V. (2021b)
Sorption mechanism of Fe(II) on illite: sorption and modelling. Submitted for publication in Applied Geochemistry.

Diomidis N., Cloet V., Leupin O.X., Marschall P., Poller A., Stein M. (2016)
Production, consumption and transport of gases in deep geological repositories according to the Swiss disposal concept. Nagra Technical Report NTB 16-03, Nagra, Wettingen, Switzerland.

Glaus M.A., Frick S., Van Loon L.R. (2021)
Competitive effects of cations on the diffusion properties of strongly sorbing trace cations in compacted illite and Opalinus Clay. ACS Earth and Space Chemistry, 5(10), 2621–2625.

Greeshma G., Baptiste D., Gernot R., Michael C.C., Bourg I. (2017)
Hydrophobic Solvation of Gases (CO_2, CH_4, H_2, Noble Gases) in Clay Interlayer Nanopores. The Journal of Physical Chemistry C 121 (47), 26539-26550.

Holmboe M. & Bourg I. (2014)
Molecular Dynamics Simulations of Water and Sodium Diffusion in Smectite Interlayer Nanopores as a Function of Pore Size and Temperature. The Journal of Physical Chemistry C. 118. 1001-1013.

Krejci P., Gimmi T., Van Loon L.R. (2021)
On the concentration-dependent diffusion of sorbed cesium in Opalinus Clay. Geochimica et Cosmochimica Acta, 298, 149-166.

Maes N., Glaus M.A., Baeyens B., Marques Fernandes M., Churakov S.V., Dähn R., Grangeon S., Tournassat C., Geckeis H., Charlet L., Brandt F., Poonoosamy J., Hoving A., Havlova V., Fischer C., Scheinost A.C., Noseck U., Britz S., Siitari-Kauppi M., Missana T., (2021)
State-of-the-Art report on the understanding of radionuclide retention and transport in clay and crystalline rocks. Final version as of 30.04.2021 of deliverable D5.1 of the HORIZON 2020 project EURAD. EC Grant agreement no: 847593.

Soltermann D., Baeyens B., Bradbury M.H., Fernandes M.M. (2014)
Fe(II) uptake on natural montmorillonites. II. Surface complexation modeling. Environmental Science and Technology 48, 8698-8705.

Van Loon L.R. & Mueller W. (2014)
A modified version of the combined in-diffusion/abrasive peeling technique for measuring diffusion of strongly sorbing radionuclides in argillaceous rocks: A test study on the diffusion of caesium in Opalinus Clay. Applied Radiation and Isotopes 90, 197–202.

Yeh I.C. & Hummer G. (2004)
System-Size Dependence of Diffusion Coefficients and Viscosities from Molecular Dynamics Simulations with Periodic Boundary Conditions. The Journal of Physical Chemistry B 2004, 108, 15873−15879.

5 RADIOACTIVE WASTE CHARACTERISATION

Wieland E., Churakov S.V., Curti E., Kulik D.A., Dähn R., Kunz D., Laube A., Marafatto F., Miron G.D., Pfingsten W., Prasianakis N.I., Tits J.

5.1 Introduction

This chapter presents the progress made in research activities on the characterisation of radioactive waste, such as irradiated steel, spent fuel and vitrified high-level waste as well as cemented radioactive waste. The work carried out in this project will provide important information on the source term (e.g. release rates, speciation) of radionuclides released from the waste materials in the planned repositories for high-level waste and spent fuel (HLW/SF) and low- and intermediate-level waste (L/ILW). The source term directly and indirectly influences several parameters of the safety assessment and safety calculations with reference to other repository compartments (near field, geosphere, biosphere). The source term is a time-dependent parameter that is strongly influenced by the temporal evolution of the waste materials as they are subject to chemical degradation processes over time, such as the corrosion of irradiated steel, the (bio)chemical degradation of organic material or the dissolution of SF and HLW. For this reason, investigations of the long-term behaviour of wastes have been identified as an area of research that is important for the Swiss waste management programme in the coming years and possibly beyond the general licence application.

5.2 Carbon-14 Project: Release and speciation of ^{14}C-bearing carbon compounds

Carbon-14 (^{14}C) is a key radionuclide in the safety assessment of a deep geological repository (DGR) for radioactive waste (e.g. Nagra 2002). ^{14}C has been identified in safety assessments (SA) as a dose-determining radionuclide for several reasons: i) due to its long half-life (5700 years), ii) ^{14}C may be present as both dissolved and gaseous species in the repository and host rock, iii) gaseous and dissolved ^{14}C-containing organic compounds migrate readily in the near field and geosphere due to weak interaction with mineral surfaces under alkaline to near-neutral conditions, and iv) ^{14}C may be taken up by humans via food chain. The chemical form of the ^{14}C-bearing carbon species, i.e. either as a dissolved or gaseous ^{14}C-bearing carbon compound, determines the pathway of ^{14}C migration into, and retention by the engineered barrier system (EBS) of a DGR and the surrounding host rock. The chemical form thus determines the long-term contribution of ^{14}C to the dose release from a DGR for radioactive waste. For example, if ^{14}C in the inorganic chemical form can be retained within the EBS of the DGR for a sufficiently long time, it will decay and not contribute to dose release, whereas the radiological consequences must be considered if ^{14}C is released in the dissolved and gaseous form.

In the framework of the ^{14}C project, a corrosion experiment with irradiated stainless steel was set up to identify and quantify the ^{14}C-containing carbon compounds released under anoxic and strongly alkaline conditions that simulate the long-term conditions in a cement-based DGR for L/ILW. The project was started in 2012 with the acquisition of the necessary analytical instruments. In further phases, a compound-specific radiocarbon analysis (CSRA) based on ^{14}C quantification by accelerator mass spectrometry (AMS) as well as the experimental set-up were developed. Finally, the corrosion experiment was started in 2016 and has been sampled regularly since then.

The new analytical development required for this project is based on chromatographic separation techniques (ion chromatography and gas chromatography) in combination with ^{14}C detection by AMS, which allows the determination of ^{14}C-bearing carbon compounds in both the solution and gas phases (Cvetković et al. 2018, Guillemot et al. 2020, Guillemot et al. 2021a). AMS is the most sensitive method for quantifying ^{14}C. Scoping calculations carried out before the start of the experiment had shown that due to the very low corrosion rate of irradiated steel in alkaline solution, the limited sample size and the relatively low ^{14}C inventory of the irradiated steel samples mounted in the reactor, extremely low ^{14}C concentrations are released to the liquid and gas phases.

The project was completed at the end of 2021 with a technical report summarising the experimental results (Guillemot et al. 2021b) and the preparation of a summary report. The latter report presents an overview of the current state of knowledge on the ^{14}C speciation and an overall assessment of the consequences for ^{14}C release from a DGR (Wieland et al. 2021). The following section summarises few conclusions regarding the ^{14}C speciation originating from the degradation of ^{14}C-containing waste materials and highlights possible implications for safety analysis. An extension of the project with further samplings from the reactor containing the irradiated steel nut samples is currently planned.

5.2.1 ^{14}C speciation in DGRs for HLW/SF and L/ILW

The most important sources of ^{14}C in the light water reactors (LWR) operated in Switzerland are nuclear fuel components, reactor core structural materials and reactor coolant. ^{14}C is mainly produced from ^{14}N impurities present in the materials through the nuclear reaction ^{14}N(n,p)^{14}C. A DGR for vitrified high-level waste (HLW) and spent fuel (SF) contains ^{14}C in irradiated steel, Zircaloy cladding and spent fuel. In contrast, ^{14}C in L/ILW is distributed among several waste sorts (Fig. 5.1). The main source of ^{14}C in the already existing and future arising L/ILW is irradiated steel (~ 75 %), while the inventories of other ^{14}C-containing waste materials, such as nuclear fuel components (e.g. Zircaloy) and waste resulting from the treatment of reactor coolants (spent ion exchange resins (IER), filter cartridges) and reprocessing (e.g. $BaCO_3$ crud), are much smaller (Nagra 2014). Some wastes are generated by medicine, industry and research (MIF waste). The ^{14}C inventory in waste from nuclear power plants depend on the type of reactor operated to produce electricity, the material properties (e.g. content of ^{14}N impurities), the operation conditions of the LWRs, the treatment applied to the coolant during reactor operation and reprocessing technology.

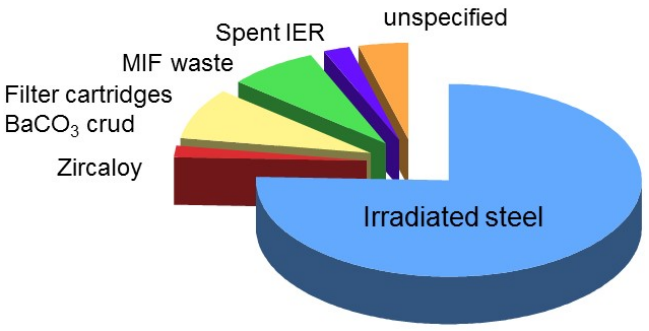

Fig. 5.1: ^{14}C inventories in L/ILW according to MIRAM14 classifications (Nagra 2014). Abbreviations: IER: ion exchange resins, MIF (German): Medizin, Industrie und Forschung.

New experimental information from the literature, in particular from corrosion experiments with irradiated materials (steels, Zircaloy) including also the in-house experiments, provides the basis for a preliminary assessment of the chemical forms of ^{14}C released from HLW/SF and L/ILW repositories (Fig. 5.2).

The current scenarios for the L/ILW repository assume that breaching of the steel drums and concrete containers containing the waste will occur as early as 100 years after closure of the repository (Nagra 2016). Canister breaching will expose the internal components of the canister and the L/ILW to the pore water present in the saturated near field. Upon exposure to water, several processes will control ^{14}C release over time. In contact with water, some ^{14}C is expected to be released immediately from the oxide layers (corrosion layer) of Zircaloy and irradiated steels. These corrosion layers form on the metals exposed to oxic conditions, e.g. during the operation phase of the reactor or interim storage. There is evidence that this ^{14}C fraction is present in both inorganic and organic form, while the proportions of instantaneously released ^{14}C in the gaseous form is comparatively small. It is assumed that the fraction of ^{14}C immediately released from the irradiated metals consists of 50% organic and 50% inorganic ^{14}C. In the long term, however, ^{14}C is mainly released in the gaseous form in accordance with the corrosion rate of the corresponding metal.

^{14}C is also expected to be released immediately from spent ion exchange resins (IER), filter cartridges and crud. The ^{14}C released from spent IERs and filters is likely to be predominantly in the inorganic form, with only a small portion in the organic form. The ^{14}C released from $BaCO_3$ crud is likely to be predominantly inorganic carbon.

It is further assumed that the release of ^{14}C from MIF waste is due to the corrosion of irradiated metals in the waste matrix and only a small portion of the inventory is due to the degradation of small ^{14}C-bearing organic molecules. The largest fraction is inorganic ^{14}C origniating from military and industrial waste. The release of ^{14}C from irradiated metals has already been discussed above. The release of organically bound ^{14}C will occur through microbially-induced decomposition of the ^{14}C-bearing organics, which is assumed to produce equal amounts of gaseous and inorganic ^{14}C. It is proposed that the MIF waste and the unspecified waste are treated in the same way.

In the case of HLW/SF, the corrosion of irradiated steel and Zircaloy as well as the dissolution of SF are the main sources of ^{14}C. The ^{14}C speciation during the corrosion of irradiated steel under HLW/SF disposal conditions is probably identical to that occurring under L/ILW conditions. Note, however, that the corrosion rate of steel under HLW/SF conditions is greater than under L/ILW conditions. Also in the case of Zircaloy, ^{14}C is expected to be released in two phases: i) an immediate release corresponding to the instant release fraction (IRF), partly in organic and partly in inorganic form, ii) slow release of ^{14}C in gaseous form in accordance with the corrosion rate of Zircaloy. In the case of SF, ^{14}C is produced by the activation of the very small amounts of ^{14}N impurities in the matrix, but also by the nuclear reaction ^{17}O(n,α)^{14}C in the UOx and MOx-type fuel matrices. Activation calculations showed that ^{17}O activation in UO_2 contributes ~ 30 % to the ^{14}C inventory of fuel assemblies (Gras 2017).

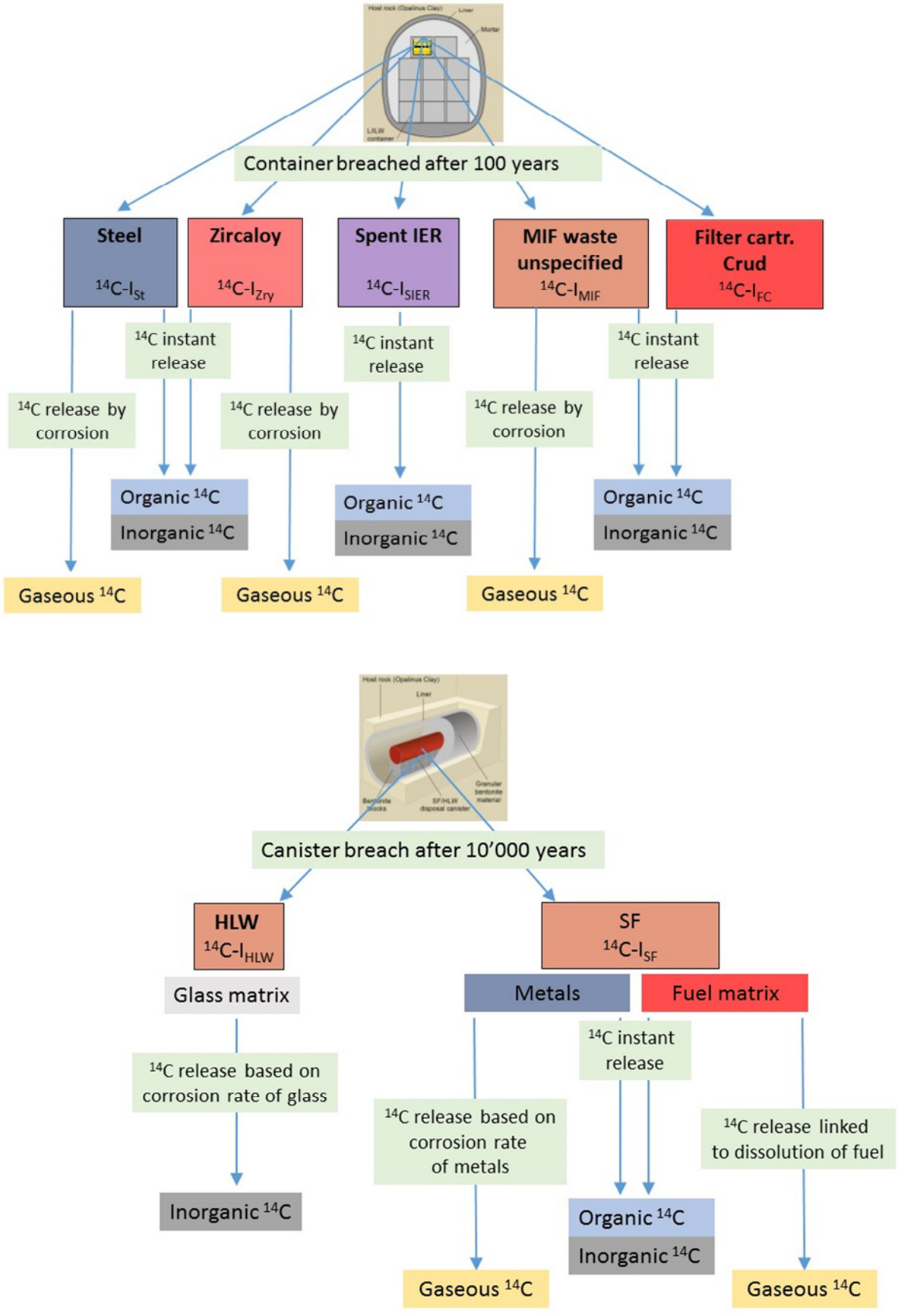

Fig. 5.2: Overview of the chemical forms of ^{14}C released from the repositories for L/ILW (top) and HLW/SF (bottom). "Metals" in HLW/SF refers to mainly Zircaloy and smaller amounts of activated steels and alloys.

It should be noted that the main uncertainties in the concentrations of ^{14}C in fuel as well as the structural materials result from uncertainties in the N contents of the un-irradiated materials. As with Zircaloy and irradiated steels, ^{14}C is assumed to be released from the fuel matrix in two steps, i.e. a rapid release as dissolved ^{14}C-bearing carbon compounds and, over the long time of concern for a DGR, release in gaseous form consistent with the dissolution of SF.

Knowledge of the chemical nature of the carbon compounds acting as ^{14}C carriers to the liquid and gas phases enables a more detailed assessment of their retention in the near field of the L/ILW and HLW/SF repositories. The following compounds have been identified as representing the different chemical forms of carbon: i) ^{14}C-bearing methane for the gaseous form, ii) ^{14}C-bearing carboxylates, such as ^{14}C-bearing formate and acetate, for the organic form, and iii) ^{14}C-bearing carbonate ($^{14}CO_2$(aq) and its bases) for the inorganic form. The retention of the first two chemical forms of carbon in the near fields of the L/ILW and HLW/SF repositories is very weak or non-existent. However, ^{14}C-bearing carbonate is retained through interaction with the backfill materials, i.e. cementitious materials in the L/ILW repository and bentonite in the HLW/SF repository. In addition, strong retention also occurs in the host rock. It is assumed that retention originates from an isotopic dilution with the surface layers of the calcite present in the backfills and the host rock. Thus, ^{14}C in the gaseous and organic form contribute to dose release, while ^{14}C in the inorganic form decays in the repository environment.

5.3 DisCo Project: Spent fuel behaviour

In the framework of the Horizon 2020 EU project DisCo (Modern spent fuel **Dis**solution and chemistry in failed **Co**ntainer conditions) LES was responsible for the development of thermodynamic models to predict the behaviour of doped and non-doped UO_2 fuels from LWRs, both under in-pile and repository conditions. In the last PSI contribution to DisCo, we focused on the evolution of aqueous and secondary solid chemistry at the water-saturated canister-fuel interface.

Thermodynamic equilibrium calculations were carried out to model chemical conditions after canister breaching and intrusion of pore water from the surrounding bentonite buffer material, based on the disposal concept currently foreseen in Switzerland. Two types of models were applied:

(i) A batch equilibration model (BEM) in which progressively increasing amounts of the materials involved (UO_2 spent fuel, Zircaloy, steel canister and other structural materials) react with intruded bentonite pore water filling the open spaces in the canister. The canister is assumed to be partially corroded (50 % Fe and 50 % Fe_3O_4) at the onset of the reaction. The amounts of materials reacted are scaled to the respective corrosion rates.

(ii) A reactive transport model (RTM) simulating thermodynamic equilibrium during counter-diffusion of solutes from saturated bentonite on one side and oxidatively corroding SF on the opposite side ($[U]_{tot}$ = 1 mM) across a 1-dimensional 4 cm long fissure through a failed iron canister. The fissure is filled with saturated bentonite and with fragments of partially corroded canister (50% Fe, 50% Fe_3O_4).

The calculations were carried out with GEM-Selektor using the PSI-Nagra database 12/07 with auxiliary solid solution data (dolomite-ankerite solid solution). In the BEM calculations realistically slow reductive SF dissolution rates and detailed material inventories (McGinnes 2002) were assumed. The focus was on the effect of redox reactions. Specifically, three cases were distinguished:

case 1: both C(IV) and S(VI) reduction are suppressed to simulate conditions in which H_2 is chemically inert and sulphate reduction cannot take place due to lacking microbial activity;

case 2: S(VI) reduction to S(IV), S(0) or S(-II) allowed, but not C(IV) reduction;

case 3: In addition to reduction of S(VI), also reduction of C(IV) to C(0) or (C-IV) is permitted (full thermodynamic equilibrium).

In all three cases the equilibrated solutions were predicted to be more alkaline and more reducing than the initial input bentonite pore water. However, the results indicate large differences in pH and Eh between *case 1* and *case 2/3*. The results obtained for *case 2* and *case 3* are very similar, indicating that sulphate reduction reactions have a major impact on pH and Eh (Fig. 5.3). The following alkaline reaction (anaerobic iron to magnetite conversion coupled with sulphate reduction to pyrite) was identified to be responsible for the initial pH increase from 7.5 to 9.6 in *case 2/3* calculations:

$$5.5\ Fe(cr) + 2\ H_2O + 2\ SO_4^{2-} = 1.5\ Fe_3O_4\ (cr) + FeS_2(cr) + 4\ OH^- \quad (1)$$

The subsequent plateau is explained by the onset of Mg-hydroxide (brucite) precipitation, which compensates the hydroxyl production at fractions of canister reacted (FCR) > 6×10^{-6}.

The aim of the reactive transport simulations (RTM) was to assess whether the environment within a fissured canister would provide sufficient chemical resistance to the propagation of the radiolytic oxidation front into the bentonite buffer. To this end, we simulated solute transport with instantaneous chemical

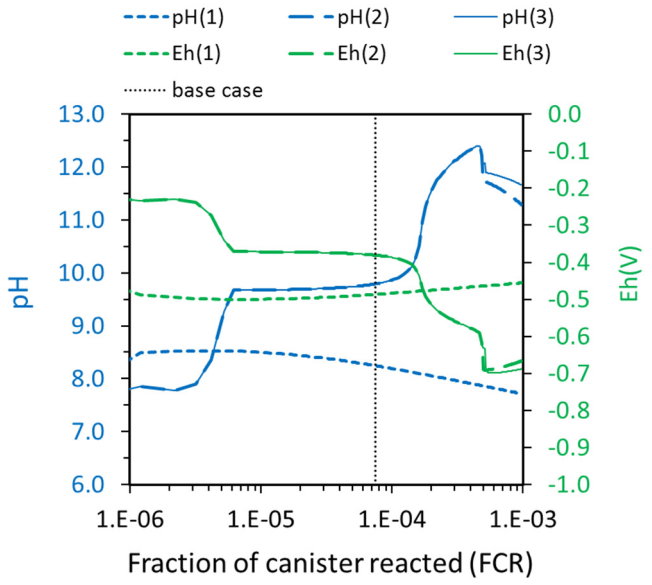

Fig. 5.3: Eh and pH evolution in disposal canisters as a function of reaction progress for the three cases discussed in the text. The vertical dotted line indicates the amount of reacted canister corresponding to one water exchange cycle (estimated to last about 11 years based on a water diffusion coefficient of 6×10^{-11} m^2 s^{-1} in compacted bentonite).

equilibria within a fissure filled with saturated bentonite intersecting a steel canister (Fig. 5.4). On the left boundary, the permeable spent fuel is filled with bentonite pore water containing 1 millimolar uranium. This constant concentration condition simulates the effect of oxidative UO_2 dissolution. On the opposite boundary, bentonite pore water with a background concentration of 1 nanomolar dissolved uranium is assumed. The solutes counter-diffuse and interact with small fragments of canister material inside the fissure, initially consisting of a 50%-50% mixture of metallic iron and magnetite.

The calculations were carried out using the GEM2MT module of GEM-Selektor (v. 3.7.0) for the case 2 scenario, i.e. allowing for sulphate reduction. Due to anaerobic iron corrosion and sulphate reduction, the pH inside the fissure rises abruptly. However, diffusion across both boundaries rapidly reduces the pH, so that a "baseline" at pH between 9.5-10.0 is reached, which slowly recedes with time (Fig. 5.4a). The radiolytic front, represented by the high uranium concentrations at the spent fuel side, slowly moves towards the canister/bentonite interface (Fig. 5.4b). After about half a year, it has propagated about three millimetres away from the canister SF interface. Finally, Fig. 5.5 shows the calculated inventories of secondary solids across the fissure in moles per kg of water. The main minerals formed within the fissure are brucite, pyrite and ankerite-dolomite solid solution. Close to the SF boundary, we predict formation of UO_2, goethite, schoepite and uranophane, while close to the bentonite interface calcite, dolomite-ankerite and goethite are formed. The most abundant secondary solids within the fissure are pyrite and brucite, which are produced according to the following reaction:

$$Fe_3O_4(cr) + 22\ H_2(g) + 6\ MgSO_4(aq) \rightarrow 3\ FeS_2(cr) + 16\ H_2O + 6\ Mg(OH)_2(cr) \quad (2)$$

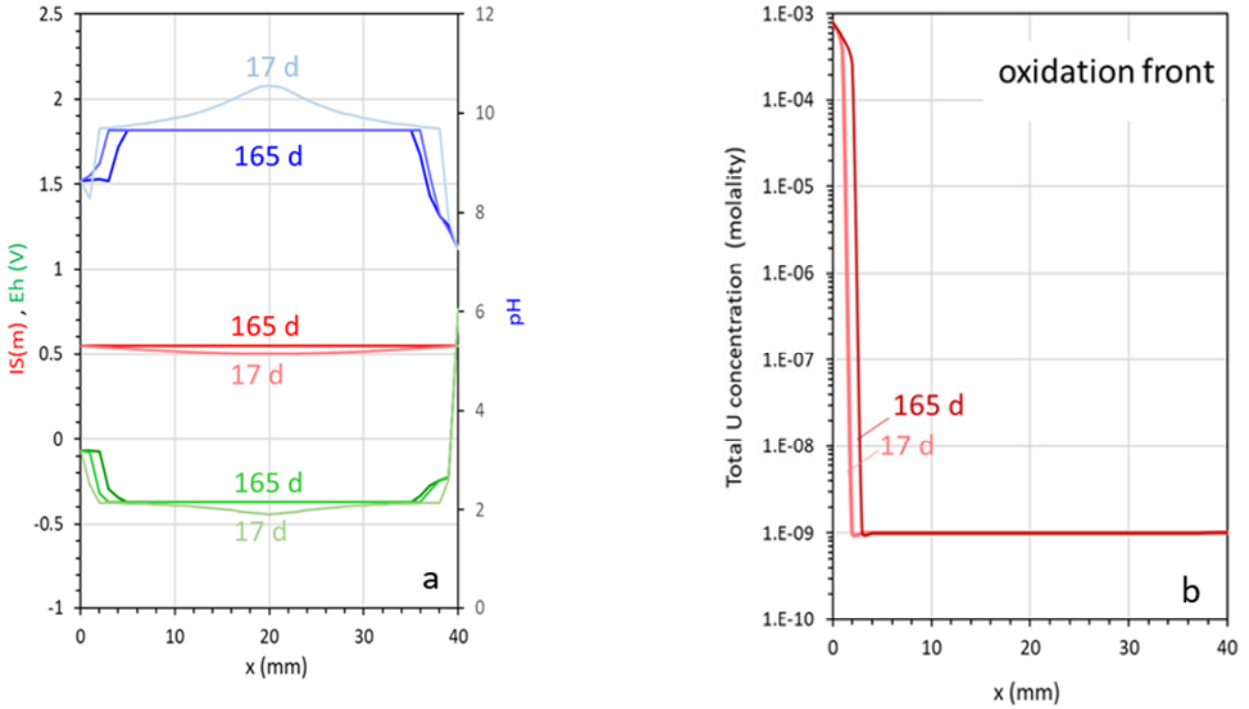

Fig. 5.4: Selected results of RTM calculations: (a) Evolution of pH, ionic strength and Eh across the fissure between 17 and 165 days diffusion time; (b) corresponding evolution of aqueous U concentration.

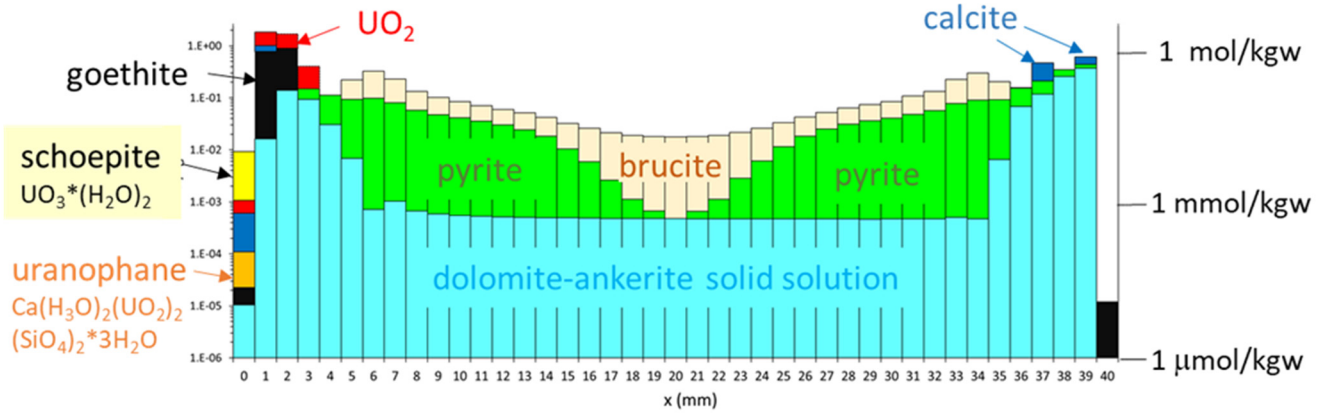

Fig. 5.5: Inventories of solids across the fissure calculated from RTM after 165 days diffusion time. Magnetite (the dominating solid) was excluded from the graph for the sake of clarity.

In other words, hydrogen reduces Fe^{3+} from magnetite and sulphate diffusing from the bentonite, releasing alkalinity, which is neutralized via brucite precipitation.

Normally H_2 is considered to be inert at the expected repository temperatures (40-60 °C), unless appropriate microbial activity or specific abiotic activation mechanisms are operating. In the system under consideration, hydrogen activation mediated by noble metal inclusions has been proven an effective mechanism for consuming radiolytic oxidants produced in a narrow region near the corroding UO_2 surface (Johnson 2005, Broczkowski et al. 2005, Trummer et al. 2010). The aforementioned H_2-consuming reaction would however mostly proceed at some distance from the fuel surface, where analogous abiotic activation mechanism cannot be assumed *a priori* (Truche et al. 2009). Reduction of sulphate and carbonate at low temperatures in the bulk solution according to the overall reactions (1) and (2) would thus probably require microbial mediation, which is unlikely in a γ-radiation field. Moreover, it has been shown that microbial activity in compacted bentonite rapidly decreases as the degree of bentonite compaction increases (Stroes-Gascoyne 2011). These circumstances make microbial mediation of redox processes unlikely, prompting us to consider *case 1* model to be the most realistic of the three examined.

Two main conclusions thus arise from the comparison of the results of the different model variants:

I. Assessment of C(IV)/S(VI) redox kinetics and of H_2 chemical reactivity under *faithful* repository conditions (realistic temperature, radiation field, clay compaction) is critical as these reactions can profoundly affect the water chemistry inside a breached steel canister in contact with UO_2 spent fuel assemblies. It is recommended to carry out dedicated experiments in future in order to determine under which conditions H_2 and S(VI) reduction are activated.

II. Although the mechanism of spent fuel matrix dissolution (reductive vs. oxidative dissolution) profoundly affects the solubility of U and radionuclide release rates, it has only a minor effect on the bulk aqueous and solid chemistry inside the breached canister. This is simply because the chemical environment is buffered by a few reactive major elements. The pH, Eh and major element concentrations will be largely controlled by the redox-sensitive Fe, C and S systems.

5.4 EU Project CORI: Degradation of ISA and cellulose

In the framework of the Horizon 2020 EU project CORI ("Cement-Organics-Radionuclides-Interactions") LES is investigating the possibility of the abiotic degradation of cellulose and isosaccharinc acid (ISA) under the anaerobic, alkaline condition relevant to a cement-based L/ILW repository. This project aims at investigating whether abiotic degradation can occur at elevated partial pressure of H_2 and in the presence of iron as a possible catalyst under alkaline conditions.

In many countries, L/ILW is planned to be stored in DGRs. Prior to storage, the waste is typically solidified in a cement matrix and, after disposal, caverns and access tunnels will be backfilled with cementitious materials that establish highly alkaline conditions in the near field. L/ILW may contain significant amounts of organic materials, such as cellulose-based materials (lab coats, tissues, paper,…), that can degrade over time, possibly resulting in the formation of gaseous products (Nagra 2014). Under the highly alkaline, anaerobic conditions of an L/ILW repository, cellulose degradation will mainly occur through abiotic processes due to limited microbial activity under these

conditions. It was observed that abiotic cellulose degradation processes lead to the formation of mainly α- and β- ISA together with a series of low molecular weight (LMW) organic compounds in smaller amounts (e.g. Glaus et al. 1999). Furthermore, Glaus & Van Loon (2009) found indications that α-ISA might be unstable in the presence of portlandite, which was attributed to the presence of traces of residual oxygen, while an experimental proof could not be given. Thermodynamic modelling further suggests that, under repository conditions, organic compounds are unstable and decompose to produce mainly CO_2(aq), HCO_3^-, CO_3^{2-} and CH_4 (Wieland & Hummel 2015). However, it is uncertain whether complete thermodynamic equilibrium is achieved over the period of concern of a DGR or the organics are metastable and their degradation occurs only very slowly at ambient temperatures. Furthermore, the presence of catalysts, such as metallic Fe or magnetite, are known to catalyse decomposition reactions of LMW organic compounds (e.g. McCollom & Seewald 2003a, b).

Cellulose degradation and α-ISA stability is being investigated in artificial cement pore water (ACW) with pH 13.3 in the presence of portlandite and metallic Fe powder at a temperature of 90°C to accelerate potential degradation reactions. The presence of metallic Fe gives rise to increased H_2 partial pressures caused by progressive corrosion, which creates reducing conditions. The experiments were carried out in gas-tight reaction vessels, i.e. either in autoclaves where only the liquid phase can be analysed at the end of the experiment, or in gas-tight pressure reactors (Versoclave type 3E, Büchi Glas AG) that allow sampling of the liquid and the gas phase during the experiment without opening the reactor. The organic degradation products in the liquid and gas phase were identified and quantified with high performance ion exchange chromatography coupled with mass spectrometry (HPIEC-MS) or gas chromatography coupled with MS (GC-MS), respectively. Total dissolved organic carbon was determined as non-purgeable organic carbon (NPOC).

Stability tests with α-ISA performed in the autoclaves show that its concentration decreased with progressing reaction time during the first 30 days and then remained constant (Fig. 5.6a). It was also observed that the α-ISA concentration decreased significantly with the presence of increasing amounts of metallic Fe (Fig. 5.6b). In contrast, the presence of portlandite did not affect the α-ISA concentration (data not shown). NPOC measurements and the sum of the carbon concentrations of all analysed organic compounds (Σ(C)), both expressed in terms of the ISA-related carbon contents (i.e. C_6), show the same behaviour. Mass balance calculations based on the carbon concentration in solution reveal that the decrease in the α-ISA concentration was significantly higher than the increase in the concentration of the organic degradation products in solution determined by HPIEC-MS. This finding suggests that the decrease in α-ISA could be the result of a sorption process on the corroded metallic Fe surface or a precipitation process rather than ISA

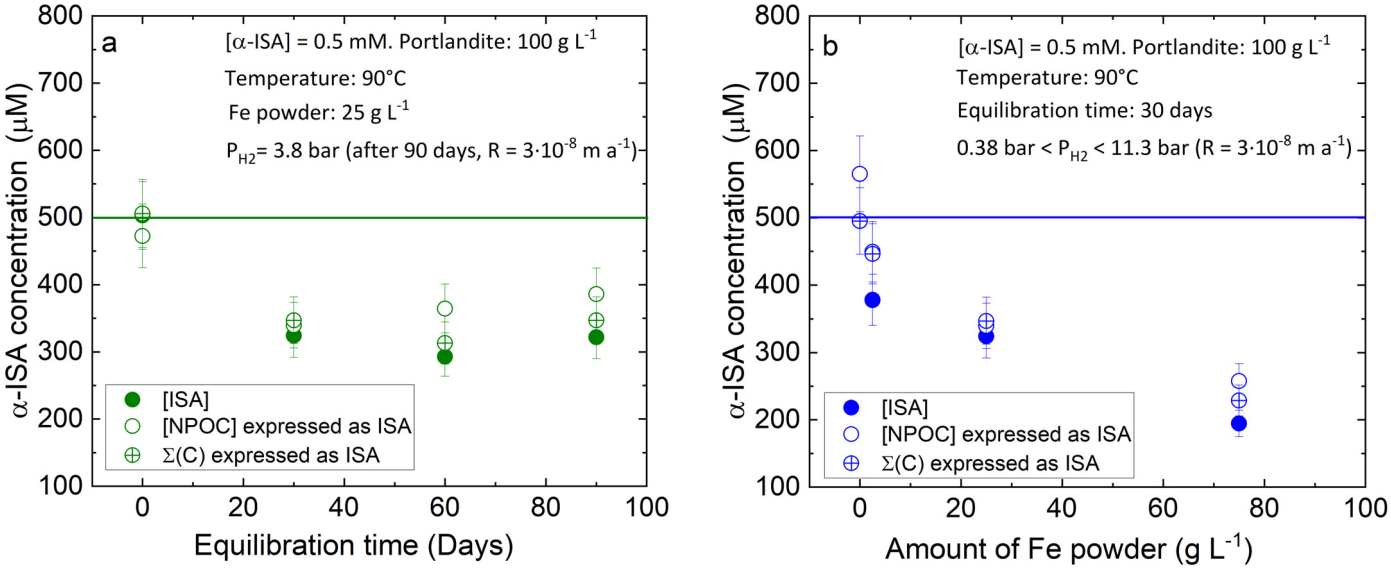

Fig. 5.6: α-ISA stability at 90°C in ACW at pH = 13.3 in the presence of portlandite and metallic Fe powder: (a) α-ISA concentration in ACW as a function of equilibration time in the presence of 100 g L^{-1} portlandite and 25 g L^{-1} metallic Fe powder; (b) Influence of the presence of increasing amounts of Fe powder on the α-ISA concentration in ACW after an equilibration time of 30 days. H_2 partial pressures reported in the figures are calculated assuming an Fe corrosion rate of 3×10^{-8} m a^{-1}, an initial specific surface area of the Fe powder of 0.87 m^2 g^{-1} and a decreasing surface area with progressing corrosion.

degradation. Note, however, that the mass balance is still incomplete as the composition of the gas phase could not be analysed in these autoclave experiments. The experiments are currently repeated in gas-tight Versoclave reactors allowing the gas phase to be analysed in order to test whether α-ISA could be decomposed into gaseous organic components and to complete the mass balance. Additional experiments with cellulose are planned with the aim of testing whether its degradation under the given conditions produces gaseous species in addition to dissolved α- and β-ISA.

5.5 EU Project PREDIS: Development of a digital twin of cemented waste packages

The Horizon 2020 EU project PREDIS ("The pre-disposal management of radioactive waste") aims to develop new methods, processes and technologies for the management of radioactive waste streams during interim storage. The project runs over 4 years (01/09/2020 to 31/08/2024). LES is contributing to the development of digital twins of cemented waste packages by experimental investigations of old waste packages and model development.

In many European countries, radioactive waste from the nuclear and non-nuclear industries as well as from medicine and research is stored in interim storage facilities until a final disposal site is available. The handling of cemented L/ILW has been identified by end-users (waste producers, waste management organisations) as a high priority area where improvements are desirable. In several countries, problems have been documented with already conditioned cemented waste packages that need to be repackaged and reconditioned. These experiences demonstrate the importance of adequate monitoring and control of these waste packages, as well as the need for numerical tools that can predict the behaviour and evolution of the waste packages during the period of interim storage. In addition, in many countries the final disposal of waste is delayed, which implies a prolongation of the interim storage period and appropriate monitoring and control methods of the waste packages.

Within work package 7 (WP 7) of PREDIS, LES is participating in task 7.4, which foresees the development of a digital twin for cemented waste packages during (extended) interim storage. The task consists of three subtasks:

1. Application of numerical geochemical evolution and mechanical integrity models to produce data for training of surrogate models (e.g. neural networks) in the digital twin tool.
2. Experimental characterisation of old cemented waste packages for model validation and calibration.
3. Development of a toolkit "Digital Twin".

LES has taken over the coordination of this task as well as the coordination of subtasks 2 and 3.

The work carried out during the first year mainly consisted of the development of a concept for a digital twin of cemented waste packages during predisposal together with the international partners involved in this task. This concept accounts for the purpose, the structure, the level of detail of the integrated models and the geochemical processes, as well as the main input and output parameters. The definition of a digital twin was reported by Madni et al. (2019): "A digital twin is a virtual instance of a physical system (twin) that is continually updated with the latter's performance, maintenance, and health status data throughout the physical system's life cycle". Such a digital twin is intended for systems where changes occur on the time scale of minutes, seconds, or hours. The physical object could be a car, a building, a bridge, or a jet engine connected to sensors that collect data, which feeds into the digital model. The data collected by sensors is thus continuously used to improve/refine the models that form the digital twin. The user of a digital twin can observe how the physical object behaves in real time in the real world.

In contrast, the evolution of radioactive waste packages during predisposal is controlled by very slow chemical processes whose effects first become visible on the time scales of years to decades. Examples of these slow processes are: organic matter degradation (10^{-3}-10^{-5} mol a^{-1}), corrosion of metals (10^{-5}-10^{-8} mol a^{-1} for aluminium and steel), mineral dissolution/precipitation (10^{-14}-10^{-16} (mol m^{-2} s^{-1}), quartz dissolution; 10^{-7}-10^{-11} (mol m^{-2} s^{-1}), calcite precipitation), ion diffusion in cement (10^{-12} m^2 s^{-1}; gas diffusion 10^{-7} m^2 s^{-1}) (Wieland et al. 2020). Models describing the evolution of radioactive waste packages during interim storage should therefore cover similar time scales. A definition of a digital twin that is more suitable for application to the predisposal of waste packages is therefore the one proposed by Bankhead et al. (2018): "A digital twin is a virtual framework capable of predicting the most important variables of a physical asset, built from several components (or sub-models) integrated into a single powerful tool that enables the end user to predict the outcome of scenarios and to predict the values of outputs as a function of the inputs".

We envisage the digital twin of PREDIS as a user-friendly and accessible tool designed to predict and evaluate different scenarios of waste package evolution during interim storage using specific input information, such as the dimensions, the initial composition of the waste package and the storage conditions (Fig. 5.7). To this end, the tool should take into account a selection of independent and/or coupled processes (usually a few main processes are responsible for most of the changes) related to the evolution of mineralogical and mechanical properties. At this stage, a full thermal-hydrological-mechanical-chemical (THMC) coupling is not foreseen yet. Based on the available waste package data (composition and properties), a set of reference waste types, predefined compositions, and materials will be available for the users to create their desired waste package "recipe" (matrix, waste type, material amount and volume) and run the digital twin tool over the desired time period. In this way, not only can different compositions be tested for potential problems in future waste packages (e.g. use of appropriate aggregates and new phosphate-rich cements), but also different "what-if" scenarios for older waste packages for which only limited data is available.

Numerical models for waste package evolution in the digital twin are computationally very time-consuming and are therefore replaced by surrogate models using machine learning and neural network models. These neural network models are trained with large amounts of chemical, physical and mechanical data of the cemented waste package during its stay in the interim storage facility. Such large amounts of data cannot possibly be measured experimentally. They are provided by a combination of chemical interaction and chemical-mechanical process models that cover the main chemical and physical-mechanical processes potentially taking place in the waste package during interim storage. Examples of chemical processes are cement hydration, carbonation, moisture evolution, alkali-silica reactions (ASR), sulphate attack, gas generation, metal corrosion, etc. The various partners involved in the development of the digital twin will apply such numerical models to calculate the chemical and mechanical evolution of cemented waste packages with different geometries and compositions during interim storage under different storage conditions. The results of these model calculations will then be used to train the surrogate neural network model in the digital twin tool. To validate these numerical models, their results will be compared with a small amount of experimental data from the characterisation of old cemented waste packages stored for many years in an interim storage facility under known conditions. For this purpose, a limited number of 27-year-old, decayed, cemented, 200-litre drums of radioactive waste from the federal interim storage facility in Würenlingen, Switzerland, will be opened and their contents characterised using various geochemical methods. Applications to the Swiss Federal Nuclear Safety Inspectorate (ENSI) for the necessary authorisations are currently being prepared.

The digital twin will be implemented using the Python programming language as a link for the various methods and codes. Python offers a suite of libraries for data processing, statistical analysis, visualisation, and machine learning. Codes written in C++ can be used in Python with the addition of a C++ - Python API for the

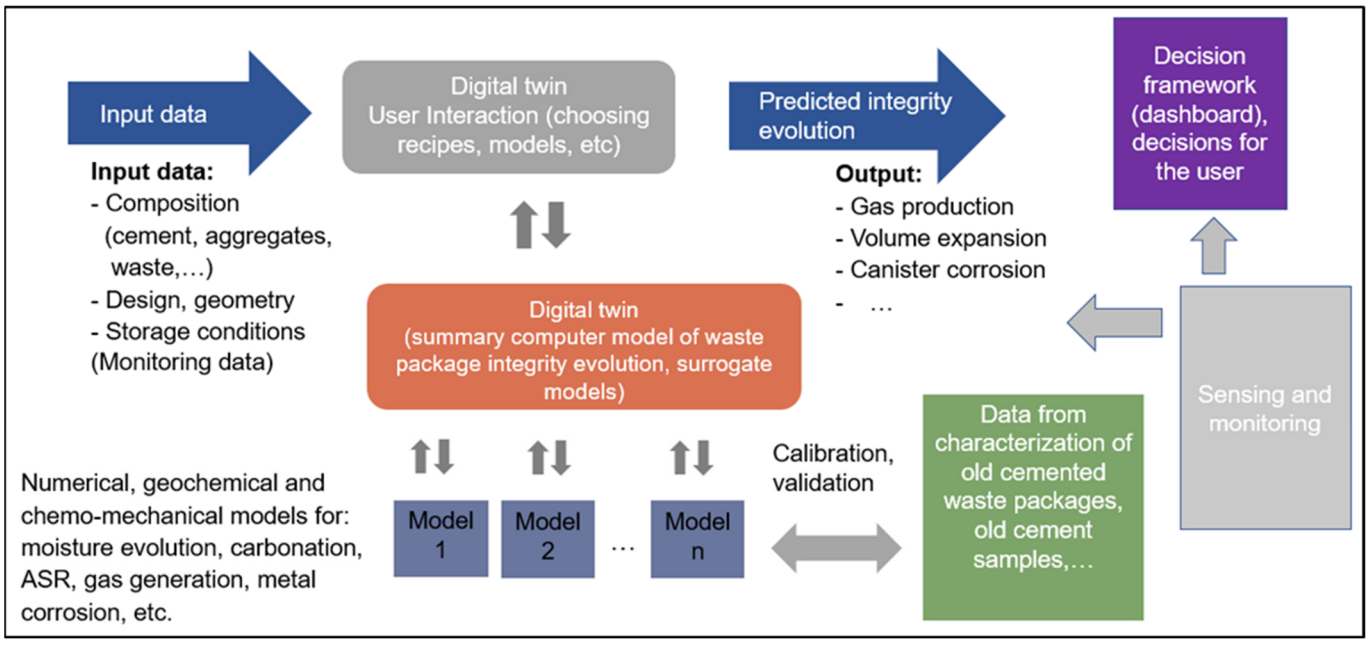

Fig. 5.7: Schematic overview of a digital twin concept for cemented waste package in interim storage.

main functionality using the pybind11 library. Data from other codes that are closed source or available in other programming languages can be exchanged with the digital twin using simple input/output ascii/text files in CSV (comma separated value) format that can be easily converted to other formats and in principle uploaded to an actual database (for large amount of data).

The development environment will be on the LES GeoML.EU service (https://geoml.eu) in JupyterLab environment (https://jupyter.org). This is a web-based, collaborative interactive development environment, supported by common web-browsers. In this environment, simple demonstrative web applications can be easily created and shared between developers and users with no or minimum requirements for installing dependencies.

5.6 X-ray emission spectroscopy mapping for sulphur speciation investigations

Synchrotron-based spectroscopy is a unique tool for the non-destructive physical and chemical characterisation of a wide range of materials. In particular, X-ray absorption spectroscopy (XAS) is sensitive to the valence of elements under investigation and can therefore provide information on the redox speciation of samples, down to trace concentrations. For heterogeneous samples, such as soils, sediments, cement and biological samples, such redox information can be obtained with micrometre spatial resolution by scanning a two-dimensional sample with a micro-focused beam. Knowledge of the redox state of sulphur is important in the context of assessing the redox conditions in radioactive waste. The aim of this project was to develop the basis for a fast X-ray emission spectroscopy (XES)-based method to distinguish the different redox states of sulphur in heterogeneous samples with micrometre spatial resolution.

Because the acquisition of a full XAS spectrum is a time-consuming step, the traditional approach to obtaining spatially resolved redox information involves the acquisition of 2D maps at discrete energies across the absorption edge of the element under investigation (Fig. 5.8, top left). Visual analysis of XAS spectra of reference compounds that are representative of the sample allows to choose the energies at which the maps are collected. The images are aligned using features that do not change at the different energies (to account for the energy-dependent beam shift). Therefore, a simplified spectrum can be obtained from each pixel, which can then be compared with reference spectra as is the case with bulk XAS (Marafatto et al. 2021, Marcus 2010). This XAS approach has a drawback in the alignment step, although it can be applied even at low concentrations of the probed element in the sample thanks to the measurements in fluorescence mode and sensitive detectors. In particular, the approach requires i) the acquisition of features with a good contrast that do not vary across the energies studied, ii) if the instrument crashes during a measurement, the entire map at that energy is often affected and requires manual processing to recover data, and iii) important beam drifts can hinder obtaining information from features at the edge of the map (Fig. 5.8, bottom left).

In this work, a proof of concept study for chemical redox mapping by XES was developed. This approach was made possible thanks to a hybrid pixel-counting detector in a von Hamos setup installed at the Phoenix beamline of the Swiss Light Source (Borca et al. 2016, Forster et al. 2019). We applied this technique to investigate the speciation of sulphur in a synthetic concentrated sample (a mixture of gypsum and pyrite in a pressed pellet) (Fig. 5.8 right). The results were then compared with those obtained with the chemical redox mapping approach by using XAS (Fig. 5.8 left).

The results show that it is possible to obtain the redox speciation of sulphur within one single shot using XES, which has significant advantages over the classical disadvantages of the chemical redox mapping by XAS. The latter method requires multiple maps at different energies. The main advantage to the XES approach is that no image alignment is required, and a “live” indication of the oxidation state is possible with a simple programme. Furthermore, no particular knowledge of the species present in the material is required, as we obtain a full spectrum with a single shot. The data can be fitted to references in a second moment, even away from the beamline, allowing exploratory measurements during beam time with unknown oxidation states.

In summary, XES, which has already been used as a complementary technique in bulk measurements (Glatzel and Juhin, 2014), was used here for the first time for a chemical mapping approach. This technique can be complementary to XAS, since the energies at which X-ray emission occurs are just above the absorption edge of the probed element, without increasing acquisition times considerably, and therefore can be combined with XAS at little to no time expense.

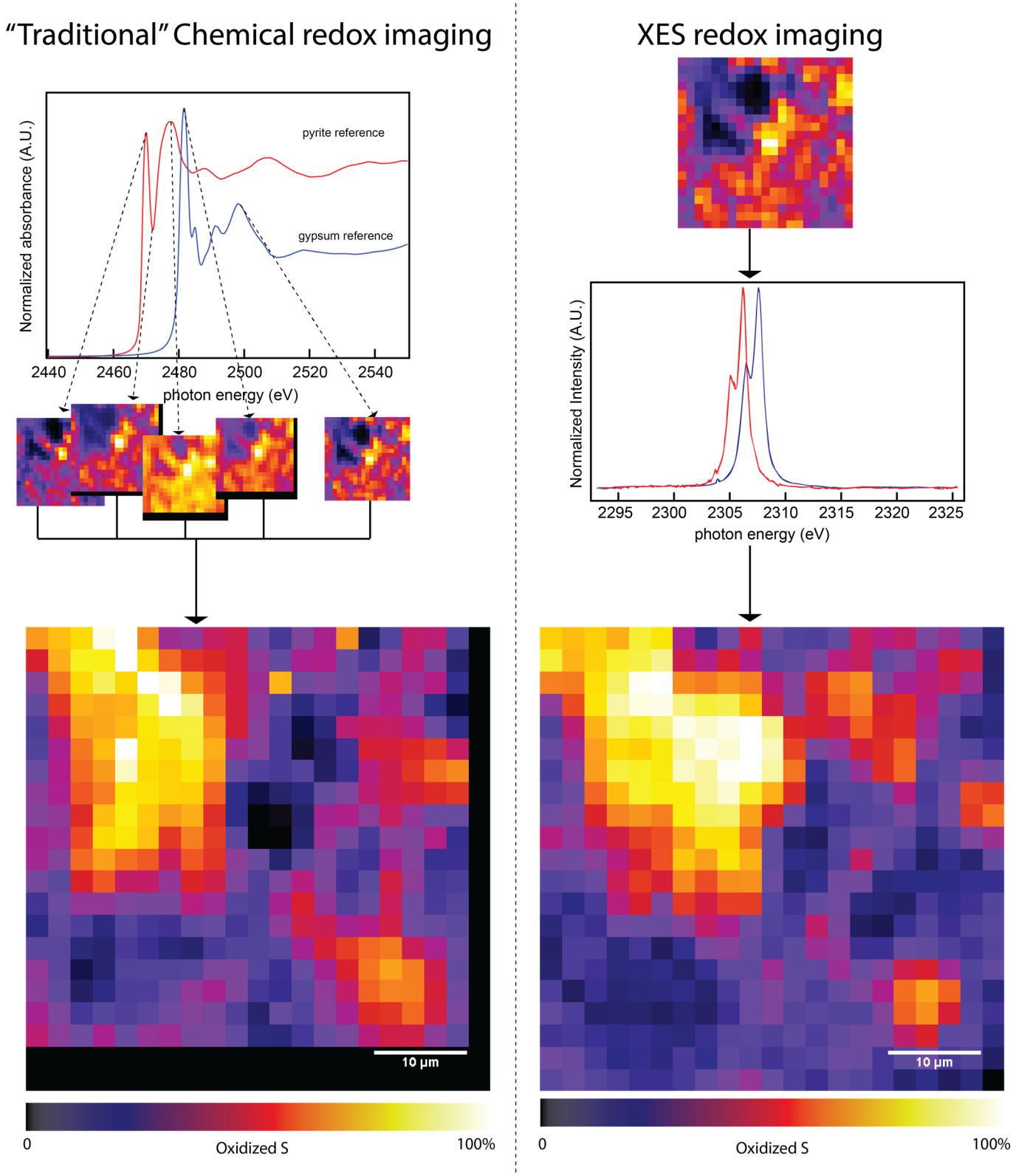

Fig. 5.8: Comparison of the sulphur oxidation state evaluated on given references. Left: the approach for XAS-based mapping: based on distinctive features in the spectra of the species present in the sample, 2D maps are acquired at different energies, aligned and then a linear combination fitting is performed to assess the oxidation state(s) present. Right: when acquiring X-ray emission spectra, a single shot above the absorption edge of S will yield a full spectrum for each pixel, where the individual components can be deconvoluted either by peak fitting or by linear combination fitting with reference spectra.

5.7 References

Bankhead M., Fritsch K., MacDonald-Taylor J., Trivedi D., Ecclestone G., O'Brien W.J. (2018)
Digital twin of nuclear waste management facilities, 8th Int. Work. Reliab. Eng. Comput. "Computing With Confidence".

Borca C.N., Wetter R., Frieh C., Henzler K., Xto J., Janousch M., Huthwelker T. (2016)
PHOENIX: a tender energy beamline for in-situ X-ray studies. Acta Crystallographica A-Foundation and Advances 72, S425-S425.

Broczkowski M.E., Noël J.J., Shoesmith D.W. (2005)
The inhibiting effects of hydrogen on the corrosion of uranium dioxide under nuclear waste disposal conditions. Journal of Nuclear Materials 346, 16-23.

Cvetković B.Z., Salazar G., Kunz D., Szidat S., Wieland E. (2018)
Analysis of ^{14}C-containing compounds released by corrosion of irradiated steel using accelerator mass spectrometry. Analyst 143, 3059-3067.

Forster A., Brandstetter S., Schulze-Briese C. (2019)
Transforming X-ray detection with hybrid photon counting detectors. Philosophical Transactions of the Royal Society A 377, 20180241.

Glatzel P. & Juhin A. (2014)
X-ray absorption and emission spectroscopy. Inorganic Materials Series, 89-171.

Glaus M.A., Van Loon L.R., Achatz S., Chodura A., Fischer K. (1999)
Degradation of cellulosic materials under the alkaline conditions of a cementitious repository for low and intermediate level radioactive waste. Part I: Identification of degradation products. Analytica Chimica Acta 398, 111–122.

Glaus M.A. & Van Loon L.R. (2009)
Chemical reactivity of α-isosaccharinic acid in heterogeneous alkaline systems. PSI Technical Report 08-01.

Gras J.-M. (2014)
State of the art of ^{14}C in Zircaloy and Zr alloys - ^{14}C release from zirconium alloy hulls (D3.1). CAST WP3 Report Deliverable D3.1.

Guillemot T., Salazar G., Cvetković B.Z., Kunz D., Szidat S., Wieland E. (2020)
Determination of ultra-low concentrations of gaseous ^{14}C-bearing hydrocarbons produced during corrosion of irradiated steel using accelerator mass spectrometry. Analyst 145, 7870-7883.

Guillemot T., Cvetković B.Z., Kunz D., Salazar G., Rauber M., Szidat S., Wieland E. (2021a)
Development of analytical methods for the detection of ^{14}C-bearing carbon compounds at ultra-low concentrations. Nagra Working Report NAB 21-03.

Guillemot T., Kunz D., Salazar G., Rauber M., Szidat S., Wieland E. (2021b)
Long-term monitoring of dissolved and gaseous ^{14}C-bearing carbon compounds during anoxic alkaline corrosion of irradiated steel. Nagra Working Report NAB 21-26.

Johnson L.H. (ed.) (2005)
Spent fuel evolution under disposal conditions. Synthesis of results from the EU spent fuel stability (SFS) project. Nagra Technical Report NTB 04-09.

Madni A., Madni C., Lucero S. (2019)
Leveraging digital twin technology in model-based systems engineering. Systems 7(1), 7-13.

Marafatto F.F., Dähn R., Grolimund D., Göttlicher J., Voegelin A. (2021)
Thallium sorption by soil manganese oxides: Insights from synchrotron X-ray micro-analyses on a naturally thallium-rich soil. Geochimica et Cosmochimica Acta 302, 193-208.

Marcus M.A. (2010)
X-ray photon-in/photon-out methods for chemical imaging. TrAC-Trends in Analytical Chemistry 29, 508-517.

McCollom T.M. & Seewald J.S. (2003a)
Experimental constraints on the hydrothermal reactivity of organic acids and acid anions: I. Formic acid and formate. Geochimica et Cosmochimica Acta 67, 3625–3644.

McCollom T.M. & Seewald J.S. (2003b)
Experimental study of the hydrothermal reactivity of organic acids and acid anions: II. Acetic acid, acetate, and valeric acid. Geochimica et Cosmochimica Acta 67, 3645–3664.

McGinnes D.F. (2002)
Model radioactive waste inventory for reprocessing waste and spent fuel. Nagra Technical Report NTB 01-01.

Nagra (2002)
Project Opalinus Clay - Safety Report. Demonstration of disposal feasibility for spent fuel, vitrified high-level waste and long-lived intermediate-level waste (Entsorgungsnachweis). Nagra Technical Report NTB 02-05.

Nagra (2014)
Modellhaftes Inventar für radioaktive Materialien MIRAM 14. Nagra Technical Report NTB 14-04.

Nagra (2016)
Waste management programme 2016 of the waste producers. Nagra Technical Report NTB 16-01E.

Stroes-Gascoyne S. (2011)
Microbiological characteristics of compacted bentonite for a dry density of 1'450 kg/m^3: A literature review. Nagra Working Report NAB 11-05.

Truche L., Berger G., Destrigneville C., Pages A., Guillaume D., Giffaut E., Jacquot E. (2009)
Experimental reduction of aqueous sulphate by hydrogen under hydrothermal conditions: Implication for the nuclear waste storage. Geochimica et Cosmochimica Acta 73, 4824-4835.

Trummer M. & Jonsson M. (2010)
Resolving the H_2 effect on radiation induced dissolution of UO_2-based spent nuclear fuel. Journal of Nuclear Materials 396, 163–169.

Wieland E., Kosakowski G., Lothenbach B., Kulik D.A. (2020)
Geochemical modelling of the effect of waste degradation processes on the long-term performance of waste forms. Applied Geochemistry 115, 104539.

Wieland E. & Hummel W. (2015)
Formation and stability of ^{14}C-containing organic compounds in alkaline iron-water systems: preliminary assessment based on a literature survey and thermodynamic modelling. Mineralogical Magazine 79, 1275–1286.

Wieland E., Miron G.D., Tits J., Curti E., Van Loon L.R. (2021)
Carbon-14 source, speciation and release in a deep geological repository for radioactive waste. Nagra Technical Report (in prep.).

6 THERMODYNAMIC MODELS AND DATABASES

Hummel W., Kulik D.A., Miron G.D.

6.1 Introduction

The aim of this project is to develop thermodynamic models and databases used for the preparation of various reports for the general license applications (RBG). Among others, the solubility and sorption databases and synthesis reports are an important part of the documentation for RBG.

The timely finalisation of the thermodynamic database is essential because the carefully selected unified thermodynamic data provide the basis for pore water definition, for the solubility limits calculations, the development of the sorption databases and simulation of the repository *in situ* conditions. The consistent and consequent use of the approved thermodynamic dataset throughout all types of thermodynamic calculations is of crucial importance.

To support the thermodynamic calculations and to maintain the thermodynamic databases, the GEM Software (GEMS) code collection has been developed at PSI/LES since 2000 by a community team lead by D.A. Kulik. The most recent application of GEMS focuses on the development of a new, flexible and extendable calcium aluminium silicate hydrate (CASH+) sublattice solid solution model describing accurately the stability, solubility, density, water content and mean silicate chain length of CASH phases – the main product of cement hydration.

6.2 Update of the Thermodynamic Data Base (TDB)

A high-quality Thermodynamic Data Base (TDB) is currently in place. This database needs to be kept up to date and to be improved continuously filling remaining gaps where this is safety relevant. The availability of an approved TDB is an essential prerequisite for defining pore water models and for preparing solubility limits and sorption database reports for the next safety assessments related to Nagra's RBG. The latest update of the TDB to "TDB 2020" was carried out in the period 2017 – 2021 with a final document to be published in 2022. New data for radium species were revised and an extended thermodynamic model for CASH+ solid solution was developed in 2021.

6.2.1 Data selection for radium compounds and complexes

Radium isotopes are produced in all actinide decay chains. The longest-lived isotope of radium is Ra-226, a member of the naturally occurring uranium-238 ($4n + 2$) family of radioelements, with a half-life of 1600 ± 7 years. Ra-226 contributes in dose-relevant quantities to the inventory of radioactive waste coming from nuclear power plants. For this reason radium is included into Nagra/PSI TDB 01/01 (Hummel et al. 2002).

The thermodynamic properties of radium included in the Nagra/PSI TDB 01/01 were all taken from Langmuir & Riese (1985). Due to a lack of experimental investigations, all data were based on estimates only, with the notable exception of the solubility product for $RaSO_4$(cr).

Meanwhile, new reviews of the solubility of alkaline earth sulphate and carbonate phases (Brown et al. 2019) have been published, which are considered in the present update of radium data. In addition, this review provides new estimates for aqueous radium species based on data for Mg, Ca, Sr and Ba selected in TDB 2020 (Hummel & Thoenen 2022).

Data estimation can be done by calculating weighted or unweighted means and linear regressions of selected data. In all NEA TDB books, Appendix C (see e.g. Grenthe et al. 1992), weighted mean and weighted linear regression (for SIT analysis) are discussed and recommended, based on the formulae given by Bevington (1969). The estimated standard errors (s) of unweighted means, i.e. $y_{mean} = \Sigma y_i / N$ where N is the number of data,

$$\sigma_{dispersion} \cong s = \sqrt{[\ 1 / (N - 1) \cdot \Sigma\ (y_i - y_{mean})^2\ ]}$$

and unweighted linear regressions $y = a + b \cdot x$

$$\sigma_{dispersion} \cong s = \sqrt{[\ 1 / (N - 2) \cdot \Sigma\ (y_i - a - b \cdot x_i)^2\ ]}$$

solely depend on the dispersion of the data. By contrast, uncertainties derived from weighted means and weighted linear regressions depend on the uncertainties (σ_i) associated with the data but not on their dispersion

$$\sigma_{weights} = \sqrt{[\ 1 / \Sigma\ (1 / \sigma_i^2)\ ]}.$$

Note that the uncertainty bars shown in the following figures for Mg, Ca, Sr and Ba data represent the 95% confidence level, and are denoted here as $2\sigma_i$ for formal consistency with the other σ values discussed in this paragraph.

Bevington (1969) discusses a third option (p. 73): "It often happens that the relative values of the σ_i are

known, but the absolute magnitudes are not. … In such a case the *relative* values of $\sigma_i' \cong \sigma_i$ should be included as weighting factors in the determination of the mean and its uncertainty, and the *absolute* magnitudes of the σ_i can be estimated from the dispersion of the data points around the mean". This leads to the average uncertainty of the data, used for calculating the weighted mean,

$$\sigma_{average} \cong s = \sqrt{ \{ N \cdot \Sigma [(1 / \sigma_i'^2) \cdot (y_i - y_{mean})^2] / [(N-1) \cdot \Sigma (1 / \sigma_i'^2)] \} }$$

or likewise to the average uncertainty of the data, used for calculating a weighted linear regression

$$\sigma_{average} \cong s = \sqrt{ \{ N \cdot \Sigma [(1 / \sigma_i'^2) \cdot (y_i - a - b\, x_i)^2] / [(N-2) \cdot \Sigma (1 / \sigma_i'^2)] \} }$$

All these variants have been explored in this review for estimating values and their uncertainties for aqueous radium species. The examples given here concern radium fluoride, chloride and sulphate complexes.

Radium fluoride complexes

Estimates of thermodynamic data for RaF^+ seem to have never been published. This review used the $\log_{10}K_1°$ and $\Delta_r H_m$ values of Mg^{2+}, Ca^{2+}, Sr^{2+} and Ba^{2+} selected in TDB 2020 (Hummel & Thoenen 2022) and plotted them versus their effective ionic radii in 8-fold coordination (Shannon 1976).

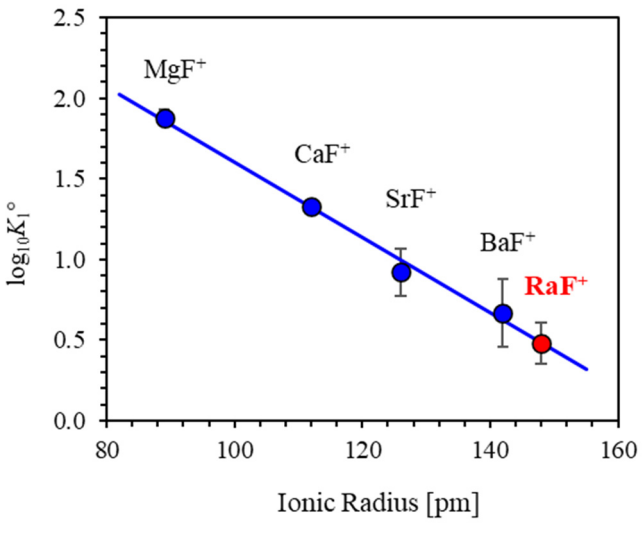

Fig. 6.1: The equilibrium constant $\log_{10}K_1°$ for $M^{2+} + F^- \rightleftharpoons MF^+$ as function of effective ionic radius. Solid line: unweighted regression of all selected data (blue circles). Red circle: $\log_{10}K_1°$ (298.15 K) = 0.48 ± 0.13 calculated from the unweighted linear regression for $Ra^{2+} + F^- \rightleftharpoons RaF^+$.

The $\log_{10}K_1°$ values indicate a negative linear correlation versus their effective ionic radii (Fig. 6.1). The results of an unweighted linear regression are $\log_{10}K_1°$ (RaF^+) = 0.48 with $2\sigma_{dispersion}$ = 0.13. A weighted linear regression results in $\log_{10}K_1°$ (RaF^+) = 0.46 with $2\sigma_{weights}$ = 0.03 and $2\sigma_{average}$ = 0.05. The $\log_{10}K_1°$ values obtained by weighted and unweighted regression analyses are the same within their uncertainties. The results of the unweighted linear regression with the higher uncertainty have been selected by this review.

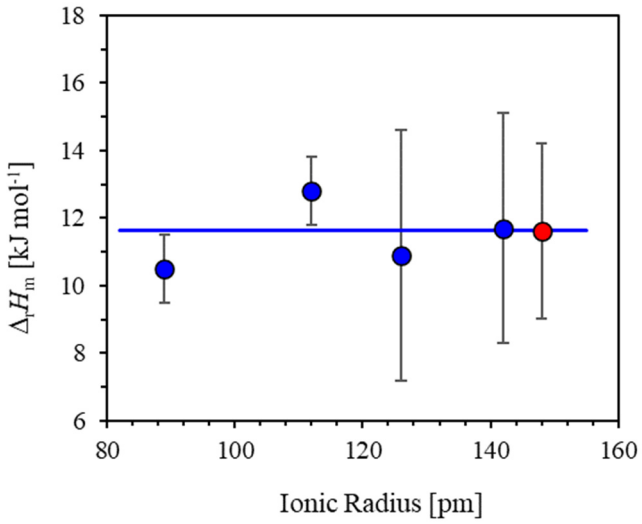

Fig. 6.2: Reaction enthalpy $\Delta_r H_m°$ for $M^{2+} + F^- \rightleftharpoons MF^+$ as function of effective ionic radius. Solid line: weighted mean of all selected data (blue circles). Red circle: $\Delta_r H_m°$ (298.15 K) = (11.6 ± 2.6) kJ · mol^{-1} for $Ra^{2+} + F^- \rightleftharpoons RaF^+$.

The $\Delta_r H_m$ values do not show any correlation with the effective ionic radii (Fig. 6.2) and hence, their means have been calculated. The unweighted mean is $\Delta_r H_m$ (RaF^+) = 11.5 with $2\sigma_{dispersion}$ = 2.0. The weighted mean is $\Delta_r H_m$ (RaF^+) = 11.6 with $2\sigma_{weights}$ = 0.7 and $2\sigma_{average}$ = 2.6. The weighted and unweighted means of $\Delta_r H_m$ are the same within their uncertainties. The weighted mean with the higher uncertainty has been selected by this review

$$\Delta_r H_m \text{ (298.15 K, 1 M)} = (11.6 \pm 2.6) \text{ kJ} \cdot \text{mol}^{-1}$$

No attempt has been made to extrapolate $\Delta_r H_m$ to zero ionic strength. This value is considered as an approximation of $\Delta_r H_m°$ (298.15 K).

Radium(II) chloride complexes

This review does not consider the formation of weak alkaline earth chloride complexes, but includes possible ion interactions in their SIT interaction coefficients. There are no isopiestic or any other experimental data concerning $RaCl_2 \cdot 2H_2O$ which could be used to derive the value for $\varepsilon(Ra^{2+}, Cl^-)$.

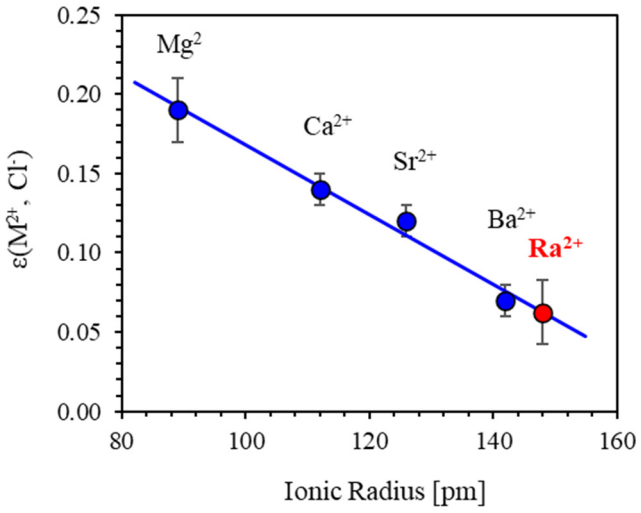

Fig. 6.3: SIT interaction coefficients $\varepsilon(M^{2+}, Cl^-)$ as function of effective ionic radius. Solid line: linear regression of all selected data (blue circles). Red circle: $\varepsilon(Ra^{2+}, Cl^-) = (0.06 \pm 0.02)$ kg · mol^{-1} calculated from the linear regression.

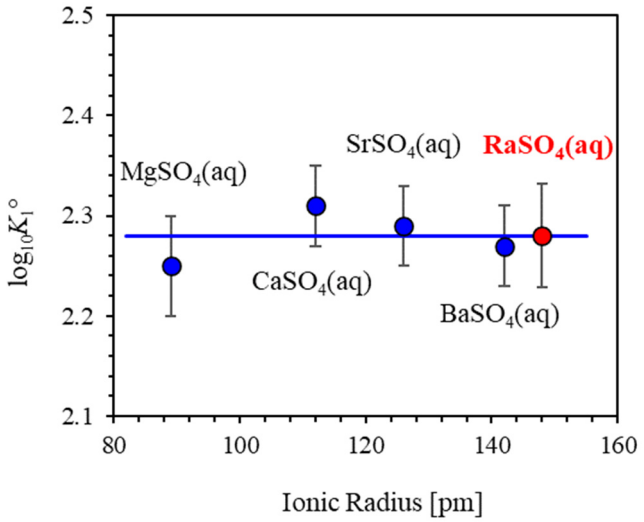

Fig. 6.4: The equilibrium constant $\log_{10}K_1°$ for $M^{2+} + SO_4^{2-} \rightleftharpoons MSO_4(aq)$ as function of effective ionic radius. Solid line: mean of all selected data (blue circles). Red circle: $\log_{10}K_1°$ (298.15 K) = 2.28 ± 0.05 for $Ra^{2+} + SO_4^{2-} \rightleftharpoons RaSO_4(aq)$.

This review used the $\varepsilon(M^{2+}, Cl^-)$ values for $M^{2+} = Mg^{2+}$, Ca^{2+}, Sr^{2+} and Ba^{2+} selected in TDB 2020 (Hummel & Thoenen 2022) and plotted them versus their effective ionic radii in 8-fold coordination (Shannon 1976). The $\varepsilon(M^{2+}, Cl^-)$ values indicate a negative linear correlation versus their effective ionic radii (Fig. 6.3). The results of an unweighted linear regression are $\varepsilon(Ra^{2+}, Cl^-) = 0.063$ with $2\sigma_{dispersion} = 0.016$. A weighted linear regression results in $\varepsilon(Ra^{2+}, Cl^-) = 0.062$ with $2\sigma_{weights} = 0.006$ and $2\sigma_{average} = 0.017$. Hence, the weighted and the unweighted linear regressions give the same results and this review selected:

$$\varepsilon(Ra^{2+}, Cl^-) = (0.06 \pm 0.02) \text{ kg} \cdot \text{mol}^{-1}$$

Radium(II) sulphate complexes

Langmuir & Riese (1985) estimated $\log_{10}K_1°$ and $\Delta_rS_m°$ for the reaction:

$$Ra^{2+} + SO_4^{2-} \rightleftharpoons RaSO_4(aq)$$

by using the Fuoss equation (Fuoss 1958). They obtained:

$$\log_{10}K_1° \text{ (298.15 K)} = 2.75$$

and calculated $\Delta_rH_m°$ from $\Delta_rS_m°$

$$\Delta_rH_m°(298.15 \text{ K}) = 1.3 \text{ kcal} \cdot \text{mol}^{-1} = 5.4 \text{ kJ} \cdot \text{mol}^{-1}$$

This review used the $\log_{10}K_1°$ and $\Delta_rH_m°$ values of Mg^{2+}, Ca^{2+}, Sr^{2+} and Ba^{2+} selected in TDB 2020 (Hummel & Thoenen 2022) and plotted them versus their effective ionic radii in 8-fold coordination (Shannon 1976).

The $\log_{10}K_1°$ values do not show any correlation with the effective ionic radii (Fig. 6.4) and hence, their means have been calculated. The unweighted mean is $\log_{10}K_1°$ ($RaSO_4(aq)$) = 2.28 with $2\sigma_{dispersion} = 0.05$. The weighted mean is $\log_{10}K_1°$ ($RaSO_4(aq)$) = 2.28 with $2\sigma_{weights} = 0.02$ and $2\sigma_{average} = 0.05$. The weighted and unweighted means are numerically identical and have been selected by this review:

$$\log_{10}K_1° \text{ (298.15 K)} = 2.28 \pm 0.05$$

This value is considerably different from the value estimated by Langmuir & Riese (1985) using the Fuoss equation.

The $\Delta_rH_m°$ values indicate a negative linear correlation versus the effective ionic radii (Fig. 6.5). The results of an unweighted linear regression are $\Delta_rH_m°$ ($RaSO_4(aq)$) = 0.6 with $2\sigma_{dispersion} = 7.4$. A weighted linear regression results in $\Delta_rH_m°$ ($RaSO_4(aq)$) = 1.4 with $2\sigma_{weights} = 0.5$ and $2\sigma_{average} = 4.4$. The $\Delta_rH_m°$ values obtained by weighted and unweighted regression analyses are the same within their uncertainties. The results of the weighted linear regression have been selected by this review:

$$\Delta_rH_m°(298.15 \text{ K}) = (1.4 \pm 4.4) \text{ kJ} \cdot \text{mol}^{-1}$$

This value is, within its uncertainty limits, in fair agreement with the value estimated by Langmuir & Riese (1985) using the Fuoss equation.

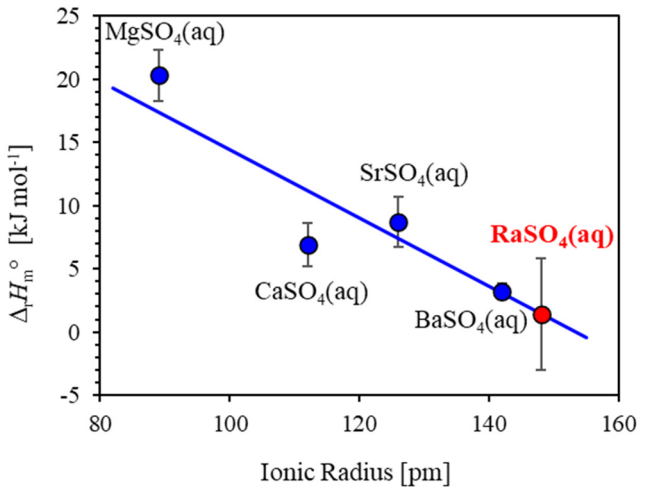

Fig. 6.5: Reaction enthalpy $\Delta_r H_m°$ for $M^{2+} + SO_4^{2-} \rightleftharpoons MSO_4(aq)$ as function of effective ionic radius. Solid line: weighted regression of all selected data (blue circles). Note that the error bars for $BaSO_4(aq)$ are about the same size as the circle. Red circle: $\Delta_r H_m°(298.15\ K) = (1.4 \pm 4.4)\ kJ \cdot mol^{-1}$ calculated from the linear regression for $Ra^{2+} + SO_4^{2-} \rightleftharpoons RaSO_4(aq)$.

6.2.2 A PHREEQC version of the PSI Chemical Thermodynamic Data Base 2020

The thermodynamic data from PSI Chemical Thermodynamic Data Base 2020 (Hummel & Thoenen 2022) is now available in electronic form in the ThermoHub database format (https://thermohub.org/thermohub). To broaden the availability of the critically selected thermodynamic data for the popular PHREEQC geochemical toolkit (https://www.usgs.gov/software/phreeqc-version-3), the database has been converted into the PHREEQC ".dat" file format. The original data in the database are defined in terms of master components (species) and reactions with standard state thermodynamic properties at reference temperature (25 °C) and pressure (1 bar). These reactions can be of the type: formation, dissociation, stepwise complexation, or mineral dissolution. To be used in PHREEQC, the thermodynamic data needs to be redefined in terms of reactions for master species (aqueous), reactions for secondary master species (aqueous) and reactions for dependent (or product) species (aqueous, gaseous and solid).

The process of generating a database of PHREEQC compatible reactions and exporting it into a PHREEQC '.dat' file format, consisting of three main steps, was implemented using the ThermoMatch (https://thermohub.org/thermomatch) thermodynamic data management tool, along with its reactions generator and export to foreign formats modules.

- Step 1: Create a list of chemical elements with the designated primary (PM) and secondary (SM) master species. One primary master species is required per element, and one additional master species for different oxidation state of one element (e.g. for iron, Fe^{2+} is designated as PM and Fe^{3+} as SM).
- Step 2: Using the automatic reactions generator, create all reactions for the SM from the PM, and for the dependent species from PM and SM.
- Step 3: Export the generated reactions dataset into the PHREEQC '.dat' text format using the ThermoMatch export-to-PHREEQC script.

For some of the reactions, the original thermodynamic database contains values for the standard enthalpy and heat capacity that are required for calculation of the reaction equilibrium constant ($\log_{10}K°$) as a function of temperature T (in K). In the reactions generation step, these values are automatically converted into the PHREEQC analytical function coefficients A[1] to A[4]:

$$\log_{10}K°(T) = A[1] + A[2]\cdot T + A[3]/T + A[4]\cdot\log_{10}(T)$$

The produced file can be used for modelling applications in the context of waste repository safety analysis using the PHREEQC geochemical modelling tool.

6.3 Estimations of thermodynamic properties of CASH+ solid solution endmembers and aqueous speciation

The new CASH+ solid solution model (Kulik et al. 2022) has been consistently extended to describe the equilibrium uptake of alkali metals (Li, Na, K, Rb, Cs) and alkaline earth metals (Mg, Sr, Ba, Ra) (Miron et al. 2022) in calcium silicate hydrate phases (C-S-H). The sublattice solid solution model considers several endmembers that do not exist as pure mineral substances, and their thermodynamic properties need to be fitted to experimental data or to be independently estimated. The standard molar Gibbs energy ($G_{298}°$) of endmembers can be accurately fitted to the available uptake and solubility experimental data. To use the model at temperatures different than the reference temperature (25 °C) (Fig. 6.6), the values of standard molar absolute entropy ($S_{298}°$) and standard molar heat capacity ($Cp_{298}°$) are necessary. Such estimates for CASH+ endmembers can be obtained from the so-called volume-based thermodynamics (VBT) equations (Glasser & Jenkins 2016):

$$S°_{298} = V_m 1579 + 6 \ \ (\text{in J}\cdot\text{mol}^{-1}\cdot\text{K}^{-1}) \qquad (1)$$

$$Cp°_{298} = V_m 1465 + 11 \ \ (\text{in J}\cdot\text{mol}^{-1}\cdot\text{K}^{-1}) \qquad (2)$$

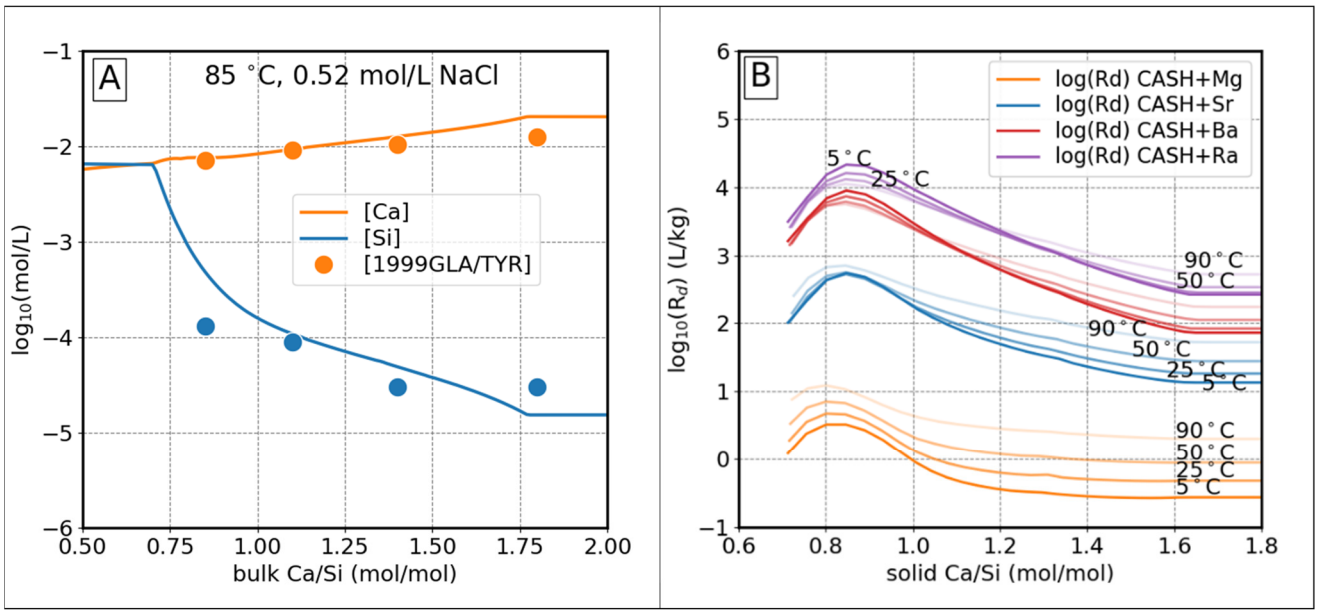

Fig. 6.6: (A) Measured (Glasser et al. 1999) and calculated Si and Ca concentrations in equilibrium with C-S-H in NaCl solution and elevated temperature. (B) The CASH+ model predicts the effect of temperature on the uptake of alkaline earth metals.

where $V_m = 10^{21} \cdot \frac{V^\circ_{298}}{N_A}$ in nm^3/(formula unit), $N_A = 6.022 \cdot 10^{23}$ is Avogadro's number, and the standard molar volume (V°_{298}) is in cm^3·mol^{-1}. The mean absolute errors are 7.4 % and 24.4 % for eqs. 1 and 2, respectively. Values for V°_{298} of endmembers are set such that the CASH+ model reproduces the known values of density as a function of Ca/Si (Kulik et al. 2022).

Exchange reactions were used to estimate properties of CASH+ endmembers for chemical systems where no or little experimental data is available. When parameterizing the uptake of Na and K, the properties of most K endmembers could be estimated from the exchange reactions with Na setting $\Delta_r G^\circ_{298} = 0$. This method was used to estimate the uptake of Li from Na and of Cs and Rb from K.

For the alkaline earth metals, based on the measured distribution coefficient (R_d), an almost linear correlation of R_d was observed when plotted against the crystalline ionic radius at different Ca/Si ratios (Fig. 6.7). From this correlation, the distribution coefficients for other alkaline earth metals can be estimated and used to optimize the stability of the endmembers containing the respective element.

In the C-S-H system, the formation of silicate metal complexes like the calcium-silica neutral complex ($CaSiO_3^0$) may be important. Complexes between other alkaline earth metals (M) and silica may also form at elevated pH. Stability constants for the reaction:

$$M^{2+} + SiO_3^{2-} = MSiO_3^0 \quad (3)$$

of 5.7 ± 0.2, 4.0 ± 0.1 and 2.9 are available in the literature for Mg (Thoenen et al. 2014), Ca (Kulik et al. 2022, Walker et al. 2016), and Sr (Felmy et al. 2003), respectively. These constants show a linear trend with the crystalline ionic radius (r, taken from Marcus (1994)) with the following relation:

$$\log_{10} K^\circ_{298}\ (MSiO_3^0) = -0.0653\ r_{M(pm)} + 10.384\ (R^2 = 0.99). \quad (4)$$

The stability of these complexes decreases from Mg to Sr suggesting that the silica complexes of Ba and Ra should be less stable than that of Sr. Using equation 4, stability constants for $BeSiO_3^0$, $BaSiO_3^0$, and $RaSiO_3^0$ can be calculated to be 8.1, 1.5, and 1.0, respectively.

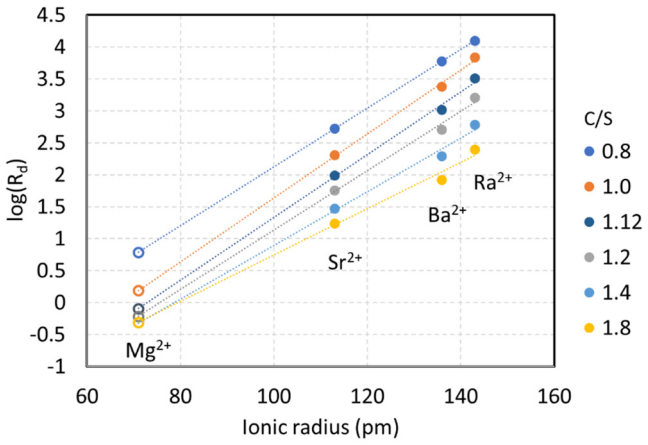

Fig. 6.7: Correlation of R_d with ionic radius (in pm) (Marcus 1994) for Mg, Sr, Ba, and Ra uptake at different Ca/Si ratios in solid. Solid symbols: calculated from the fitted CASH+ model; empty symbols: estimated values.

6.4 References

Bevington P.R. (1969)
Data Reduction and Error Analysis for the Physical Sciences. McGraw-Hill, New York, 336 pp.

Brown P.L., Ekberg C., Matyskin A.V. (2019)
On the solubility of radium and other alkaline earth sulfate and carbonate phases at elevated temperature. Geochimica et Cosmochimica Acta, 255, 88–104.

Felmy A.R., Mason M.J., Gassman P.L., Mccready D.E. (2003)
The formation of Sr silicates at low temperature and the solubility product of tobermorite-like $Sr_5Si_6O_{16}(OH)_2.5H_2O$. Am. Mineral. 88, 73–79.

Fuoss R.D. (1958)
Ionic association III. The equilibrium between ion pairs and free ions. Journal of the American Chemical Society, 80, 5059-5061.

Glasser F.P., Tyrer M., Quillin K. (1999)
The chemistry of blended cements and backfills intended for use in radioactive waste disposal, Environment Agency, Bristol, U.K., 1-378.

Glasser L. & Jenkins H.D.B. (2016)
Predictive thermodynamics for ionic solids and liquids. Phys. Chem. Chem. Phys. 18, 21226–21240.

Grenthe I., Fuger J., Konings R.J.M., Lemire R.J., Muller A.B., Nguyen-Trung C., Wanner H. (1992) Chemical Thermodynamics of Uranium. Chemical Thermodynamics, Vol. 1. North-Holland, Amsterdam, 715 pp.

Hummel W., Berner U., Curti E., Pearson F.J., Thoenen T. (2002)
Nagra/PSI Chemical Thermodynamic Data Base 01/01. Nagra Technical Report NTB 02-16, Nagra, Wettingen, Switzerland, and Universal Publishers, Parkland, Florida, 565 pp.

Hummel W. & Thoenen T. (2022)
The PSI Chemical Thermodynamic Data Base 2020. Nagra Technical Report NTB 21-03, Nagra, Wettingen, Switzerland, in press.

Kulik D.A., Miron G.D., Lothenbach B. (2022)
A structurally-consistent CASH+ sublattice solid solution model for fully hydrated C-S-H phases: Thermodynamic basis, methods, and Ca-Si-H_2O core sub-model. Cem. Concr. Res. 151, 106585.

Langmuir D. & Riese A.C. (1985)
The thermodynamic properties of radium. Geochimica et Cosmochimica Acta, 49, 1593-1601.

Marcus Y. (1994)
A simple empirical model describing the thermodynamics of hydration of ions of widely varying charges, sizes, and shapes. Biophys. Chem. 51, 111–127.

Miron G.D., Kulik D.A., Yan Y., Tits J., Lothenbach B. (2022)
Extensions of CASH+ thermodynamic solid solution model for the uptake of alkali metals and alkaline earth metals in C-S-H, Cem. Concr. Res. 152, 106667, 28 p.

Shannon R.D. (1976)
Revised effective ionic radii and systematic studies of interatomic distances in halides and chalcogenides. Acta Crystallographica A, 32, 751-767.

Thoenen T., Hummel W., Berner U.R., Curti E. (2014)
The PSI / Nagra Chemical Thermodynamic Database 12 / 07, PSI Report 14-04, Paul Scherrer Institut, Villigen, Switzerland, 417 pp.

Walker C.S., Sutou S., Oda C., Mihara M., Honda A. (2016)
Calcium silicate hydrate (C-S-H) gel solubility data and a discrete solid phase model at 25 °C based on two binary non-ideal solid solutions. Cem. Concr. Res. 79, 1–30.

7 FUNDAMENTAL ASPECTS OF MINERAL REACTIVITY AND STRUCTURAL TRANSFORMATIONS

Churakov S.V., Cametti G., Katheras A.S. (PhD student), Karalis K. (postdoc), Roos D.P. (MSc student), Krattiger N. (MSc student)

7.1 Introduction

PSI/LES and the Institute for Geological Science at the University of Bern (UBERN/IfG) collaborate in the field of mineralogy, crystallography and environmental geochemistry. The research field of the Mineralogy group at the University of Bern covers fundamental aspects of mineral dissolution and precipitation mechanisms, chemical aspects of crystal structure stability and temperature driven phase transitions in minerals. The dedicated laboratories operated by the group are equipped with powder and single-crystal diffractometers for structural studies of minerals and an atomic force microscopy laboratory for *in situ* characterisation of mineral surfaces. The experimental studies are widely supported by modelling activities. In particular, we develop and apply numerical methods for investigations of reaction mechanisms and theoretical predictions of mineral thermodynamics. Main research activities are focused on the characterisation of mineral structure transformations in natural and synthetic zeolite materials as result of dehydration and cation exchange processes. These structural characterisation studies are conducted combining single crystal X-ray diffraction experiments, spectroscopic measurements, and molecular simulations. *Ab initio* molecular dynamics simulations are further used to elucidate the mechanism of mineral surface interactions at an atomic-scale. Dedicated laboratory nucleation and re-crystallisation experiments, surface characterisations and geochemical modelling are applied to develop sustainable strategies for heavy metal extraction from contaminated water via carbonates precipitation.

7.2 The interaction of carbonate minerals with aqueous Pb^{2+}

Cation exchange is undoubtedly one of the most exploited properties of natural and synthetic zeolites. The ability to exchange the extraframework (EF) cation content with different cationic species has been widely applied not only for the removal of contaminated substances from water and soils but also to produce zeolite structures with tailored features (Wang & Peng 2010, Chen et al. 2018). Indeed, the modification of the EF cation-content strongly affects the microporous properties, such as sorption, catalytic and dehydration behaviour that can significantly differ from those of the original untreated zeolite.

Pb-exchanged zeolites have received special attention because of their importance in environmental related problems (i.e. removal of Pb from wastewater and food) and their use in industrial processes (Sökmen & Savin 2003).

Pb can occur in form of different species, Pb^{2+}, $Pb(OH)^{+}$, etc. inside the zeolitic pores. In literature, the presence of $[Pb(OH)_x]^{(2-x)}$ species was referred as "overexchange process" (Yeom et al. 1997), referring to the fact that, assuming all Pb to be present only in form of Pb^{2+}, a surplus of positive charges than that necessary to balance the negative charge of the aluminosilicate framework, was detected.

The crystal structure of a natural zeolite, stellerite (**STI**), fully exchanged with Pb, was investigated for the first time. The aim was to (i) determine eventual structural changes induced by the lead uptake; (ii) find out which Pb species are present in the structural voids; and (iii) compare the obtained data with those of the other cationic forms of stellerite. To have a complete and detailed picture of the structural features, we combined Single Crystal X-ray Diffraction (SC-XRD) with Molecular Dynamics (MD) simulations and X-ray Absorption Spectroscopy (XAS).

The combination of these methods showed that, under the used experimental conditions, Pb was uptaken in form of $[Pb(OH)_x]^{(2-x)}$ species. The crystal structure maintained the space group *Fmmm*, characteristic of the natural stellerite. Thus, in contrast to the other known forms of stellerite (i.e. Cd^{2+}-, Ag^{+}-exchanged STI) (Cametti et al. 2019a, Cametti et al. 2019b) no distortion to the monoclinic symmetry was observed. In particular, no variation in the apertures of the channels parallel to [100] occurred because of the Pb-uptake. However, the extra-framework occupants, Pb^{2+}, H_2O and OH^{-}, were characterised by a strong positional-disorder. The latter was resolved and interpreted combining Extended X-ray Absorption Fine Structure (EXAFS) analysis with Molecular Dynamics (MD) simulations.

According to experimental and theoretical data, the first coordination shell of Pb^{2+} is constituted by OH^{-} and H_2O. The average $<Pb\text{-}O_w>$ distance is in agreement with that expected from the sum of atomic radii (ca. 2.52 Å) whereas the $<Pb\text{-}O_h>$ distance is significantly smaller. Short Pb-O distances, in the

range of 2.2 and 2.3 Å, were reported for other Pb-silicate structures where Pb adopts a distorted coordination due to the stereochemical activity of the lone pair electrons. A similar configuration was also observed in our theoretical structure: Each *t-sti-1** cavity hosts one Pb atom, which is mainly surrounded by H_2O, or two Pb atoms coordinated by OH^-, H_2O and (at longer distances) by framework oxygen (Fig. 7.1a). In the first case, the arrangement of Pb resembles that of Ca in natural stellerite, that is Pb coordinated by 5 or 6 H_2O (Fig. 7.1 b). Alternatively, when $Pb_2(OH)_2$ species are present (i.e. more than one Pb atom per cavity) Pb atoms show a sided coordination with OH^- groups (at short distances < 2.3 Å) and H_2O, and longer contacts (> 2.8 Å) with the oxygen of the aluminosilicate framework (Fig. 7.1c).

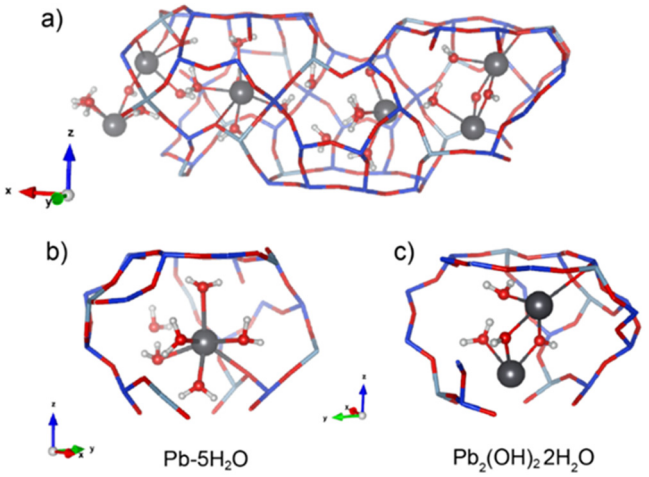

Fig. 7.1: (a) Representative snapshot from MD trajectories showing the distribution of Pb, H_2O, and OH^- within adjacent cages parallel to [100] in Pb-STI structure. Blue and red sticks represent the framework. Dark grey, red and white spheres correspond to Pb, O, and H, respectively. (b,c) Possible local environment of Pb atoms in two adjacent cages.

7.3 Electronic and structural properties of magnetite

Thick-wall steel casks are used to store radioactive waste in deep geological repositories and to prevent the release of radionuclides into the environment. Steel corrodes slowly under repository conditions forming mixed iron oxides, mainly magnetite (Fe_3O_4), and the casks are expected to eventually breach after several ten thousand years. The radionuclides on the other hand can interact with the corrosion products and either form surface complexes or become incorporated into the crystal structures of the iron oxides. The first necessary preparatory step for this theoretical study of these processes is the description of bulk magnetite to prove the validity of our applied computational model.

Under the expected repository conditions, magnetite is a cubic inverse spinel with Fe^{3+} occupying the tetrahedral lattice sites and Fe^{2+} and Fe^{3+} (ratio 1:1) the octahedral sites. Spin polarized crystal structure calculations were performed based on Density Functional Theory (DFT) using the Gaussian Plane Wave (GPW) method as it is implemented in the QUICKSTEP module of the open source CP2K code (Kühne et al. 2020). The generalised-gradient approach (GGA) with the PBE exchange-correlation functional was used and compared for the functional parametrisations of PBE and PBEsol (Perdew et al. 2008). The so-called DFT+*U* method (Liechtenstein et al. 1995) was applied to obtain more accurate results as conventional DFT is known to underestimate the Coulomb repulsion between the localized *3d*-electrons of Fe (Rollmann et al. 2004). To estimate the magnitude of the *U* parameter, several calculations with different values were performed. In a former CP2K investigation (Kéri et al. 2017), the value of 1.9 eV proved to be quite accurate for wüstite and hematite as other iron bearing minerals.

The obtained the crystal structure data (Fig. 7.2, Tab. 7.1) and electronic structure (Fig. 7.3) are in good agreement with the experimental lattice parameters and band gaps of a = 8.3985 Å (Fleet 1986) and band gaps E_g = 1.4 eV (s = + ½) and E_g = 0.1 eV (s = - ½) (Wang et al. 2013). These experimental values were determined above 120 K. In general, the lattice parameter is expected to increase and the band gaps to decrease with higher temperatures, hence the best fitting combination of the model with PBE parametrisation and *U* value is using PBEsol with U = 1.9 eV. This proves the validity of our model and will be applied to future computational investigations on radionuclide uptake mechanisms by magnetite.

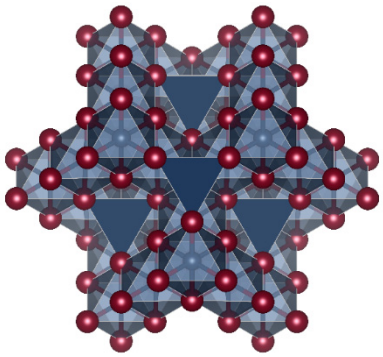

Fig. 7.2: Optimized geometry of cubic unit cell of magnetite viewed along [111] direction. The octahedra (semi-transparent) and tetrahedra (opaque) contain Fe (blue) which are surrounded by O (red).

Tab. 7.1: Lattice parameters and band gaps (s-spin) from DFT+U calculations using different parametrizations for the PBE exchange-correlation functional and different U values.

PBE parametrisation (U value)	Lattice parameters [Å]			E_g [eV]	
	a	b	c	s = + ½	s = - ½
PBE (0.0 eV)	8.4090	8.4085	8.4095	0.8437	0.0448
PBE (1.9 eV)	8.4295	8.4355	8.4325	1.5582	0.2736
PBE (3.8 eV)	8.4020	8.4075	8.4090	2.0571	0.8025
PBEsol (0.0 eV)	8.2910	8.2895	8.2955	0.7192	0.0161
PBEsol (1.9 eV)	8.3235	8.3230	8.3225	1.5491	0.1716
PBEsol (3.8 eV)	8.2970	8.2975	8.3005	2.0571	0.8021

7.4 Electrochemical properties of ASR and C-S-H phases

The alkali-silica reaction (ASR) is one of the most important concrete degradation mechanism severely impairing the service life of the infrastructure. ASR are formed by reaction of silicate minerals in the aggregates with the alkaline pore solution. The atomic structure of ASR products is similar to the natural mineral shlykovite ($KCa[Si_4O_9(OH)]\cdot 3H_2O$), which has a layered structure with SiO_4^{4-} tetrahedrons charge balanced by K^+(or Na^+) and Ca^{2+} in the main layer and by H^+ in the interlayer.

The key mechanism responsible for the ions uptake by C-S-H and ASR is the electrostatic attraction of ions with "charged" surface formed as result of deprotonation of the surface OH groups. The C-S-H and ASR surfaces have very different density of the OH groups and thus should have different sorption affinity and the surface electrokinetic properties as function of pH. These atomic scale differences should result in macroscopically different sorption dynamics and partitioning of calcium and alkali ions between C-S-H and ASR.

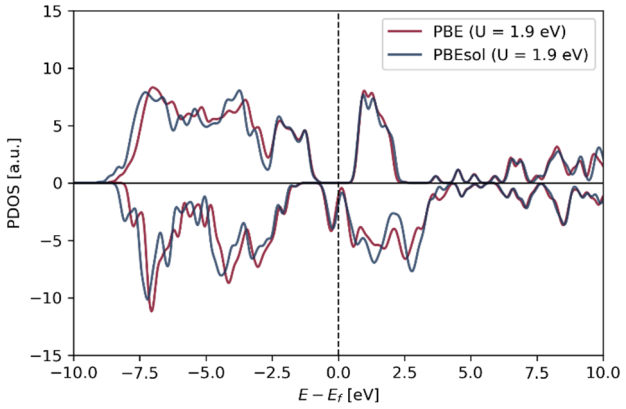

Fig. 7.3: Calculated electronic density of states for magnetite using PBE (red) and PBEsol (blue) exchange correlation potential and U value equal to 1.9 eV.

The primitive model of electrolyte was applied to simulate the titration and sorption behaviour of ASR and C-S-H in Ca^{2+}- and K^+-rich electrolytes. Comparative study of C-S-H and ASR revealed, that differences in the surface sites protonation state, evolution of surface charge and the ion adsorption as function of pH are largely determined by the distinct surface site densities in both phases (Krattiger et al. 2021). The density of the reactive >SiOH surface sites on C-S-H is nearly two times larger than that of ASR. Accordingly, the highest expected surface charge of the C-S-H surface (e.g. 100% deprotonation of surface sites) is the two times the maximal surface charge density expected for ASR. Since the ion adsorption is primary driven by electrostatic interaction of ions with the charged surface sites, the C-S-H has higher sorption capacity than ASR. At equilibrium with the same electrolyte solution C-S-H adsorb more cations and anions per unit of surface area than ASR. The model used in this study suggest that ζ-potential of the ASR remains weakly negative at the most relevant conditions. A close to zero value of ζ-potential is predicted for the system in equilibrium with 20 mM $CaCl_2$ in a wide range of pH. Model suggest that reversal surface potential in ASR-$Ca(OH)_2$ system can occur only at high pH above 12.5. For comparison, C-S-H is expected to have positive surface potential in the 20mM $CaCl_2$ and undergo surface potential reversal in $Ca(OH)_2$ at pH 11.8. The model allows to predict partitioning coefficient of Ca and K between ASR and

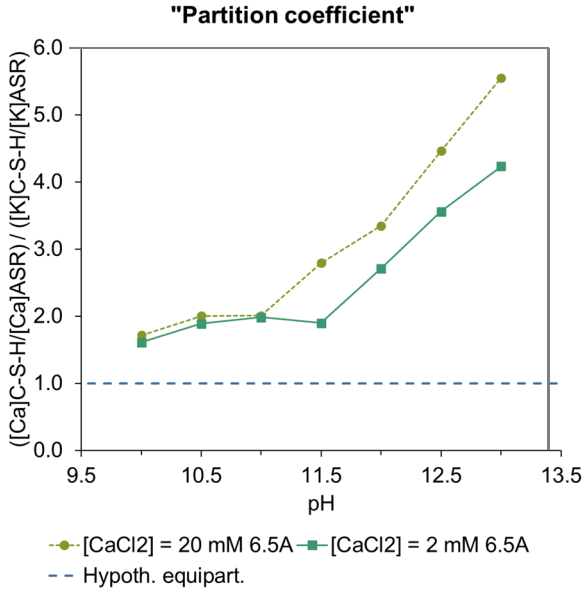

Fig. 7.4: $Ca_{[CSH]}/K_{[CSH]}$:$K_{[ASR]}/Ca_{[ASR]}$ partition coefficient between as function of pH.

C-S-H phases (Fig. 7.4). The calculated partition coefficient $Ca_{[CSH]}/K_{[CSH]}:K_{[ASR]}/Ca_{[ASR]}$ shows that K has higher affinity to ASR and Ca has higher affinity to C-S-H. The coefficient partitioning is constant up to pH 11.5 and linearly increase at higher pH. This behaviour is explained by the fact that ASR surface is almost fully deprotonated at pH above 11.5, surface, whereas the surface charge density of C-S-H continue to increase with pH (Krattiger et al. 2021).

7.5 References

Chen X., Shen B., Sun H., Zhan G. (2018)
Ion-exchange modified zeolites X for selective adsorption desulfurization from Claus tail gas: Experimental and computational investigations. Microporous Mesoporous Materials 261, 227-236.

Cametti G., Scheinost A.C., Giordani M., Churakov S.V. (2019a)
Framework modifications and dehydration path of a Ag^{+}-modified zeolite with STI framework type. Journal of Physical Chemistry C 123, 13651-13663.

Cametti G., Scheinost A.C., Churakov S.V. (2019) Structural modifications and thermal stability of Cd2+-exchanged stellerite, a zeolite with STI framework type. Journal of Physical Chemistry C 123, 25236-25245.

Fleet M.E. (1986)
The Structure of Magnetite: Symmetry of Cubic Spinels. Journal of Solid State Chemistry 62, 75–82.

Kéri A., Dähn R., Krack M., Churakov S.V. (2017) Combined XAFS Spectroscopy and Ab Initio Study on the Characterization of Iron Incorporation by Montmorillonite. Environmental Science & Technology 51, 10585–10594.

Kühne T.D., Iannuzzi M., Ben M.D., Rybkin V.V., Seewald P., Stein F., Laino T., Khaliullin R.Z., Schütt O., Schiffmann F., Golze D., Wilhelm J., Chulkov S., Bani-Hashemian M.H., Weber V., Borštnik U., Taillefumier M., Jakobovits A.S., Lazzaro A., Pabst H., Müller T., Schade R., Guidon M., Andermatt S., Holmberg N., Schenter G.K., Hehn A., Bussy A., Belleflamme F., Tabacchi G., Glöß A., Lass M., Bethune I., Mundy C.J., Plessl C., Watkins M., VandeVondele J., Krack M., Hutter J. (2020)
CP2K: An Electronic Structure and Molecular Dynamics Software Package - Quickstep: Efficient and Accurate Electronic Structure Calculations. The Journal of Chemical Physics 152, 194103.

Krattiger N., Lothenbach B., Churakov S.V. (2021) Sorption and electrokinetic properties of ASR product and C-S-H: A comparative modelling study. Cement and Concrete Research, 146, 106491.

Liechtenstein A.I., Anisimov V.I., Zaanen J. (1995) Density-Functional Theory and Strong Interactions: Orbital Ordering in Mott-Hubbard Insulators. Physical Review B 52, R5467–R5470.

Perdew J.P., Ruzsinszky A., Csonka G.I., Vydrov O.A., Scuseria G.E., Constantin L.A., Zhou X., Burke K. (2008)
Restoring the Density-Gradient Expansion for Exchange in Solids and Surfaces. Physical Review Letters 100, 136406.

Rollmann G., Rohrbach A., Entel P., Hafner J. (2004) First-Principles Calculation of the Structure and Magnetic Phases of Hematite. Physical Review B 69, 165107.

Sökmen I., Sevin F. (2003)
Oxidation of cyclohexane catalysed by metal-ion exchanged zeolites. Journal of Colloid Interface Science 264, 208-211.

Wang S., Peng Y. (2010)
Natural zeolites as effective adsorbents in water and wastewater treatment. Chemical Engineering Journal 156, 11-24.

Wang W., Mariot J.-M., Richter M.C., Heckmann O., Ndiaye W., Padova P.D., Taleb-Ibrahimi A., Fèvre P.L., Bertran F., Bondino F., Magnano E., Krempaský J., Blaha P., Cacho C., Parmigiani F., Hricovini K. (2013)
Fe T2g Band Dispersion and Spin Polarization in Thin Films of Fe3O4(001)/MgO(001): Half-Metallicity of Magnetite Revisited. Physical Review B 87, 85118.

Yeom Y.H., Kim Y., Seff K. (1997)
Crystal structure of zeolite X exchanged with Pb(II) at pH 6.0 and dehydrated: (Pb4+)14(Pb2+)18(Pb4O4) 8Si100Al92O384. Journal of Physical Chemistry B 101, 5314-5318.

8 GEOCHEMICAL ASPECTS OF WASTE MATERIALS AND THEIR DISPOSAL

Eggenberger U., Churakov S.V., Weibel G., Kulik D.A., Miron G.D., Wolffers M. (PhD student), Ingold P. (PhD student), Zappatini A., Dörfler P. (MSc student)

8.1 Introduction

The Competence Center for Secondary Raw Materials at the Institute of Geological Sciences conducts applied research in the field of environmental geochemistry and secondary raw materials. The core competencies of the Center include the topics of recycling management and disposal quality of conventional non-radioactive waste. The sustainable implementation of recycling technologies is waste type specific and requires detailed knowledge of material composition, long-term behavior and process couplings controlling material degradation.

Each year, around 800'000t of bottom ash and 80'000t of fly ash from Municipal Solid Waste Incineration (MSWI fly ash) plants are produced and deposited of at landfills in Switzerland. For metal recycling from municipal solid waste (MSW) incineration residues, detailed knowledge of the formation and composition of the incineration residues (slag, fly ash) is essential to maximise the metal recovery. Under the latest Swiss Waste Ordinance (Swiss Confederation, 2016), the requirements for residues have been increased and metal recovery must be implemented by 2026 for MSW fly ash. In addition to metal recovery, the behaviour of residues in landfills is a key component of our research. Furthermore, studies are also being carried out to assess the potential to reuse the residues in the materials cycle.

8.2 Assessing the heavy metal recoverability of MSWI fly ashes along the flue gas cooling path

MSWI fly is composed of boiler- and electrostatic precipitator ash and shows significant concentrations of heavy metals (e.g. Zn, Cu, Cd, Pb, Sb). From 2026 onwards, there will be an obligation for heavy metal recovery from Swiss MSWI fly ashes. Acid leaching (Bühler & Schlumberger 2010) represents the state-of-the-art method for heavy metal recovery prior to deposition. However, it has not yet been legally determined whether the obligation for treatment also applies to the boiler ash. An alternative disposal route would be the disposal together with the bottom ash. The available data for boiler ashes is very limited, thus their metal recovery potential has not yet been explored. Thus, detailed chemical and mineralogical characterisation was performed on the different fly ash fractions that form along the flue gas path (empty pass-ash (EA), boiler ashes (BOA) and electrostatic precipitator ash (ESPA), *Fig. 8.1*). Using a broad combination of methods (XRF, XRD, SEM), the ashes from six Swiss MSWI plants were characterised with respect to the chemical and mineralogical composition of major- and minor phases. Key parameters to estimate the recovery potential are the contents of recoverable heavy metals and the extractability of the ashes. The focus was therefore laid on matrix phases affecting leachability (e.g. alkalinity, oxidation-reduction potential), as well as on the distribution and concentration of recoverable heavy metals and their binding forms. In order to estimate the need for metal recovery before landfilling, the contents of non-mobilizable pollutants such as Sb was also recorded along the flue gas path.

EA and BOA showed comparable bulk chemical and mineralogical composition (*Fig. 8.2*) and are composed of two significantly different materials: the airborne ash particles (quenched melt droplets and refractory particles) and deposits formed on heat exchanger surfaces. It is mainly the deposits that contribute to the elevated heavy metal concentration, explained by the well-developed, large (Na,K)-$PbSO_4$ crystals and the Zn-bearing matrix sulfates (*Fig. 8.3*). The variation in the amount and chemical composition of the deposits controls the fluctuations in the bulk composition of EA and BOA. The ESPA shows different chemical and mineralogical characteristics than EA and BOA. The ESPA is enriched in the more volatile metals Zn, Pb, Cu, Cd, which are mainly present as chlorides and sulfates. The high content of salt-bound and thus easily soluble heavy metals together with the lower alkalinity and oxidation-reduction potential indicates, that ESPA has a better leachability compared to EA and BOA. These observations suggest that individual treatment of ESPA has higher potential for heavy metal recovery. Comparing the EA and BOA, however, no significant differences could be found in the parameters affecting extractability.

The obtained results (full text in Wolffers et. al. 2021) provide important insights into the formation of the different ash fractions and its geochemical characteristics. The data may serve as basis for re-evaluating disposal routes of ash fractions with poor extraction properties.

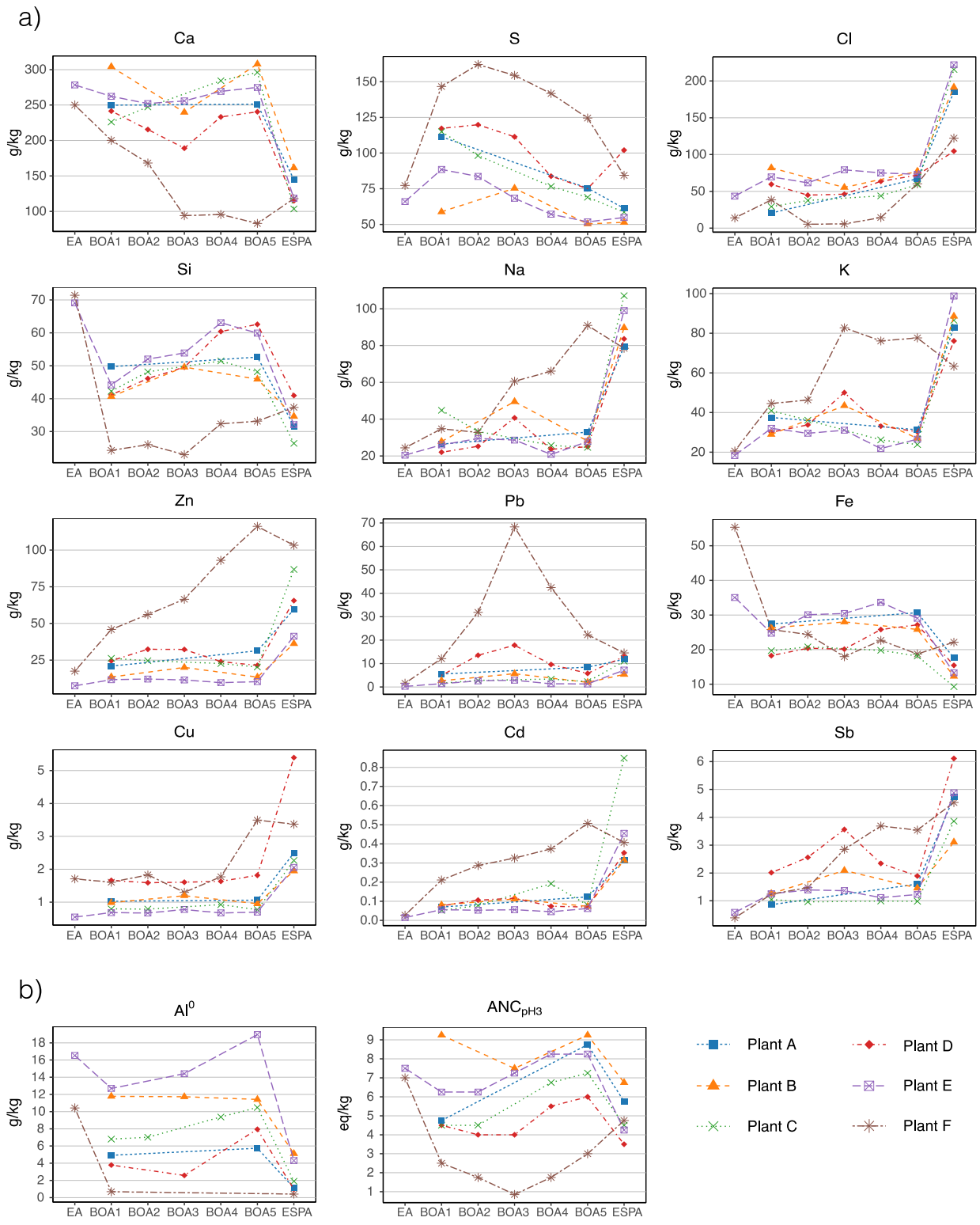

Fig. 8.1: Chemical composition of different ash fractions arising along the flue gas cooling path (a) and proxies for estimating leachability (b): content of metallic Al and acid neutralizing capacity (ANC).

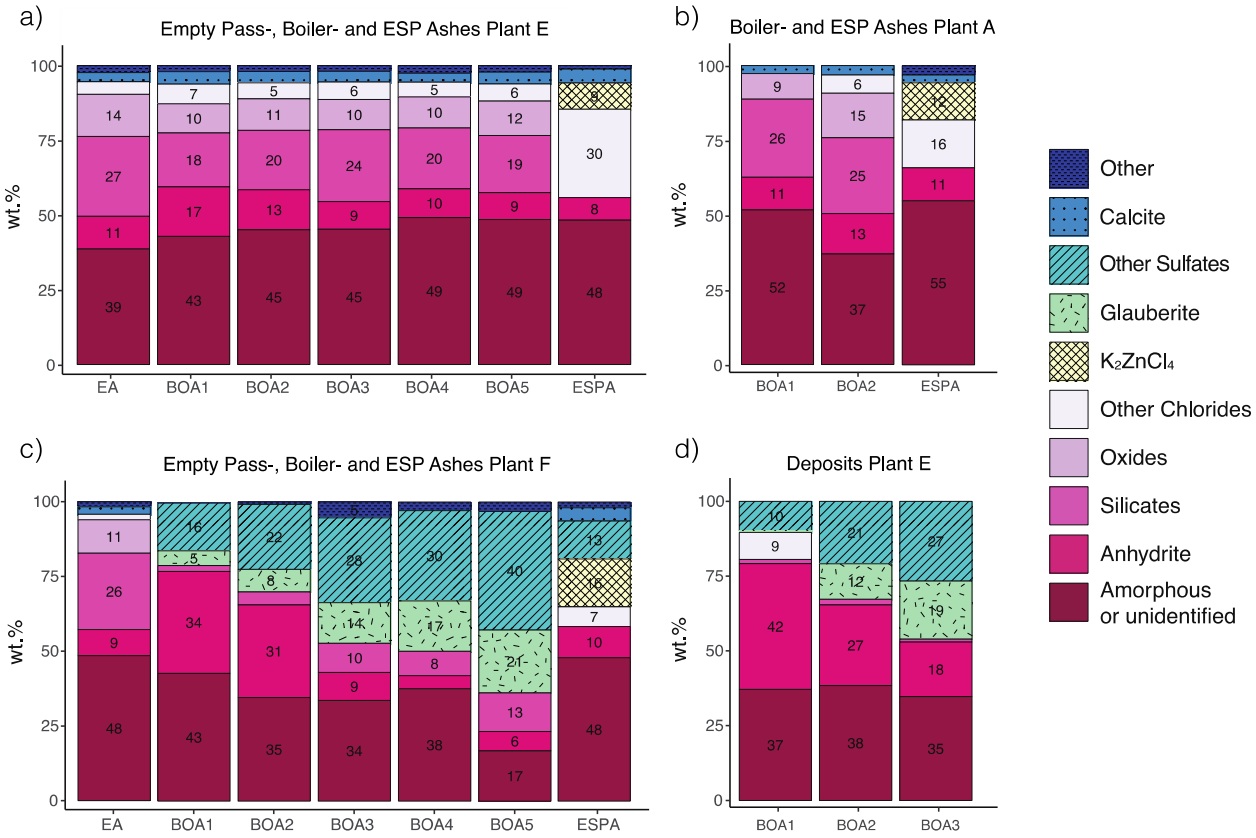

Fig. 8.2: Mineralogical composition of the different ash fractions and deposits formed on heat exchangers.

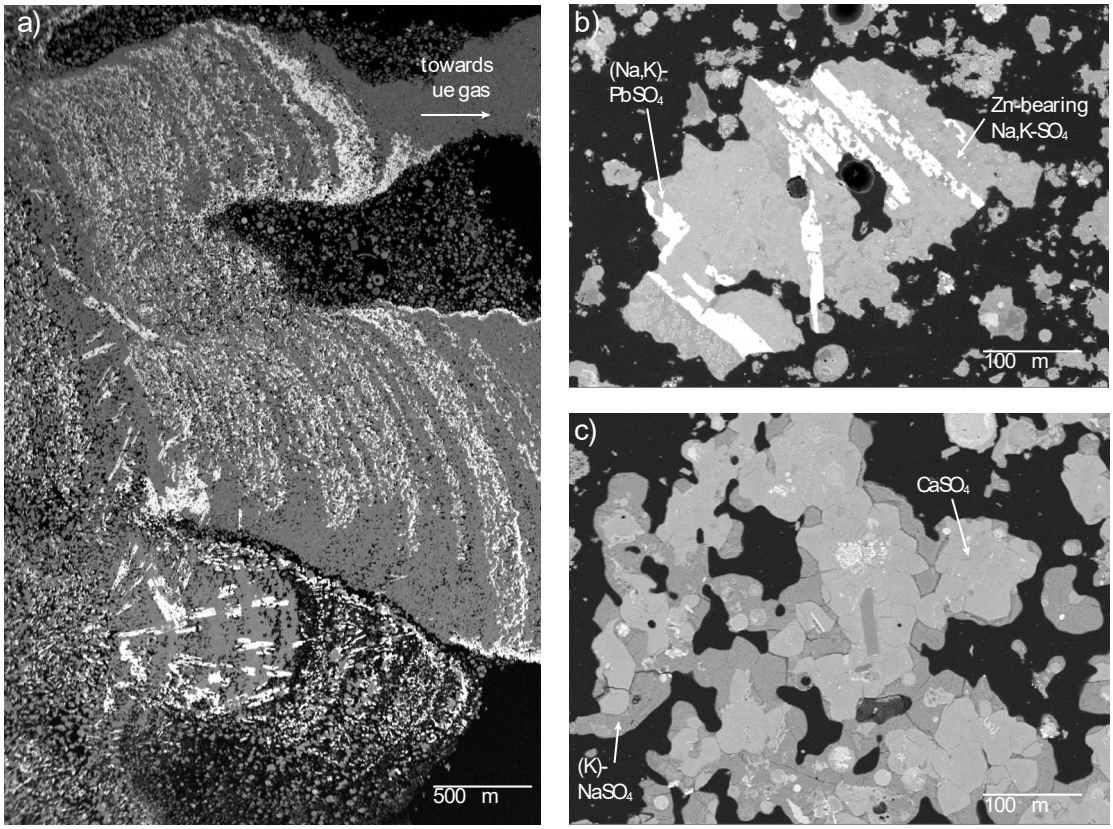

Fig. 8.3: Backscattered electron (BSE) images of deposits (a-c) and ESPA (d-e). Deposit-like BOA from plant F (a), particle piece of a deposit from plant D rich in $PbSO_4$ (b), coexistence of different matrix compositions (c).

8.3 Biomass Bottom Ash from Fluidised Bed Incinerators: Upcycling Potential for Cement Production

Cement manufacturers need new raw materials. Conventionally used raw materials such as limestone are becoming unfavourable due to the high CO_2 emissions arising from calcination reactions and land use conflicts often related to open-pit mines (Andrew 2018). Currently used supplementary cementitious materials (SCMs) such as coal fly ash were previously thought to be environmentally friendly alternatives, but they are expected to become unavailable in Europe since their production is, again, often related to high-carbon-emission productions (Reid et al. 2020).

On the search for modern raw materials with a low-carbon-footprint, the cement industry has evaluated waste materials from biomass power plants. The solid biomass energy market is expected to grow 20-30 % by 2050, which makes it an important future energy type (IEA 2021). Due to their constant volume and composition, bottom ashes from fluidised bed boilers are especially attractive to the cement industry (Maschowski et al. 2019 & 2020). They occur as gravitational output at the bottom of the first, second, or third draws of a fluidised bed incinerator (Fig. 8.4a).

In fluidised bed incineration, a bubbling bed of a hot, sand-like material functions as a heat bank. It increases the efficiency of the energy conversion: within the 0.5-1.5 m high bed, temperatures remain relatively stable even if the input material has variable quality. This is the case for wood energy plants, where different wood types (waste wood or natural wood) with variable water content and chemistry are fed into the boiler. Currently, quartz sand is used as a bed material. In the boiler, inorganic compounds form a thin rim of around the sand particles. This way, the bed material itself is the main component of the output ashes. Replacing the quartz sand as bed material thus opens the opportunity to design a new cement raw material. This design may include the lowering of the heavy metal content by fractionation and enrichment in other ash fractions of the incinerator or the activation of the new bed material.

To estimate the potential for element fractionation, mass fluxes of three Swiss wood energy plants were evaluated. In spring 2021, an ash sampling campaign was carried out. Using the indications on the share of each ash fraction (values in the legend) provided by the technical staff and the chemical composition (WDX-XRF) of those fractions, a mass balance could be established. The diagram in Fig. 8.4b shows the fractionation of heavy metals across the ash fractions within one plant. Values below the total indicated in the legend means relative depletion of the element, values above the total indicate relative enrichment. With this information, it is possible to predict, how the inorganic compounds of the wood will contribute to the chemistry of the ash types. They also hint to possible fractionation processes that could have an effect on the bed material itself. This way, incineration may result in an improvement or deterioration of the bottom ash (draws 1-3, green colours) with regard to its use as cement raw material. Bed material could, on the one hand, be "cleaned" from elements such as Cl or Pb, and enriched in generally hazardous elements such as Co or Cu. Since the fractionation depends on the mineralogical composition of the ashes, XRD results are evaluated simultaneously and results are upcoming.

In order to evaluate the activation potential of the substitution candidates, the research strategy comprises a comparison of the mineralogical composition before and after heating in a lab-scale rotary kiln as well as XRD heating-stage experiments. Based on these preliminary tests as well as other tests covering the

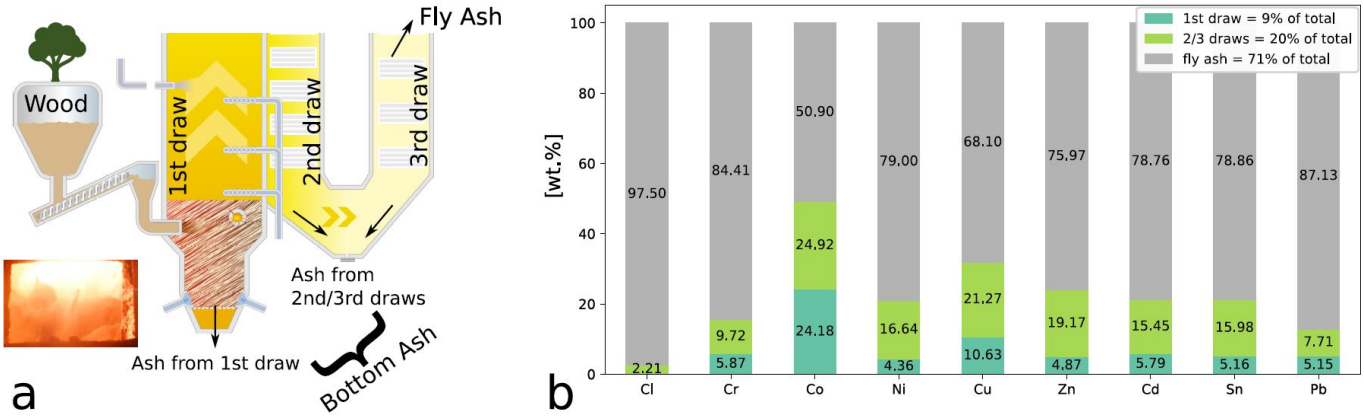

Fig. 8.4: Sketch of a fluidised wood incinerator with output locations of the bottom ashes (a) and transfer coefficients for the Basel wood energy plant (b). The values in (b) indicate the amount of the fraction of the total input.

mechanical and thermal stability and their behaviour in the fluidised bed incinerator as modelled by Bertsch, an incinerator engineering company, two materials will eventually be tested in a bench scale incinerator run by the TU Vienna. These batch runs will produce ashes, which will be tested for use as cement supplement by Holcim.

After careful evaluation of all tests and bench-scale experiments, a test run in an industry-scale incinerator is planned for Summer 2022.

8.4 Hydraulic aspects of bottom ash landfills

In Switzerland, more than 3 million tons of waste are collected annually from households and industry and incinerated in waste incineration plants across the country (VBSA, 2018). The residues after the incineration, mainly bottom ash (approx. 800'000 tons per year), are treated for metal recovery and deposited at around 30 landfill sites of Type D (BAFU, 2016).

The waste disposal ordinance defines an aftercare period of 50 years, in which landfills and their leachates can be treated in order to achieve limit values (BAFU, 2016). After this period, active measures to protect the environment should no longer be necessary. Furthermore, the potential for pollutants and releases, as well as the significance and exposure of the protected property (e.g. surface water, groundwater, soil), should be assessed with the help of a hazard assessment (BAFU, 2019).

The time horizon of landfill aftercare reflects only a small part of its life cycle and is not based on scientific studies. Therefore, reliable predictions for future behavior of Type D landfills are challenging. Due to the obvious knowledge gap, the project aims to investigate the dynamics of pollutants found in such bottom ash landfills in more detail. The main goal is the formulation of a model-like description of the ongoing processes. In addition to chemical parameters, the focus is also on hydraulic properties, since these are usually unknown, but have a significant influence on the interaction between liquid phases (e.g. rainwater, leachate) and the deposited solid material. To get an overview, the current situation of different bottom ash landfills are being documented and investigated. The results of these primary investigations provide the basis for the chemical and hydraulic models.

For a better understanding of the rainwater flow through a bottom ash landfill, a dye tracer experiment was carried out. The occurring flow system was visualized by using Brilliant Blue as a color tracer. The dye was applied homogeneously on an area of approx. 2 m^2, which had been previously sprinkled with water. On the following day, the landfill body was opened laterally with an excavator.

With the help of the dye tracer, the flow of water was documented on several lateral cuts through the entire sampling domain (Fig. 8.5). The flow path visualization revealed that a large part of the bottom ash body is not in contact with the incoming water. Furthermore, most of the water is transported along preferential flow paths, which seem to emerge stochastically within the domain. Although some zones show dry conditions, wet areas seemed to take up more volume.

Based on these observations, it is suggested that a bottom ash landfill body can be considered as highly inhomogeneous two-component system:

- Saturated zone, defining preferential flow paths, which is responsible for most of the liquid transport.
- Partially saturated contact zone, in which water and solutes are transported by diffusion only.

Based on the results of the dye tracer experiment, it can be assumed that the pollutants released in the leachate of the landfill originate from interaction of rainwater with only a small volume of fraction of disposed solid (approx. 5 %). It is suggested that solutes inventory located in contact zone, is only mobilized and flushed out during heavy rainwater events. The conducted tracer experiment indicates that the detailed investigation of hydraulic properties of bottom ash landfill bodies is of great importance for a better understanding of their future pollutant and release potential.

Upcoming field experiments will focus on the liquid flow in unsaturated zones, residence time and leaching processes. Chemical analyses of fresh and altered bottom ash, as well as of landfill leachate should provide further information about hydrology and its influence on the solid-liquid reaction.

Fig. 8.5: Lateral view of the excavated experimental site. The used dye tracer Brilliant Blue visualized the occurring preferential flow paths through the bottom ash landfill body.

8.5 References

Andrew R.M. (2018)
Global CO 2 emissions from cement production. Earth System Science Data, 10(1), 195-217.

Bundesamt für Umwelt, BAFU (2016)
Verordnung über die Vermeidung und Entsorgung von Abfällen (VVEA).

Bundesamt für Umwelt, BAFU (2019)
Vollzugshilfe Gefährdungsabschätzung bei Deponien.

A. Bühler & S. Schlumberger (2010)
Schwermetalle aus der Flugasche zurückgewinnen 'Saure Flugaschenwäsche - FLUWA-Verfahren' ein zukunftsweisendes Verfahren in der Abfall-verbrennung.

Verband der Betreiber Schweizerischer Abfall-verwertungsanlagen, VBSA (2018)
Siedlungsabfallaufkommen Schweiz 2050.

IEA (2021)
World Energy Outlook 2021, IEA, Paris https://www.iea.org/reports/world-energy-outlook-2021.

Maschowski C., Kruspan P., Garra P., Arif A.T., Trouvé G., Gieré R. (2019)
Physicochemical and mineralogical characterization of biomass ash from different power plants in the Upper Rhine Region. Fuel 258, 116020.

Maschowski C., Kruspan P., Arif A.T., Garra P., Trouvé G., Gieré R. (2020)
Use of biomass ash from different sources and processes in cement. Journal of sustainable cement-based materials, 9(6), 350-370.

Reid I., Carpenter A.M., Masili A. (2020)
Beneficial uses of coal fly ash. Report CCC/303.

Wolffers M., Eggenberger U., Schlumberger S., Churakov S.V. (2021)
Characterization of MSWI fly ashes along the flue gas cooling path and implications on heavy metal recovery through acid leaching. Waste Management, 134, 231–240.

9 PUBLICATIONS

9.1 Peer reviewed research articles

Adams D.J., Wang L.[1], Steinle-Neumann G.[1], Passerone D.[2], Churakov S.V. (2021)
Anharmonic effects on the dynamics of solid aluminium from *ab initio* simulations. Journal of Physics: Condensed Matter, 33(17), 175501 (8 pp.).
[1] Bayerisches Geoinstitut, Universität Bayreuth, D-95440 Bayreuth, Germany
[2] Empa-Swiss Federal Laboratories for Materials Science and Technology, 8600 Dübendorf, Switzerland

Águila J.F.[1], Montoya V.[2,3], Samper J.[1], Montenegro L.[1], Kosakowski G., Krejci P., Pfingsten W. (2021)
Modeling cesium migration through Opalinus clay: a benchmark for single- and multi-species sorption-diffusion models. Computational Geosciences, 25(4), 1405–1436.
[1] Centro de Investigaciones Científicas Avanzadas (CICA), Universidad de A Coruña, A Coruña, Spain
[2] Institute for Nuclear Waste Disposal, Karlsruhe Institute for Technology, Karlsruhe, Germany
[3] Department of Environmental Informatics, Helmholtz Centre for Environmental Research - UFZ, Leipzig, Germany

Cametti G., Scheinost A.C.[1,2], Churakov S.V. (2021)
Cd^{2+} incorporation in small-pore LEV/ERI intergrown zeolites: a multi-methodological study. Microporous and Mesoporous Materials, 313, 110835 (11 pp.).
[1] The Rossendorf Beamline at the European Synchrotron Radiation Facility (ESRF), Avenue des Martyrs 71, 38043, Grenoble, France
[2] Helmholtz Zentrum Dresden Rossendorf, Institute of Resource Ecology, Bautzner Landstrasse 400, 01328, Dresden, Germany

Cramer K.[1], Prasianakis N.I., Niceno B., Ihli J., Holler M., Leyer S.[1] (2021)
Three-dimensional membrane imaging with X-ray ptychography: determination of membrane transport properties for membrane distillation. Transport in Porous Media, 138(2), 265-284.
[1] University of Luxembourg, L-1359 Luxembourg

Dähn R., Baeyens B., Marques Fernandes M. (2021)
Zn uptake by illite and argillaceous rocks. Geochimica et Cosmochimica Acta, 312, 180-193.

Di Lorenzo F., Arnold T., Churakov S.V. (2021)
Pb^{2+} uptake by magnesite: the competition between thermodynamic driving force and reaction kinetics. Minerals, 11(4), 415 (18 pp.).

Di Lorenzo F., Steiner K., Churakov S.V. (2021)
The effect of pH, ionic strength and the presence of Pb^{II} on the formation of calcium carbonate from homogenous alkaline solutions at room temperature. Minerals, 11(7), 783 (15 pp.).

Geng G.[1], Barbotin S.[2], Shakoorioskooie M.[3], Shi Z.[3], Leemann A.[3], Sanchez D.F., Grolimund D., Wieland E., Dähn R. (2021)
An in-situ 3D micro-XRD investigation of water uptake by alkali-silica-reaction (ASR) product. Cement and Concrete Research, 141, 106331 (8 pp.).
[1] National University of Singapore, Singapore
[2] Swiss Federal Institute of Technology (EPFL), Lausanne, Switzerland
[3] Empa, Dübendorf, Switzerland

Glaus M.A., Frick S., Van Loon L.R. (2021)
Competitive effects of cations on the diffusion properties of strongly sorbing trace cations in compacted illite and Opalinus Clay. ACS Earth and Space Chemistry, 5(10), 2621-2625.

Huang Y.[1,2], Shao H.[2,3], Wieland E., Kolditz O.[2,4], Kosakowski G. (2021)
Two-phase transport in a cemented waste package considering spatio-temporal evolution of chemical conditions. Npj Materials Degradation, 5(1), 4 (14 pp.).
[1] Key Laboratory of Shale Gas and Geoengineering, Institute of Geology and Geophysics, Chinese Academy of Sciences, Beijing, China
[2] Department of Environmental Informatics, Helmholtz Centre for Environmental Research – UFZ, Leipzig, Germany
[3] Freiberg University of Mining and Technology – TUBAF, Freiberg, Germany
[4] Applied Environmental Systems Analysis, Dresden University of Technology, Dresden, Germany

Jaquenoud M.[1], Elam W.T.[2], Grundl T.[3], Gimmi T., Jakob A., Schefer S.[4], Cloet V.[5], de Cannière P.[6], Van Loon L.R., Leupin O.X.[1] (2021)
In-situ X-ray fluorescence to investigate iodide diffusion in opalinus clay: Demonstration of a novel experimental approach. Chemosphere 269, 128674 (11 pp.).
[1] National Cooperative for the Disposal of Radioactive Waste, Wettingen, Switzerland
[2] Applied Physics Lab, University of Washington, Seattle, WA, 98105, USA
[3] School of Freshwater Sciences, University of Wisconsin-Milwaukee, WI, 53201, USA
[4] Swisstopo, Route de la Gare 63, 2882, St-Ursanne, Switzerland
[5] Arcadis, Ifangstrasse 11, 8952, Schlieren, Switzerland
[6] FANC-AFCN, 1000, Brussels, Belgium

Karalis K., Zahn D.[1], Prasianakis N.I., Niceno B., Churakov S.V. (2021)
Deciphering the molecular mechanism of water boiling at heterogeneous interfaces. Scientific Reports, 11(1), 19858 (10 pp.).
[1] Lehrstuhl für Theoretische Chemie/Computer Chemie Centrum, Friedrich-Alexander Universität Erlangen-Nürnberg, Erlangen, Germany

Khatoonabadi M., Prasianakis N.I., Mantzaras J., (2021)
Lattice Boltzmann model with generalized wall boundary conditions for arbitrary catalytic reactivity. Physical Review E, 103(6), 063303 (13 pp.).

Khatoonabadi M., Safi M.A., Prasianakis N.I., Roth J., Mantzaras J., Kirov N., Büchi F.N. (2021)
Insights on the interaction of serpentine channels and gas diffusion layer in an operating polymer electrolyte fuel cell: numerical modeling across scales. International Journal of Heat and Mass Transfer, 181, 121859 (13 pp.).

Klinkenberg M.[1], Brandt F.[1], Baeyens B., Bosbach D.[1], Marques Fernandes M. (2021)
Adsorption of barium and radium on montmorillonite: a comparative experimental and modelling study. Applied Geochemistry, 135, 105117 (11 pp.).
[1] Forschungszentrum Julich, 52425 Julich, Germany

Krattiger N., Lothenbach B.[1], Churakov S.V (2021)
Sorption and electrokinetic properties of ASR product and C-S-H: a comparative modelling study. Cement and Concrete Research, 146, 106491 (11 pp.).
[1] Empa, Dübendorf, Switzerland

Krejci P., Gimmi T., Van Loon L.R. (2021)
On the concentration-dependent diffusion of sorbed cesium in Opalinus Clay. Geochimica et Cosmochimica Acta, 298, 149-166.

Kulik D.A., Winnefeld F.[1], Kulik A.D.[2], Miron G.D., Lothenbach B.[1,3] (2021)
CemGEMS – an easy-to-use web application for thermodynamic modeling of cementitious materials. RILEM Technical Letters, 6, 36-52.
[1] Empa, Swiss Federal Laboratories for Materials Science and Technology, 8600 Dübendorf, Switzerland
[2] CONGINEER LLC, 5200 Brugg, Switzerland
[3] NTNU, Norwegian University of Science and Technology, 7491 Trondheim, Norway

Maier M.-L.[1], Patel R.A.[1], Prasianakis N.I., Churakov S.V., Nirschl H.[1], Krause M.J.[1] (2021)
Coupling of multiscale lattice Boltzmann discrete-element method for reactive particle fluid flows. Physical Review E, 103(3), 033306 (15 pp.).
[1] Karlsruhe Institute of Technology (KIT), Karlsruhe, Germany

Mancini A., Lothenbach B.[1], Geng G.[2], Grolimund D., Sanchez D.F., Fakra S.C.[3], Dähn R., Wehrli B.[4], Wieland E. (2021)
Iron speciation in blast furnace slag cements. Cement and Concrete Research, 140, 106287 (18 pp.).
[1] Empa, Dübendorf, Switzerland
[2] National University of Singapore, Singapore
[3] Lawrence Berkeley National Laboratory, Berkeley, USA
[4] ETH Zürich, Zürich, Switzerland

Mancini A., Wieland E., Geng G.[1], Lothenbach B.[2], Wehrli B.[3], Dähn R. (2021)
Fe(II) interaction with cement phases: method development, wet chemical studies and X-ray absorption spectroscopy. Journal of Colloid and Interface Science, 588, 692-704.
[1] National University of Singapore, Singapore
[2] Empa, Dübendorf, Switzerland
[3] ETH Zürich, Zürich, Switzerland

Marafatto F.F., Dähn R., Grolimund D., Göttlicher J.[1], Voegelin A.[2] (2021)
Thallium sorption by soil manganese oxides: insights from synchrotron X-ray micro-analyses on a naturally thallium-rich soil. Geochimica et Cosmochimica Acta, 302, 193-208.
[1] Karlsruhe Institute of Technology, Eggenstein-Leopoldshafen, Germany
[2] Eawag, Dübendorf, Switzerland

Marsiske M.R.[1], Debus Ch.[1], Di Lorenzo F., Bernard E.[2], Churakov S.V., Ruiz-Agudo C.[1] (2021)
Immobilization of (aqueous) cations in low pH M-S-H cement. Applied Sciences, 11(7), 2968 (18 pp.).
[1] Department of Physical Chemistry, University of Konstanz, 78457 Konstanz, Germany
[2] Department of Civil and Environmental Engineering, Imperial College London, South Kensington, Skempton Building, London SW7 2AZ, UK

Nakarai K.[1], Shibata M.[2], Sakamoto H.[2], Owada H.[3], Kosakowski G. (2021)
Calcite precipitation at cement-bentonite interface. Part 1: effect of carbonate admixture in bentonite. Journal of Advanced Concrete Technology, 19(5), 433-446.
[1] Hiroshima University, Civil and Environmental Engineering Program, Hiroshima, Japan
[2] Taiheiyo Consultant Co. Ltd., Electric and Nuclear Power Technology Department, Sakura-shi, Japan
[3] Radioactive Waste Management Funding and Research Center, Research and Development of Geological Disposal Barrier System, Tokyo, Japan

Nakarai K.[1], Watanabe M.[2], Koibuchi K.[3], Kosakowski G. (2021)
Calcite precipitation at cement-bentonite interface. Part 2: acceleration of transport by an electrical gradient. Journal of Advanced Concrete Technology, 19(5), 447-461.
[1] Hiroshima University, Civil and Environmental Engineering Program, Hiroshima, Japan
[2] Gunma University, Department of Civil and Environmental Engineering, Gunma, Japan
[3] Global Material Research Corporation, Chiba, Japan

Nedyalkova L., Tits J., Bernard E., Wieland E., Mäder U. (2021)
Sorption experiments with HTO, 36-Cl, 125-I and 14-C labeled formate on aged cement matrices retrieved from long-term in-situ rock laboratory experiments. Journal of Advanced Concrete Technology, 19(7), 811-829.

Patel R.A, Churakov S.V., Prasianakis N.I. (2021) A multi-level pore scale reactive transport model for the investigation of combined leaching and carbonation of cement paste. *Cement and Concrete Composites*, *115*, 103831 (18 pp.).

Roos D.P., Scheinost A.C.[1,2], Churakov S.V., Nagashima M.[3], Cametti G. (2021)
On the nature of Pb species in Pb-exchanged zeolite stellerite (STI): a combined experimental and theoretical study. Microporous and Mesoporous Materials, 327, 111444 (8 pp.).
[1] The Rossendorf Beamline at the European Synchrotron Radiation Facility (ESRF), Avenue des Martyrs 71, 38043, Grenoble, France
[2] Helmholtz Zentrum Dresden Rossendorf, Institute of Resource Ecology, Bautzner Landstrasse 400, 01328, Dresden, Germany
[3] Graduate School of Sciences and Technology for Innovation, Yamaguchi University, Yamaguchi, 753-8512, Japan

Sarraf F.[1], Abbatinali E.[1,2], Gorjan L.[1], Sebastian T.[1], Colombo P.[2], Churakov S.V., Clemens F.[1] (2021) Effect of MgO sintering additive on mullite structures manufactured by fused deposition modeling (FDM) technology. Journal of the European Ceramic Society, 41(13), 6677-6686.
[1] Empa-Swiss Federal Laboratories for Materials Science and Technology, 8600, Dübendorf, Switzerland
[2] University of Padova, 35122, Padova, Italy

Schliemann R., Churakov S.V. (2021)
Atomic scale mechanism of clay minerals dissolution revealed by ab initio simulations. Geochimica et Cosmochimica Acta, 293, 438-460.

Schliemann R., Churakov S.V. (2021)
Pyrophyllite dissolution at elevated pressure conditions: an ab initio study. Geochimica et Cosmochimica Acta, 307, 42-55.

Stockmann M.[1], Fritsch K.[1], Bok F.[1], Marques Fernandes M., Baeyens B., Steudtner R.[1], Müller K.[1], Nebelung C.[1], Brendler V.[1], Stumpf T.[1], Schmeide K.[1] (2021)
New insights into U(VI) sorption onto montmorillonite from batch sorption and spectroscopic studies at increased ionic strength. Science of the Total Environment, 806(2), 150653 (13 pp.).
[1] HZDR/IRE, Dresden, Germany

Weibel G., Zappatini A., Wolffers M., Ringmann S.[1] (2021)
Optimization of Metal Recovery from MSWI Fly Ash by Acid Leaching: Findings from Laboratory- and Industrial-Scale Experiments. Processes 2021, 9(2), 352.
[1] KVA Linth, Niederurnen, Switzerland

Wick S.[1,2], Baeyens B., Marques Fernandes M., Pfenninger N.[1], Voegelin A.[1] (2021)
Exploring the geochemistry of thallium in soils by x-ray absorption spectroscopy and chemical soil extractions. Chimia, 75(1-2), 103.
[1] Eawag, Swiss Federal Institute of Aquatic Science and Technology, Dübendorf, Switzerland
[2] ETH Zürich, Zürich, Switzerland

Wolffers M., Eggenberger U., Schlumberger S.[1], Churakov S.V. (2021)
Characterization of MSWI fly ashes along the flue gas cooling path and implications on heavy metal recovery through acid leaching. Waste Management, 134, 231-240.
[1] Zentrum für nachhaltige Abfall- und Ressourcennutzung ZAR, Zuchwil, Switzerland

Wolffers M., Weibel G.[1], Eggenberger U. (2021)
Waste Wood Fly Ash Treatment in Switzerland: Effects of Co-Processing with Fly Ash from Municipal Solid Waste on Cr(VI) Reduction and Heavy Metal Recovery. Processes, 9(1), 146 (15 pp.).
[1] Zentrum für nachhaltige Abfall- und Ressourcennutzung ZAR, Hinwil, Switzerland

9.2 Books

Patel R.A., Prasianakis N.I. (2021)
Pore-scale numerical modeling tools for improving efficiency of direct carbon capture in compacts. Springer Nature, RILEM Bookseries, 33, 141-149.

Schliemann R., Churakov S.V. (2021)
Ab initio simulations of clay minerals reactivity and thermodynamics. In: Sainz-Díaz, C.I. (Ed.), Computational modeling in clay mineralogy, 175-210.

9.3 Technical reports

Aschwanden L., Camesi L., Gimmi T., Jenni A., Kiczka M., Mäder U., Mazurek M., Rufer D., Waber H.N., Wersin P., Zwahlen C., Traber D. (2021) TBO Trüllikon-1-1: Data Report. Dossier VIII, Rock Properties, Porewater Characterisation and Natural Tracer Profiles, Nagra Working Report NAB 20-09.

Curti E. (2021)
Bentonite Pore Waters (BPW) for the Sectoral Plan, phase SGT-3: model development and testing. PSI Technical Report TM-44-21-02.

Curti E. (2021)
Thermodynamic modelling of “inside canister” conditions during UO_2 spent fuel dissolution in a failed steel container. European Commission, Brussels, DisCo WP5, Deliverable 5.6.

Guillemot T., Cvetković B.Z., Kunz D., Salazar G., Rauber M., Szidat S., Wieland E. (2021a)
Development of analytical methods for the detection of ^{14}C-bearing carbon compounds at ultra-low concentrations. Nagra Working Report NAB 21-03.

Guillemot T., Kunz D., Salazar G., Rauber M., Szidat S., Wieland E. (2021b)
Long-term monitoring of dissolved and gaseous ^{14}C-bearing carbon compounds during anoxic alkaline corrosion of irradiated steel. Nagra Working Report NAB 21-26.

Mäder U., Aschwanden L., Camesi L., Gimmi T., Jenni A., Kiczka M., Mazurek M., Rufer D., Waber H.N., Wersin P., Zwahlen C., Traber D. (2021)
TBO Marthalen-1-1: Data Report. Dossier VIII, Rock Properties, Porewater Characterisation and Natural Tracer Profiles, Nagra Working Report NAB 21-20.

Maes N., Glaus M.A., Baeyens B., Marques Fernandes M., Churakov S.V., Dähn R., Grangeon S., Tournassat C., Geckeis H., Charlet L., Brandt F., Poonoosamy J., Hoving A., Havlova V., Fischer C., Scheinost A.C., Noseck U., Britz S., Siitari-Kauppi M., Missana T., (2021)
State-of-the-Art report on the understanding of radionuclide retention and transport in clay and crystalline rocks. Final version as of 30.04.2021 of deliverable D5.1 of the HORIZON 2020 project EURAD. EC Grant agreement no: 847593.

Marques Fernandes M., Baeyens B. (2021)
Application of the "bottom up" approach for the sorption of Cs(I), Co(II), Ni(II), Eu(III), Th(IV) and U(VI) onto sedimentary rocks. Nagra Technical Report NTB 19-04.

Marques Fernandes M., Baeyens B. (2021)
Competitive adsorption on illite and montmorillonite: Experimental and modelling investigations. Nagra Technical Report NTB 19-05.

Mazurek M., Aschwanden L., Camesi L., Gimmi T., Jenni A., Kiczka M., Mäder U., Rufer D., Waber H.N., Wanner P., Wersin P., Traber D. (2021)
TBO Bülach-1-1: Data Report. Dossier VIII Rock Properties, Porewater Characterisation and Natural Tracer Profiles, Nagra Working Report NAB 20-08.

Miron G.D. (2021)
Fate of H_2 in the repository. PSI Technical Report TM-44-21-05.

Miron G.D. (2021)
Thermodynamic Data for Boron and Chromium. PSI Technical Report TM-44-21-06.

Pfingsten W. (2021)
Uncertainty and Sensitivity Analysis of the Chemistry of Nickel Sorption in OPA/Reference Illite. PSI Technical Report TM-44-21-19.

Tits J., Laube A. (2021)
Experimental studies on the uptake of ^{45}Ca, ^{32}Si and ^{26}Al by cementitious materials. PSI Technical Report TM-44-21-07.

Wieland E. (2021)
Iron-cement interaction: A literature survey. PSI Technical Report TM-44-21-08.

9.4 Conferences/workshops/presentations

Adams D., Churakov S.V. (2021)
Decoupled Anharmonic Mode Approximation: New insights considering full quantum anharmonicity in the nuclear motion. CECAM workshop, Capturing Anharmonic Vibrational Motion in First-Principles Simulations, 06–09 December 2021, CECAM-HQ-EPFL, Lausanne, Switzerland.

Detilleux V.[1], Swahn J.[2], Miksova J.[3], Pellegrini D.[4], Pfingsten W., Zeleznik N.[5] (2021)
SITEX_network for the development of sustainable and independent technical expertise on radioactive waste management: general overview of the network and its interactions with civil society. In Vol. IAEA-CN-266. International conference on challenges faced by technical and scientific support organizations (TSOs) in enhancing nuclear safety and security: ensuring effective and sustainable expertise (17 pp.). IAEA.
[1] Bel V, Brussels, Belgium
[2] MKG, Göteborg, Sweden
[3] SURO, Rez, Czech Republic
[4] IRSN, Paris, France
[5] EIMV, Ljubljana, Slovenia

Garibay-Rodriguez J., Kosakowski G., Lu R., Kolditz G., Montoya V. (2021)
Reactive transport model of a low and intermediate-level waste disposal cell evolution in clay rock. TransRet2020 conference, 12–13 October 2021, Dresden, Germany.

Gysi A., Hurtig N., Miron G.D., Kulik D.A, Harlov D.E. (2021)
Fluid-rock interaction and ore deposits in the Earth's crust: coupling of field and experimental methods with numerical modeling. Goldschmidt 2021.

Jaeger T., Mokos A., Prasianakis N.I., Leyer S. (2021)
Pore-level Multiphase Simulations of Realistic Distillation Membranes for Water Desalination. 16th conference on Sustainable development of Energy, Water and Environment Systems (SDEWES 2021), 10–15 October 2021, Dubrovnik, Croatia.

Krattiger N., Lothenbach B., Churakov S.V. (2021) Sorption and electrochemical properties of ASR products and C-S-H: a comparative modelling study. In B. L. A. Pichler, P. J. McDonald, B. Lothenbach, K. Scrivener, V. Bortolotti, M. Ben Haha (Eds.), ERICA CASH II final conference (69-70 pp.), Technische Universität Wien.

Mahrous M., Poonoosamy J., Curti E., Bosbach D., Churakov S.V., Deissmann G., Prasianakis N.I. (2021) A Bridging Experimental-Modeling Approach Towards Mechanistic Understanding of Minerals Co-precipitation. 7th International Workshop on Crystallization in Porous Media (CRYSPOM VII), 7–9 June 2021, Pau, France.

Niceno B., Karalis K., Prasianakis N.I., Patel R., Churakov S.V., Sato Y. (2021)
Numerical prediction of boiling crisis considering surface characteristics. Swiss Nuclear Tag der Forschung, 12 and 18 January 2021.

Pfingsten W. (2021)
Sorption parameter uncertainty propagation in reactive transport modeling using the example of cesium diffusion in clay. EUROSAFE 2021, Paris, France, 22–23 November 2021.

Poonoosamy J., Prasianakis N.I., Curti E., Mahrous M., Deissmann G., Churakov S.V., Bosbach D. (2021) Lab-on-a-chip approach for resolving controversies on crystallization processes in porous media. Scientific Workshop Processes Influencing Radionuclide Transport and Retention, Investigations Across Scales, TransRet2020, Karlsruhe, Germany, 12–13 October 2021.

Poonoosamy J., Prasianakis N.I., Lönartz N., Yang Y., Deissmann G., Churakov S.V., Bosbach D. (2021) A lab on a chip concept for rationalizing hydro-geochemical processes at the pore scale. ACS Spring meeting 2021.

Roos D., Scheinost A.C., Churakov S.V., Cametti G. (2021)
Nature of Pb species in Pb-exchanged zeolite stellerite. 3rd European Mineralogical Conference, EMC, Krakow, Poland.

Wolffers M., Eggenberger U., Schlumberger S., Churakov S.V. (2021)
Recoverability of heavy metals of MSWI fly ashes along the flue gas cooling path. 3rd European Mineralogical Conference, EMC, Krakow, Poland.

Wolffers M., Eggenberger U., Schlumberger S., Churakov S.V. (2020)
Heavy metal recoverability of MSWI fly ashes along the flue gas cooling path. 3rd European Mineralogical Conference, EMC, Krakow, Poland.

9.5 Invited Talks

Churakov S.V. (Plenary Talk 2021)
Reactive transport and retention of solutes in pores media: Current state of the art and the challenges TransRet2020 Radionuclide Transport and Retention. 12–13 October 2021, Karlsruhe, Germany.

Churakov S.V. (Plenary Talk 2021)
Fundamental and applied research on geochemistry of nuclear waste disposal in Switzerland. RWM RSO Annual Conference 15–16 September 2021, Manchester UK.

9.6 Teaching

Churakov S.V.

Bachelor course: Kristallographie I+II, Institut für Geologie, Universität Bern, spring and fall semester 2021.

Bachelor course: Kristalloptik. Institut für Geologie, Universität Bern, fall semester 2021.

Master course: Atomistic simulations of geomaterials, Institut für Geologie, Universität Bern, fall semester 2021.

Master course: Atomistic simulations of fluids and solids, Institut für Geologie, Universität Bern, fall semester 2021.

Eggenberger U., Weibel G., Zucha W., Wolffers M. Master Course: Geochemical Analysis of Rocks, Institut für Geologie, Universität Bern, fall semester 2021.

Master Course: X-Ray Powder Diffraction, Institut für Geologie, Universität Bern, spring semester 2021.

Non-Radioactive Waste and Remediation, fall semester 2021.

CAS Course: Inorganic and Organic Pollutants, Institut für Geologie, Universität Bern, June 2021.

CAS Course: Remediation of Contaminated Sites, Institut für Geologie, Universität Bern, June 2021.

Gimmi T.
CAS Course: Ausbreitung von Schadstoffen in Böden und Grundwasser: Von der Realität zum Modell – und zurück, in Verhalten von organischen und anorganischen Schadstoffe in der Umwelt, Universität Bern, 24.–25. Juni 2021.

Gimmi T., Alt-Epping P.
Master Course: Geochemical Modelling II: Reactive Transport, Universität Bern, spring semester 2021.

Kosakowski G.
Master course: Geostatistics, Institute for Geological Sciences, University of Bern, spring semester 2021.

Kulik D.A.
Online CemGEMS training course, 53 participants, February 2021.

Mazurek M., Wersin P., Curti E.
Master Course: Geological disposal of radioactive waste, Institut für Geologie, Universität Bern, spring semester 2021.

Plötze L.M., Hummel W.
Master Course: Landfilling, Contaminated Sites and Radioactive Waste Repositories, ETH Zurich, fall semester 2021.

Prasser H.-M., Hummel W., Kämpfer T.
Master Course: Nuclear Energy Systems, ETH Zurich, spring semester 2021.

9.7 PhD thesis defences

Glauser A.
Development of quality of bottom ash from municipal solid waste incineration in Switzerland, Universität Bern, 30 March 2021.

Hax Damiani L.
A novel reactive transport framework for fluid-rock interaction analysis: Computational approach, applications and benchmarks, Universität Bern, 22 October 2021.

9.8 Other

Gimmi T.
Associate Editor of Applied Geochemistry.

Kulik D.A.
Associate editor of Applied Geochemistry.

Wieland E. (2021)
Examinateur at PhD thesis defence, L. Bouzouaid, “Impact of small organic molecules on the nucleation and growth of C-S-H, the main hydrate of cement”, 25.11.2021, Université de Bourgogne, Dijon, France.

Paul Scherrer Institut :: Forschungsstrasse 111 :: 5232 Villigen PSI :: Switzerland :: Tel. +41 56 310 21 11 :: www.psi.ch